KU Leuven
Biomedical Sciences Group
Faculty of Medicine
Department of Neurosciences

Doctoral thesis:

Measures of auditory brain responses in children and adolescents with and without dyslexia.

Raúl Granados Barbero

Supervisor	Prof. Dr. Jan Wouters
Co-supervisor	Prof. Dr. Pol Ghesquière
Jury members	Prof. Dr. Monique Beullens (chair, KU Leuven, BE)
	Prof. Dr. Patrick Dupont (KU Leuven, BE)
	Prof. Dr. Maaike Vandermosten (KU Leuven, BE)
	Dr. Robin Gransier (KU Leuven, BE)
	Prof. Dr. Caroline Witton (Aston University, UK)
	Prof. Dr. Robert Oostenveld (Radboud University, NL)

Dissertation presented in partial fulfillment of the requirements for the degree of Doctor in Biomedical Sciences

Leuven, 2022



This work is licenced under a Creative Commons Attribution-Non Commercial-Share Alike 4.0 International License.

To view a copy of this licence, please visit: http://creativecommons.org/licenses/by-nc-sa/4.0/.

© 2022 **Raúl Granados Barbero**

Acknowledgments

First, I would like to acknowledge the time the examination committee has spent carefully reading my thesis and raising a number of pertinent questions and comments that led to this final version. The continuous support of Prof. Patrick Dupont and Prof. Maaike Vandermosten as well as their comments after every doctoral evaluation greatly helped to shape the present document. The time spent in Nijmegen with Prof. Robert Oostenveld and in Birmingham with Prof. Caroline Witton significantly contributed to the growth of my interest towards this research field and to the development of certain skills that allowed me to overcome major challenges during my research. Furthermore, the insightful conversations held with Dr. Robin Gransier paved the way for one of the chapters of the thesis.

I would like to thank Prof. Pol Ghesquière for his continuous supervision that provided with the necessary clinical and psychological context for two of the main studies of this doctoral project. Above all, I want to thank my supervisor Prof. Jan Wouters for the opportunity of developing my research and myself towards new places. His continuous guidance, his insightful scientific perspective and his patience are the main reasons all the research done during these years crystallised in the main chapters of this thesis. Thanks to the opportunity he handed me I had the chance of being part of the international ChildBrain project. There, I had the chance to improve my hard and soft skills through different and multidisciplinary training. In these years I had the chance to meet my fellow colleagues that soon grew to become friends. For all the time we spent together doing scientific and not that scientific activities, I would like to thank Abinash, Aimit, Anna, Caroline, Maria Carla, Pragha, Weiyong, Diandra, Marios, Simon, Vân, Gloria, Cecilia and Sam. They, together with their supervisors, helped create a very good and comfortable environment.

I would also like to thank the people from ExpOrl for all the moments that led to interesting scientific conversations or to distended and casual chats, which I found both very fruitful. Especially, I would want to thank Ehsan, because the time we spent together in the lab gave me the chance of learning from a passionate and humble person. All the conversations we had definitely had an impact on a scientific and a personal level. I am also grateful to Astrid De Vos, because her support and expertise laid the foundations of the research questions that became the core of this project. I would also like to thank Elien, Maria, Sara, Jair, Andreas,

Anouk, Tine, Jonas and Robert Luke for all the time we spent in the lab talking about science or other interesting topics that helped me understand more about neuroscience and Belgian culture.

In Leuven, I had the chance to meet wonderful people that helped me often feel at home. I would like to thank my football mates, for all the games played under the roof or under the sun. I am also thankful to my Spaniard colleagues I met in the Hospital. Especially for all the time spent trying to find the best bites in the cafeteria and aiming to replicate them in long and fun dinners afterwards. I am also thankful for my fellow group of European southerners, that helped me discover the wonders of the Jeneverfeesten and other prodigies of the Belgian drinking culture.

Finally, I am very thankful for the support of my parents and my brother, all their efforts kept me in the path to become what I am today. Lastly, I want to thank my fiancée for all of her unwavering support along these years, especially during the difficult ones. The time we spent together allowed me to maintain my balance and and gave me the strength to carry on.

Raúl Granados Barbero
July of 2022

Abstract

Developmental dyslexia is a neurodevelopmental disorder defined by poor word-reading ability. Dyslexia exists in every culture and affects approximately 10% of the population. It significantly interferes with academic, personal, social and emotional functioning. Although, up to date the most plausible theory that explains dyslexia is the phonological deficit theory, the underlying neural mechanisms remain unknown.

Different studies have suggested that language and developmental disorders such as dyslexia are associated with a disturbance of auditory entrainment and of the functional hemispheric asymmetries during speech processing. These disorders typically result from an issue in the phonological component of language that causes problems to represent and manipulate the phonological structure of words at the syllable and/or phoneme level.

The main goal of the PhD was to investigate the auditory processing levels in adolescents and children with dyslexia. We used Auditory Steady-State Responses (ASSRs) by modulating the stimulation parameters to match relevant components related to speech. To pursue these goals we carried out three major studies that are the body of this doctoral Thesis. In the first study we developed a methodology capable of measuring the source activation patterns during speech-related stimulation. We combined Denoising Source Separation (DSS) and Independent Component Analysis (ICA) to successfully reduce the number of reconstructed brain activity sources, that is components, as well as to extract the most relevant ASSR brain activity. We applied this methodology by modulating our stimulation frequencies in order to

match important speech characteristics, i.e. 4, 10 and 20 Hz at group and individual level in EEG adolescent data. The anatomical brain location for these low stimulation frequencies showed results in the temporal gyrus, the region of the brain where the auditory cortex is, with relatively small dispersion. However, for 40 and 80 Hz, results with regard to the number of components and the anatomical origin were less clear. At all stimulation frequencies the outcome measures were consistent with literature. Furthermore, the methodology we used reduced the effect of inter-subject variability, which led to more accurate results. The findings of this first study were promising for the future applications in group comparison involving dyslexia in adolescents and in children.

For the second study we used ASSRs in combination with the methodology developed in the first study. We used EEG recordings in adolescents to investigate the brain activation and hemisphere asymmetry of theta, alpha, beta and low-gamma range oscillations in typical readers and readers with dyslexia. The aim was to analyse whether the group differences found in previous electrode level studies were caused by a different source activation pattern or conversely was an effect that could be found on the active brain sources. We could not find differences in the brain locations of the main active brain sources. However, we observed differences in the extracted waveforms. The group average of the first DSS component of all signal-to-noise ratios of ASSR at source level was higher than the group averages at the electrode level. These analyses showed a low alpha synchronisation in adolescents with dyslexia and the possibility of compensatory mechanisms in theta, beta and low-gamma frequency bands.

It is known that differences between readers with dyslexia and typical readers evolve and change with age. That is the reason why in the third study we wanted to evaluate longitudinal data to measure how neural entrainment levels and hemispherical preference differences between children with dyslexia change in relation to typical readers of the same age. We measured neural speech processing activity using EEG recordings and ASSRs. Stimulation was modulated to make the ASSR match syllabic and phonemic rates. We measured the brain activation pattern and the hemispherical asymmetries in children at three age points (5, 7 and 9 years old). Despite the well-known heterogeneity during developmental stages, especially in children and in dyslexia, we could extract meaningful common oscillatory patterns using our methodology. In this longitudinal study we confirmed that atypical levels of neural

entrainment and connectivity already exist in pre-reading stages. Overall, these measures reflected a lower capability of the dyslectic brain to synchronise with syllabic-rate stimulation, in the form of neural entrainment and connectivity. In addition, our findings reinforced the hypothesis that beta rhythms are the result of brain processes in later maturation stages in dyslexia.

Overall, in the PhD thesis we developed a methodology that allowed us to observe the following: Differences in auditory EEG experiments would, according to our findings, have their origin in the intrinsic oscillatory mechanisms of the brain cortical sources related to speech perception. Furthermore, the project has shown the importance of longitudinal studies in dyslexia, especially in children, where differences between the two groups can change in the span of a year.

Contents

Acknowledgements **iv**

Abstract **vii**

Table of contents **xi**

Abbreviations and acronyms **xiii**

List of figures **xv**

List of tables **xix**

1 General introduction **1**

1.1 Auditory processing and auditory pathways 1

1.2 Neural speech processing 5

1.3 Developmental dyslexia 7

1.4 Brain analysis techniques 9

1.5 Auditory Steady-State Responses 10

1.6 Neural source analysis and brain source modelling 11

1.7 Objectives of the project and thesis outline 21

2 Identification of predominant ASSR brain sources using DSS. **25**

2.1 Introduction 26

2.2 Materials and Methods 31

2.3 Results . . . 40
2.4 Discussion . . . 45
2.5 Conclusion . . . 60
2.6 Appendix . . . 62

3 Atypical processing in neural source analysis in adolescents with dyslexia. 67
3.1 Introduction . . . 68
3.2 Materials and Methods . . . 71
3.3 Results . . . 81
3.4 Discussion . . . 88
3.5 Conclusion . . . 94

4 Speech envelope modulations in the brain in atypical developing children. 97
4.1 Introduction . . . 98
4.2 Materials and Methods . . . 101
4.3 Results . . . 109
4.4 Discussion . . . 116
4.5 Conclusion . . . 119

5 General discussion and future prospects 121
5.1 Global Findings of this project . . . 121
5.2 Future prospects . . . 125

References 129

Scientific acknowledgments 146

Personal contribution and conflict of interest statement 147

Abbreviations and acronyms

AC	Auditory cortex
AEP	Auditory evoked potential
AM	Amplitude modulated
AMICA	Adaptive mixture independent component analysis
ASSR	Auditory steady-state response
AST	Asymmetric sampling in time
BEM	Boundary element method
BSCR	Brain to skull conductivity ratio
CSF	cerebrospinal fluid
dB	Decibel
DC	Direct current
DFT	Discrete Fourier transformation
DR	Reader[s] with dyslexia
DSS	Denoising source separation
ECD	Equivalent current dipole
EEG	Electroencephalography
EFR	Envelope following response
ERP	Event-related potential
FDR	False discovery rate
FEM	Finite element method
FFR	Frequency following response

FFT	Fast Fourier transform
fMRI	Functional magnetic resonance imaging
GMM	Gaussian mixture model
GEVD	Generalised eigenvalue decomposition
HG	Heschl's gyrus
HL	Hearing level
Hz	Hertz
ICA	Independent component analysis
IQ	Intelligence quotient
LI	Laterality index
LIST	Leuven intelligibility sentence test
MEG	Magnetoencephalography
mf	Modulation frequency
MGB	Medial geniculate body
MNE	Minimum-norm estimate
MRI	Magnetic resonance imaging
PCA	Principle component analysis
PET	Positron emission tomography
PLV	Phase-locking value
PtoP	Peak to peak
ROI	region of interest
SD	Standard deviation
SNR	Signal-to-noise ratio
SPL	Sound pressure level
SVD	Singular value decomposition
SWN	Speech weighted noise
TFS	Temporal fine structure
TR	Typically developing reader[s]

List of Figures

1.1 The central auditory system. . . . 4
1.2 Auditory Steady-State Response. . . . 11
1.3 Electrophysiological superposition in EEG. . . . 12
1.4 Forward and inverse model schemas. . . . 14
1.5 Construction steps of a BEM head model based on an MRI. . . . 15

2.1 General overview of the methodological pipeline used. . . . 31
2.2 Total number of DSS components with ASSR. . . . 36
2.3 BEM layers. . . . 38
2.4 MRI orientations used for the visualisation of the dipoles fitted. . . . 39
2.5 Frequency spectrum of a DSS first component for 20 Hz left ear stimulation in the group analysis data. . . . 41
2.6 Number of reconstructed time-series carrying ASSR. . . . 42
2.7 Comparison of the SNR levels between different methodologies. . . . 43
2.8 Relative response amplitudes and SNRs from the group analysis. . . . 44
2.9 Comparison between group and individual results of the first component estimates. . . . 45
2.10 First Component cluster location for different modulation frequencies in left ear stimulation. . . . 57
2.11 First Component cluster location for different modulation frequencies in right ear stimulation. . . . 58

2.12 Brain coordinates of the first DSS component. Dipole locations were obtained together with the standard deviation estimates for left ear stimulation. 59
2.13 Brain coordinates of the first DSS component. Dipole locations were obtained together with the standard deviation estimates for right ear stimulation. 59
2.14 Cluster locations of ICA components with the highest SNR obtained from ICA mixing matrix at an individual level for left ear stimulation 65
2.15 Cluster locations of ICA components with the highest SNR obtained from ICA mixing matrix at an individual level for right ear stimulation 66

3.1 Stimulus parameters. 73
3.2 Neuromag coordinate system. 76
3.3 Brain coordinates of the first DSS component. Dipole locations were obtained together with the standard deviation estimates for left ear stimulation. 82
3.4 Brain coordinates of the first DSS component. Dipole locations were obtained together with the standard deviation estimates for right ear stimulation. 82
3.5 Comparison of the obtained SNR of the first component at the stimulation frequency. . 84
3.6 Comparison of the obtained SNR of the second component at the stimulation frequency. 84
3.7 Violin plots showing the SNR distribution, mean and variance for the individual subject analysis for both groups at 4 and 10 Hz 85
3.8 Violin plots showing the SNR distribution, mean and variance for the individual subject analysis for both groups at 20 and 40 Hz 85
3.9 Phase Coherence of the first and second component at the stimulation frequencies. . . . 87
3.10 Phase Coherence comparison of left and right ear stimulation effect in the phase coherence of the first and second component. 87
3.11 Laterality Index measures for the first component at 4 Hz and 20 Hz modulation frequencies. 88

4.1 Neuromag coordinate system. 105
4.2 Dipole locations of the first DSS component for the typical readers along different ages. 110
4.3 Dipole locations of the first DSS component for the readers with dyslexia along different ages. 111
4.4 Group comparison of the SNR for the first DSS component at 4 Hz. 112
4.5 Group comparison of the SNR for the first DSS component at 20 Hz. 112
4.6 Comparison of the phase coherence for the two first DSS components at 4 Hz for both groups. 113

4.7 Comparison of the phase coherence for the two first DSS components at 20 Hz. 114
4.8 Comparison of the laterality index of the first DSS component at 4 Hz. 114
4.9 Comparison of the laterality index of the first DSS component at 20 Hz. 115

List of Tables

2.1 Number of subjects whose first DSS component is showing the highest SNR at the modulation frequency. . . . 42
2.2 Number of subjects whose first ICA component carrying ASSR is showing the highest SNR at the modulation frequency. . . . 43
2.3 SNR differences between the means of group and individual data measured at the stimulation frequency. . . . 45
2.4 Table with source information for group analysis. . . . 51
2.5 Table with cluster information for individual analysis. . . . 53
2.6 DSS component number with the highest SNR at the stimulation frequency for the individual analysis. . . . 62

3.1 First and second DSS component signal-to-noise ratios and p values of a two-sample t test comparing the means of the two DSS components. . . . 83
3.2 Comparison of signal-to-noise ratios distribution obtained after an individual analysis of both groups. . . . 86

CHAPTER 1

General introduction

1.1 Auditory processing and auditory pathways

Sound is a mechanical waveform that can be produced by different generators. Humans can detect the frequencies that are comprised within the range of 20 $Hz - 20$ kHz. In air, sound propagates as a longitudinal wave. It is perceived and transformed into electrical impulses by the human hearing in the peripheral auditory system, that consists of the outer ear, middle ear and inner ear.

1.1.1 Amplitude Modulated processing

The human auditory system can perceive and process sounds very fast in comparison to other sensory systems. Natural selection has provided us with a system that can analyse rapid changes in acoustic pressure at the two ears very efficiently (Joris et al., 2004). The auditory system in humans has specialised in processing the temporal dimension of sounds. As it will be explained in following sections, the temporal information of sound is what describes the changes of the signal amplitude. This sensitivity of the human auditory system towards changes in the Amplitude Modulations (AM) of a signal has been described in very early studies (Von Helmholtz, 1863).

More recent studies (Zwicker, 1952) demonstrated that the threshold for detecting AM was very small at low modulation frequencies and increased to a maximum with increases in the modulation frequency. Once the maximum is reached, detection threshold decreases and drops below the values obtained at low modulation frequencies. However, in this modulation range, subjects were able to perceive the signal carrier and the modulation frequency as distinct tones. In the study of Zwicker (1952) it was also determined that, for a given carrier, detection thresholds of AM and frequency modulations (FM) measured in terms of their modulation depths coincide on the upper side of the maximum of the detection threshold at a modulation frequency later named as the critical modulation frequency. Above this critical modulation frequency the carrier and sideband components are analysed in different place of the auditory pathways. This early hypothesis would explain why subjects are not sensitive to differences in the relative phase of the modulation components that enable them to distinguish AM from FM below the critical modulation frequencies (Schorer, 1986; Sek & Moore, 1994; Moore, 2012). Nevertheless, it appears that when the auditory system processes AM imposed on pure tone carriers, the signal detection may rely on spectral cues rather than temporal ones over some modulation frequency ranges.

One way of rejecting spectral cues would be to measure the detection of sinusoidal modulation imposed on noise rather than a tonal carrier. This will allow us to estimate the temporal resolving power of the auditory system and will explain our choice for the stimulation we will use in this project. It will be introduced below in section 1.5.

1.1.2 Auditory pathways

Sound waves enter the peripheral auditory system after hitting the pinna where they are reflected and attenuated. Sonic vibrations enter the auditory canal and interact with the tympanic membrane already in the middle ear. The vibrations created in the eardrum are transmitted to a set of ossicles i.e., malleus, incus and stapes. These small bones convert the lower-pressure waves into higher-pressure at the oval window and inner ear. These vibrations are then transferred through the intracochlear fluid to the basilar membrane. High-frequency fluid vibrations produce the maximum membranal displacement near the basis of the basilar membrane while low-frequency oscillations cause maximum membranal displacement at the

end of the membrane. These displacements in the basilar membrane cause the hair cells to displace as well. This effect is what converts sound waves into electrical impulses. Electrical impulses are processed by the central auditory system, which is responsible for the processing and interpretation of the auditory information. It can be divided into the primary auditory pathway and the non-primary pathway, Figure 1.1.

Fibres of the primary auditory pathway follow a pathway that starts in the cochlear nuclei. Fibres then link with the superior olivary complex, which is connected to the lateral lemniscus. Fibres ascend towards the midbrain inferior colliculus and finally reach the medial geniculate body in the thalamus, which is connected with left and right auditory cortices (Gelfand, 2018). The non-primary auditory pathway works in parallel with the primary one. It starts from the cochlear nucleus and ascends through the reticular formation to the thalamus and then to the polysensory cortices. The main difference between the two is that primary auditory cortex is purely driven by auditory stimulation while the non-primary is a multi-sensory pathway (Møller et al., 2005).

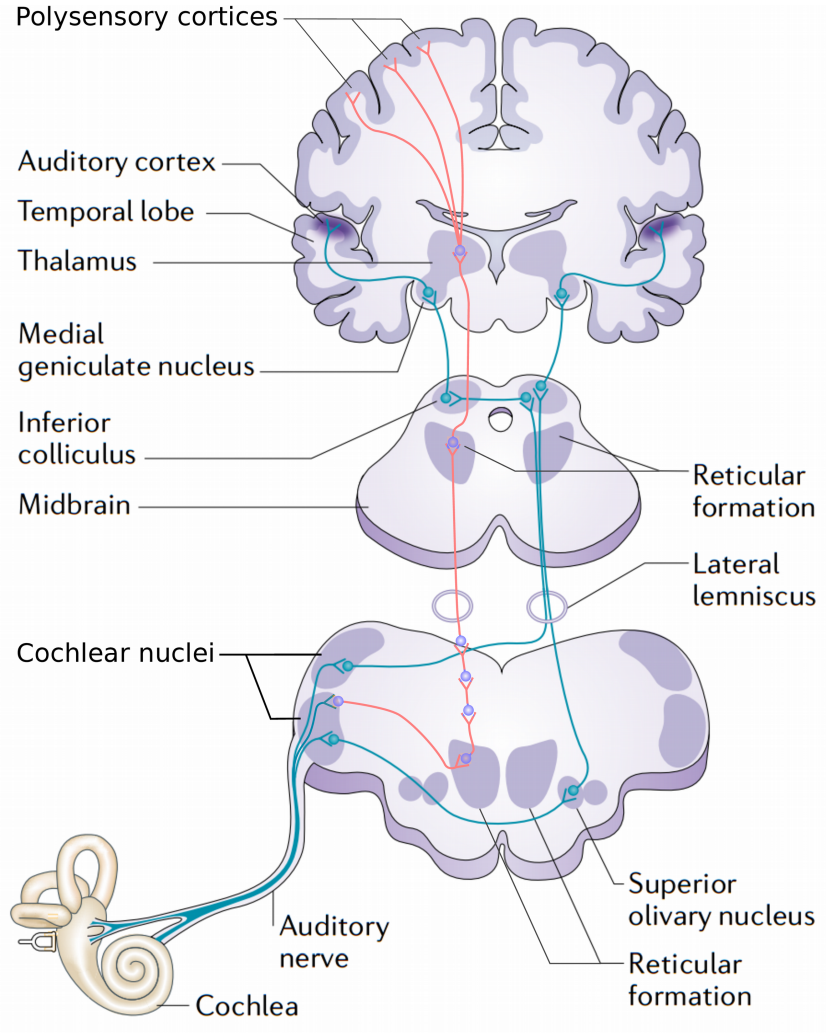


Figure 1.1: The central auditory system. The primary auditory pathway (blue) starts in the cochlear nuclei and ascends towards both auditory cortices. The non-primary auditory pathway (orange) starting also from the cochlear nuclei, however it connects with several multisensory cortices which are not fully known (Møller et al., 2005). Figure adapted from (Javitt & Sweet, 2015).

1.2 Neural speech processing

Speech is one of the most relevant signals that the human auditory system has to process, and it is key to develop communication skills. Speech perception is learned at a very young age, and it is usually executed with great ease, even by very young children. Acoustically, speech is a signal that varies in amplitude and frequency, and it can be analysed according to three features. These features are based on their acoustic, auditory, perceptual and linguistic correlates. Three main features of speech can be distinguished in the temporal domain: the envelope, the periodicity and the temporal fine structure (Rosen, 1992). The envelope of the speech signal is defined by slow fluctuations of the sound pressure waveform ($< 50Hz$) and describes the changes in the amplitude of the signal. It is typically defined as the 'temporal information' and can be described by acoustic features as intensity, duration, rise time, fall time and modulation frequency. The periodicity of the speech signal corresponds to the fundamental frequency of the waveform ($50 - 500Hz$) and results from the opening and closing of the vocal folds during voiced speech. It carries two main types of information: segmental information about voicing and manner, and prosodic information about intonation and stress. Finally, the fine structure of the speech signal is characterised by rapid changes of the waveform ($> 500Hz$) and determines the varying spectral content of the signal. Of these characteristics the sound envelope is considered as the fundamental aspect for speech perception, since the reduction of its temporal information greatly affects speech perception (Shannon et al., 1995). The most essential modulation frequencies in the envelope are between 0.4 and 20 Hz, with the most prominent at 2 to 5 Hz (Edwards & Chang, 2013; Füllgrabe et al., 2009). The latter frequency band is crucial in the identification and segmentation of phonological units in speech such as syllables ($3-10Hz$, generally around $4Hz$) and phonemes ($12 - 20Hz$).

Cortical regions in the brain are strongly linked to speech processing. Large groups of neurons firing simultaneously create the cortical responses that contain detailed information of the spectral and temporal properties of speech (Boemio et al., 2005; Luo & Poeppel, 2007; Giraud et al., 2000). This synchronised firing of neurons under auditory stimulation, known as neural entrainment, is presumed to be involved in the encoding of temporal information. This process of neural entrainment to the temporal modulations of speech is believed to make

temporal coding possible (Giraud & Poeppel, 2012). Neural temporal coding is key for speech processing, and it is key for the development of phonological representations. A phonological representation is the mental representation of the sounds and combinations of sounds that comprise words in a particular spoken language (Goswami, 2012). Neural oscillations can be classified in five different frequency ranges (Buzsaki, 2006) that can be associated to the speech envelope modulation ranges (Ghitza, 2011). The neural oscillation ranges are delta $(0.5 - 4Hz)$, theta $(4 - 8Hz)$, alpha $(8 - 12Hz)$, beta $(12 - 30Hz)$ and gamma $(30 - 80Hz)$. Beta and gamma are associated with phoneme perception, and syllables and words are linked to the theta frequency range. Series of words and sentences are associated with the slowest neural oscillation range, i.e., delta rhythm.

Along the years many different theories of speech perception have seen the light (Fant, 1970; Liberman et al., 1967; Stevens, 1960; Fowler, 1986; McClelland & Elman, 1986; Luce & Luce, 1986; Marslen-Wilson & Tyler, 1980). They suggest that there is a functional hemispherical preference towards the processing of different frequency ranges of the modulation rates. Thus, speech-related modulation frequencies are processed asymmetrically in the auditory cortices. There would be a right hemispheric preference to process syllabic rate modulations (Boemio et al., 2005; Poeppel, 2003), whereas both hemispheres would activate during the processing of phoneme rate modulations (Jamison et al., 2006; Obleser et al., 2008).

The explanation for differences in hemispherical preferences during syllable-rate stimulation and phoneme-rate stimulation is theoretically described in Poeppel (2003): It is proposed that the auditory processing of speech happens based on the intrinsic component rates of the speech signal. Specifically, the information at different temporal rates would be encoded by the stimulus-induced phase-locking of these intrinsic cortical rhythms contained in these rates. That would explain why slow rates: theta range $(0.5 - 4\ Hz)$ and delta range $(4 - 8\ Hz)$ would be dominantly processed in the right hemisphere; and why rapid rates: beta range $(13 - 30\ Hz)$ and gamma range $(30 - 80\ Hz)$ would be dominantly processed either in the left hemisphere or bilaterally.

More recent experimental studies support the theoretical hypothesis presented in Poeppel (2003). Their findings point out that theta rate modulations tend to show right processing asymmetry in adults (Poelmans et al., 2012a,b), children (Abrams et al., 2008; Vanvooren et al., 2014) and even in newborns (Telkemeyer et al., 2009, 2011).

In phonemic rates within the beta range, most of the studies support that there is a hemispheric lateralisation preference. However, in contrast to the left or bilateral preference proposed in Poeppel (2003), experimental evidence suggests that hemispherical preference during beta rate stimulations is typically ipsilateral and is more commonly found in adults (Jamison et al., 2006; Obleser et al., 2008) than in children (Vanvooren et al., 2015).

1.3 Developmental dyslexia

Developmental dyslexia is a neurobiological and hereditary disorder characterised by difficulties with accurate and fluent word reading and by poor spelling and decoding abilities (Eden et al., 2016). This often causes issues while learning to read in the context of normal intelligence and sufficient educational opportunity (Stoodley, 2016). In the last decades, dyslexia has been widely investigated (Vellutino et al., 2004). The processing of a wide range of auditory features related with developmental dyslexia has provided evidence in favour of auditory processing deficit theories (Goswami, 2011; Ramus, 2001). These theories hypothesise that atypical perception and processing of speech might be the underlying cause for the use and representation of phonological information. Different studies have proven that individuals with dyslexia present deficits or atypical responses in the phonological components of language that causes problems to represent and manipulate the phonological structure of words at the syllable and/or phoneme level (Ziegler & Goswami, 2005; Vandermosten et al., 2020; Vellutino et al., 2004). When this happens, children have difficulties to associate the phonemic sounds with the letters, leading to expected reading and writing problems. This theory of the origin of dyslexia is known as the phonological deficit theory. However, according to the multiple deficit theory: phonemic awareness deficits may be necessary but definitely not sufficient to produce dyslexia (Pennington et al., 2012). This statement is based on two main factors. The first one is that in dyslexia phonemic awareness is only the "tip of the phonological iceberg" and that "deeper" spoken-language phonological impairments among people with dyslexia appear well before the onset of reading and even at birth (Guttorm et al., 2005; Share, 2021). The second main reason is genetic, different studies performed at genetic level came to the conclusion that the aetiology of dyslexia, as of other developmental disorders, is genetically complex (Pennington, 2006). These two reasons would support that

multiple actors, e.g., visual attention, orthographic processing, executive functioning... could be potential aetiological factors that would lead to the development of dyslexia.

In summary, the multiple deficit theory states that there is no single aetiological or cognitive factor that is sufficient to dyslexia or another developmental disorder. Instead, multiple cognitive deficits caused by multiple aetiological factors need to be present to produce a disorder at the behavioural level (McGrath et al., 2020). In addition, these factors can have different impact or weight in the development of disorders at the individual level (Pennington, 2006). Thus, if multiple factors are responsible for the development of dyslexia, and they can affect differently each individual, a study that focuses in the common features that differentiate a typically developing group with a group with dyslexia will have a significant impact. Since some of the aetiological and cognitive risk factors are shared with other disorders, we will focus on the phonological processing aspects at a group level. In this project, we will develop a methodology that can minimise the individual differences and focus on the shared phonological processing features of the group with dyslexia and how they compare with the common features of a group of typically developing individuals.

Through the methodology that will be presented in following chapters, we will investigate the levels of auditory processing with amplitude modulated signals. We will evaluate these levels of auditory processing through a series of outcome measures (Section 1.6) in adolescents and children with and without dyslexia. We are expecting to find differences in the syllabic rate due to its importance for auditory and speech perception. Since it has been already proposed that disturbances and main differences in auditory processing in dyslexia are more likely to happen in the theta band (Goswami, 2011). However, the hypothesis presented in Goswami (2011) conflicts with what experimental studies have found. These studies claim that there is a deficit in the auditory processing of the group with dyslexia (Marosi et al., 1995; Arns et al., 2007; Lizarazu et al., 2015; De Vos et al., 2017b). While Goswami (2011) claims that the group presenting the deficit will be the typically developing. Moreover, despite the importance of syllabic rates for auditory perception and speech, other studies have never been able to show differences between the two groups (Hämäläinen et al., 2012; Poelmans et al., 2012a; Vanvooren et al., 2014). If we cannot find differences in this modulation range we can hypothesise that the encoding of frequency ranges other than the theta range may be more important for accurate syllabic processing, e.g., the alpha range Boets et al. (2007);

Ziegler et al. (2009); Dole et al. (2012); Poelmans et al. (2011); De Vos et al. (2017b).

We will also evaluate auditory processing in the phonemic rate. Based on the studies by Hämäläinen et al. (2012); Lehongre et al. (2011); Vanvooren et al. (2012) De Vos et al. (2017b) has proposed that beta range synchronisation differences might still emerge in later stages of reading development. We will expect then no differences in the children group, and maybe we could find differences in the auditory processing levels in adolescents with and without dyslexia.

In summary, we will evaluate auditory processing levels at syllable and phoneme rates in children and adolescents with and without dyslexia. We hypothesise we will gain interesting insight about how auditory processing levels evolve during development and the impact of formal reading instruction on them.

1.4 Brain analysis techniques

In the analysis of the brain structural and functional characteristics are relevant. They can be modelled with a wide range of techniques. Some of them can measure anatomical brain structures such as volumes, tracts and myelination levels. Within this group we can find X-ray computed tomography (CT), magnetic resonance imaging (MRI) and diffusion tensor imaging (DTI). To measure the brain functional activity imaging tools two approaches can be taken. The first one is to measure the haemodynamic activity, either directly by positron emission tomography (PET) or single photon emission tomography (SPECT); or indirectly by functional magnetic resonance imaging (fMRI). As a second option, functional brain activity can be studied through techniques that measure the electrophysiological activity that occurs inside the brain. This can be done by directly measuring the electrical potentials that reach the scalp, as electroencephalography (EEG) does. It can be done also by measuring the induced magnetic activity that any varying electrical potential induces, this is what magnetoencephalography (MEG) does.

For the PhD project, we selected a functional imaging technique with a high sensitivity to measure temporal changes. EEG as well as MEG measurements have a very high temporal resolution. MEG and EEG are sensitive to tangential dipole sources. Contrary to MEG measurements, EEG is also sensitive to radial oriented sources and to deeper sources such as

the brainstem. Nevertheless, since brain electrical responses are measured with electrodes or sensors placed on the scalp, spatial resolution is low. The spatial resolution would not only become lower the deeper the brain sources are. It is also affected by the oscillatory frequency, high frequencies are more attenuated than low frequencies. In summary, we selected EEG due to its high spatial resolution and its sensitivity towards tangential, radial and deep sources. Another important factor is that the experimental setup is relatively inexpensive and easy to use. Something of uttermost importance when young children are the main source of data. Thus, in order to measure the auditory brain responses in children and adolescents with dyslexia for this project, we used a combination of EEG with the stimulation of auditory steady-state responses (ASSRs).

1.5 Auditory Steady-State Responses

ASSRs are a periodic electrophysiological response of the brain that appear during stimulation under a periodically varying continuous signal (Rance, 2008; Picton et al., 2001). These responses oscillate with the same periodicity as the acoustic signal. The strength of these oscillations is an indicator of how the oscillatory activity synchronises to the acoustical modulation. As ASSRs show how well the brain follows the envelope of acoustic stimulation, they are an effective measure for the investigation of the temporal speech features along the central auditory system. ASSRs provide with an objective measure that is not subject-dependent and strongly correlated with speech perception (Dimitrijevic et al., 2004; Alaerts et al., 2009). ASSRs response amplitude decrease with the increment of the modulation frequency, with the exception of 40 Hz and 90 Hz, where strong responses can be observed (Picton et al., 2003; Picton, 2011; Purcell et al., 2004). Furthermore, different source analysis studies have shown that ASSRs neural generators change depending on modulation frequency (Farahani et al., 2017, 2021; Giraud et al., 2000; Herdman et al., 2002). For example, modulation frequencies in the range of $80 - 100\ Hz$) trigger the neural generators at the brainstem level. Conversely, cortical generators are commonly triggered during stimulation having a modulation frequency below 25 Hz. For the modulation frequency of 40 Hz, Herdman et al. (2002) and Farahani et al. (2017) suggested that the main neural generators of ASSRs may have overlapping cortical and subcortical activation patterns in the brainstem, thalamus, and au-

ditory cortices. However, there is still room for debate about the precise location of the ASSR neural generators as a function of the modulation frequency.

In summary, ASSRs are widely used as a neural marker in different fields to evaluate the neural response under speech-like stimulation. More specifically, ASSRs have been used in dyslexia research to evaluate auditory temporal processing (Van Hirtum et al., 2019a; De Vos et al., 2020; Vanvooren et al., 2014). These studies modulated ASSRs to match important speech-related components.

ASSRs can be easily identified in the frequency domain since their frequency components remain constant in amplitude and phase over a long period of time, Figure 1.2.

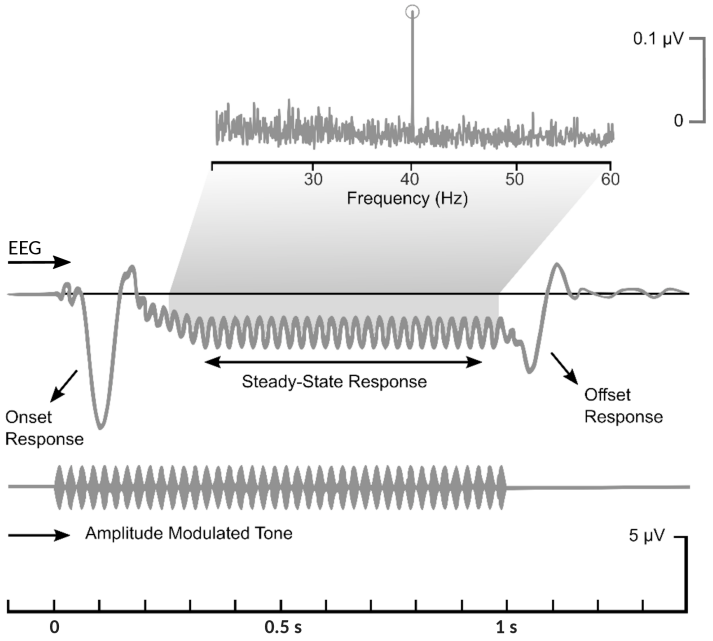


Figure 1.2: Auditory brain response to an acoustic periodical stimulation, an AM modulated tone of 40 Hz. After the onset, the auditory response becomes stable in phase and amplitude and can be identified in the frequency domain depicted above the shaded area (Picton, 2011).

1.6 Neural source analysis and brain source modelling

Multi-channel EEG recordings can provide useful information about the large-scale networks that are activated in the brain. However, we need to understand that the electrical signals we record at the scalp are generated deep in the brain tissues. Thus, what we can see at the electrode level is a superposition of brain activity that was generated in different locations,

Figure 1.3. This is what is known as the volume conduction problem.

Detected signals at the electrodes not only are a superposition of brain activity generated right below them, but the summation of activity generated in large portions of the brain. This means that due to the elemental laws of conductance, electrical potentials generated within all cortical regions will be projected and linearly added up at every electrode placed in the scalp. Thus, any EEG data picked up by scalp electrodes would be a weighted linear superposition of all the underlying cortical activity (Onton et al., 2006). Of course, these weights are dependent on many factors, such as distance to the electrode, orientation relative to the electrode, electrical conductance of the halfway tissues...

Considering the volume conduction problem, a source analysis might seem a troublesome task to perform. However, there are some advantages to consider above the electrode level analyses. A source level approach provides with straightforward neurophysiological interpretation of the results. It also diminishes the effect of reference selection, and it usually simplifies the comparison across studies as well as the pre-processing steps: With a source analysis technique normally no regions of interest need to be defined, the separation between noise and signal can be done automatically, and it will not need a manual selection of good trials or averages that can affect the level of detail of the data. Those are the main reasons why in this PhD project we decided to use a source level approach.

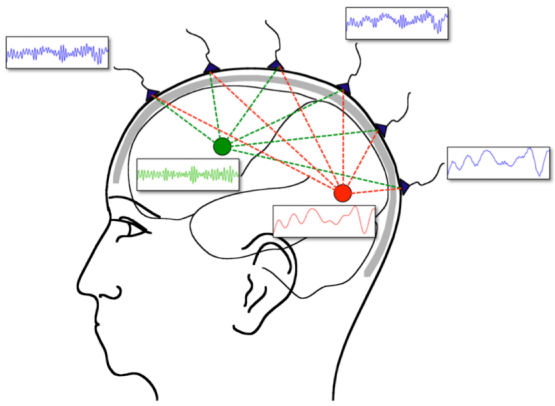


Figure 1.3: Diagram representing the electrophysiological superposition measured with EEG scalp electrodes. Figure obtained with permissions from FieldTrip workshop slides.

The modelling steps required to reconstruct the electrical information of the brain sources as well as their location is known as inverse modelling, Figure 1.4. Brain activity can be

represented with electrical currents (de Munck et al., 1988). Moreover, in far-field measurements such as EEG or MEG, the electrical activity generated by neurons can be modelled as equivalent current dipoles (ECDs) (He et al., 2018).

ECDs represent the neural activity generated by large-scale population of neurons in EEG and MEG and their features are location, strength and orientation. These features can be obtained by solving the inverse problem.

However, to solve the inverse problem we need to know how the electrical currents traverse from the brain source towards the electrodes where we are measuring. The modelling of how the potentials are created at the scalp by a specific ECD with a specific location, strength and orientation is known as the forward model.

The forward model can be calculated by resolving the Poisson's equation. Poisson's equations can be solved for: (1) static systems, where potentials and their geometrical distribution do not change with time; and for (2) dynamic systems, where potentials and their distributions change with time. Generally, the static conditions provide with analytical solutions that are much easier to implement. In our case, we would consider EEG experiments to present quasi-static conditions (Hallez et al., 2007). They are not fully static because brain activity changes with time. However, these changes are slow compared to the propagation effects and we can consider that all currents and fields behave as if they were stationary at each instance. Because at one moment in time, all the fields are triggered by the active electric source, thus, no time delay effects are introduced (Hallez et al., 2007).

The way electrical signals flow towards the scalp depends on the geometry of the head and their tissues, the conductivity of these tissues and the location of the EEG electrodes. A volume conduction model of the head describes all of these properties. This head model can be defined in different ways. The most simple approach considers the head to be spherical, and its tissues are modelled as concentric spheres with homogeneous conductivity values for each of them. For this kind of modelling, analytical solutions can be obtained. However, for more realistic head models analytical solutions cannot be obtained, and numerical approaches are required. For these more realistic head models, the geometry is defined based on 3D medical images, usually MRIs, and the most common numerical techniques to model them are the Boundary Element Method (BEM) and the Finite Element Method (FEM) (He et al., 2018). Despite needing numerical calculations instead of analytical solutions, the use of realistic head

models provides with higher localisation accuracy compared to spherical models (Akalin Acar & Makeig, 2013).

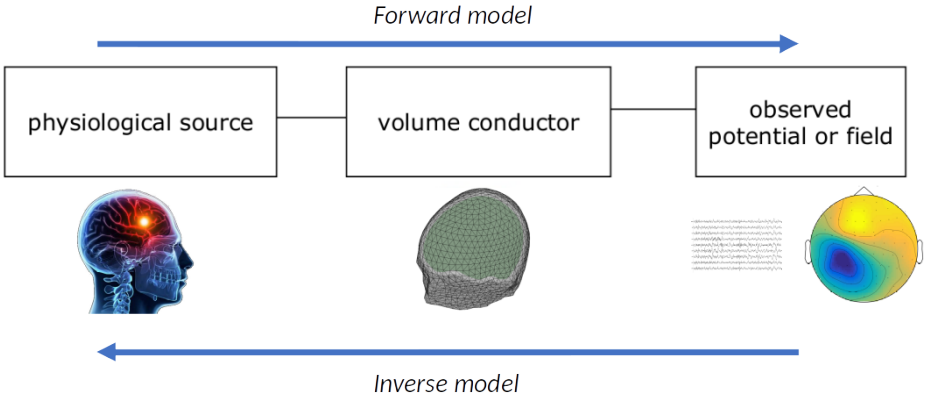


Figure 1.4: This chart represents the required steps to develop a forward and inverse models for brain source localisation.

The most realistic approach to create a head model is the FEM. This approach tessellates a 3D volume in small tetrahedra or hexahedra with a high level of detail. Each tetrahedron or hexahedron can model a different tissue, and therefore it will have its own conductivity value. FEM is the most accurate and realistic numerical method, but it is computationally quite expensive. In this project we chose BEM over FEM because of its lighter computational load and easier geometrical processing. BEM can be used independently of the source model, it is fast during its application to real data, and it can model important tissues such us scalp, skull, brain and cerebrospinal fluid. However, it requires each layer of tissue to be closed, isotropic and homogeneous, Figure 1.5 .

In the absence of subject-specific 3D scans, an averaged scan can be used as a template to create the head model. This average can be across different subjects, e.g., the ICBM152 which is the non-linear average of 152 individual magnetic resonance scans (Fonov et al., 2011); or across different measures of the same subject, e.g., the Colin27 where one individual was scanned 27 times and the images linearly registered to create an average with high SNR and structure definition (Holmes et al., 1998). Despite providing with a good quality scan suitable for BEM computation, these template images do not take into account inter-subject variability and may induce a localisation error when they are used for individual calculations (Akalin Acar & Makeig, 2013).

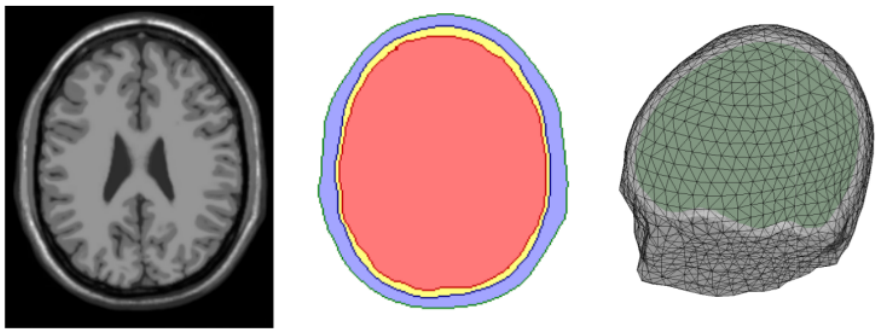


Figure 1.5: Construction of a BEM head model based on an MRI. **From left to right:** MRI source template is segmented into different tissue types. Each surface description is extracted and down sampled to a reasonable number of triangles. The final image represents the mesh and the layers that will conform the BEM head model.

EEG source modelling techniques can be classified as discrete source models or distributed source models. In discrete source modelling, the data recorded at the scalp is modelled using a limited amount of current dipoles. While in the distributed source modelling techniques a high number $(2,000 - 20,000)$ of current dipoles are employed.

In this thesis we focused on the development of our methodology following discrete source modelling techniques. We considered the lack of individual 3D scans a major factor to decide for the modelling technique. For some applications, distributed source modelling can provide with a better estimation of the brain source locations (Farahani et al., 2021). However, in distributed source modelling the head model plays a crucial role, because the forward model is computed based on it and therefore the source separation as well as the source localisation procedure is dependent on the head model used. While in discrete source modelling the separation of the EEG data into source components is done independently of the head model.

In discrete source modelling EEG data are modelled with a small number of equivalent current dipoles. This method aims to search for the location and orientation of each ECD in order to model the input data with minimum error (Grech et al., 2008). Discrete source modelling assumes that the number of brain sources is limited, and that they are focal. Nearby neural sources sharing similar activity and same orientation are modelled by a single equivalent dipole. The input data can be EEG recorded at the scalp or a subspace of EEG represented by components. In discrete source modelling of sensor-level EEG equivalent current dipoles are manually placed to model EEG data or part of it directly from the scalp recordings.

This methodology does not need a high computational load, and it is easy to interpret. Nevertheless, modelling EEG sensor data by a predetermined number of dipoles assuming their location and number is not reasonable in many scenarios. These disadvantages are one of the main reasons why discrete source modelling is often used after separating the EEG data into components.

In discrete source modelling of separated EEG data the scalp topography of EEG components (or subspace) is modelled with the current dipole. EEG components can be obtained using different source separation methods. These methods assume that the signals measured at the scalp with the EEG electrodes are a linear mixture of the activity generated by the different brain sources in the brain. This last methodology is what we used in this PhD. It combines Independent Component Analysis (ICA) and Denoising Source Separation (DSS). ICA has been used widely with the aims of detecting the primary and secondary source activation patterns (Farahani et al., 2017, 2019). We combined this technique with DSS in order to extract the primary source activation pattern and the associated electrophysiological waveforms that are shared across subjects that belong to a group under study. We decided to use DSS with ICA because we were interested in obtaining ASSR activity that would be maximally present along all the stimulation time. DSS, as it will be defined in the following section, could provide with such functionality.

There are methodologies that can condense activity of interest along one dimension or component. One of them is the Principal Component Analysis (PCA) (Kayser & Tenke, 2003). PCA or similar algorithms have been used in EEG analyses to estimate scalp topographies (Hamm et al., 2012), as well as a pre-processing step to clean data before using a methodology that could provide with dipolar patterns of the brain activity for a source localisation approach (Huang et al., 2020). These previous analyses suggested the possibility of using DSS before ICA. Furthermore, having DSS performed before ICA would produce sources and topological maps with dipolar patterns present in all of them. This would make the dipole fitting more reliable. However, our main issue was that PCA or PCA related-algorithms used as a pre-processing step aim to reduce the dimensionality of the data to make the basic ICA model hold and to avoid over-fitting or over-learning (Artoni et al., 2018). But, to avoid over-fitting, the number of mixtures or channel data must be equal or smaller than the independent components hidden in those mixtures. It is known that during stimulation there will always

be more active sources in the brain than in all the EEG channels used (Muñoz-Gutiérrez et al., 2018). Another possible issue to face if we used DSS before ICA would be to not have sufficient data for running ICA. ICA is a statistical method, and if the independence of the active distinct EEG processes is not adequately contained in the data, ICA cannot separate them. Finally, if DSS is applied before ICA we would lose the reproducibility criteria as an identifier for the most prominent activity along the recording.

Thus, we decided to select the approach of computing first ICA, and then DSS. Over-learning in ICA typically produces estimates of the Independent Components that have a single spike or bump and are practically zero everywhere else (Hyvärinen et al., 1999). As we will compute a statistical test to check how robust the signals are after computing ICA, we do not expect over-learning.

We will define these methods in depth, together with the rest of the methodology in the following paragraphs.

Independent Component Analysis

ICA is a blind source separation method that allows us to identify data components which are part of a mixture signal. In EEG ICA has been widely used to separate components or sources that are mixed due to volume conduction (Delorme & Makeig, 2004). ICA does not require a model of sources, and it is data driven, which means that it only uses the provided time series information. ICA searches for maximal independent components. Independence can be defined as the minimum mutual information or the maximal joint entropy of the data projections (Delorme & Makeig, 2004).

Mathematically ICA assumes that raw EEG data from j channels/electrodes (x_j) along t time points can be written as the sum of a number n of components (u) multiplied by a coefficient factor (w^{-1}) as shown in the Equation 1.1.

$$x_j = w_1^{-1}u_1 + w_2^{-1}u_2 + ... + w_n^{-1}u_n \tag{1.1}$$

This can be written in matrix notation as follows:

$$X_{j\times t} = W_{j\times j}^{-1}U_{j\times t} \quad \Rightarrow \quad X = W_{(ICA)}^{-1}U_{(ICA)} \tag{1.2}$$

And then by matrix algebra we obtain:

$$U_{(ICA)} = W_{(ICA)}X \tag{1.3}$$

Where U and X would have the same dimensions: channels $\times$ time ($j \times t$) and W would have $j \times j$ as dimensions.

ICA algorithm does not take any channel information and performs a blind separation of the EEG data matrix X to find the time series of ICA components U. W is the unmixing matrix and W^{-1} is the mixing matrix, where each column represents the relative projection weight at each electrode of a single component source (Onton et al., 2006). ICA was applied on our EEG data by means of using the Infomax method in FieldTrip (Oostenveld et al., 2011). The Infomax method fills the unmixing matrix with the coefficients that maximise the average Shannon mutual information between the components of the matrix U (Bell & Sejnowski, 1995). The brain source localisation and projection weights were assumed to be spatially stationary for the duration of the experiment (Onton et al., 2006).

Following the same logic, ICA can be applied in temporally concatenated EEG data. This is known as group-ICA (Delorme & Makeig, 2004; Huster et al., 2015). With this approach we aimed to extract the common activity shared by a group of subjects. This methodology assumes a similar geometrical distribution of the sources since the mixing matrices for all subjects must be identical (Huster et al., 2015). Moreover, performance may drop when source topographies vary much across subjects (Cong et al., 2013). In group-ICA with temporally concatenated data the maximum number of output components is equal to the number of input channels. The same is true in ICA with individual data.

Denoising source separation

In this project we focused our methodology in combining ICA with DSS. DSS performs a separation of the data into desirable components (signal) and undesirable components (noise) (Särelä & Valpola, 2005). The linear transformation DSS computes can be written in a similar way to ICA, Equation 1.4.

$$X = W^{-1}_{(DSS)}U_{(DSS)} \tag{1.4}$$

The denoising procedure starts with a spatial whitening of each channel from the input data. This is performed through Principal Component Analysis (PCA) (Kayser & Tenke, 2003) and normalisation. This process creates a dataset with spherical symmetry. These data are then submitted to a denoising function or bias function, followed by another PCA which specifies the orientations that maximise the bias function. This bias function was chosen to be the *proportion of epoch-averaged (evoked) activity* (de Cheveigne & Simon, 2008; de Cheveigné & Arzounian, 2015). Epochs are small segments of data, for this project we used an epoch length of 1.024 seconds.

The second PCA creates a transformation matrix which is applied to the result of the first PCA, the symmetrical data. The result of DSS analysis is a set of components sorted in terms of decreasing susceptibility to bias. In other words, first ranked components carry the most reproducible activity across trials.

By applying DSS to ICA components we had a very intuitive way of determining the amount of reproducible neural information present in each component. Mathematically this can be expressed by using the input of the Equation 1.3 in the Equation 1.4:

$$U_{(ICA)} = W^{-1}_{(DSS)} U_{(DSS)} \tag{1.5}$$

Combining the equations number 1.2 and number 1.5 we obtain:

$$X = \{W^{-1}_{(ICA)} W^{-1}_{(DSS)}\} U_{(DSS)} \tag{1.6}$$

These mathematical expressions are equivalent for group-ICA computations, because the mixing and unmixing matrices have the same dimensions. From the product of the mixing matrices ($W^{-1}_{(ICA)} W^{-1}_{(DSS)}$) the location of each component can be estimated by fitting current dipoles to its scalp topography. The columns of the mixing matrix contain the relative weights to project back the components to the scalp-level.

Laterality Index

To estimate the hemispherical preferences we can define a Laterality Index (LI). We assumed the neural origin for the DSS components could be estimated by a dipole fitting procedure.

This neural origin could be then modelled by one or two symmetrical dipoles. For components whose origin is modelled by two symmetrical dipoles, we define the LI based on the dipole magnitudes as it is shown in Equation 1.7. For components modelled by only one dipole, we calculate the LI based on the reconstructed responses and the noise level of the extracted component. If the dipole is in the right hemisphere ($x_{dip} > 0$) the noise floor is then used to estimate the neural response of the left hemisphere, see Equation 1.8. If the dipole happens to be in the left hemisphere ($x_{dip} < 0$) the noise floor is used to estimate the neural response of the right hemisphere, see Equation 1.9. Either with one or two dipoles an LI of +1 represents a response completely lateralised to the right hemisphere and an LI of -1 represents a response completely lateralised to the left hemisphere.

$$LI = \frac{mag_{right} - mag_{left}}{mag_{right} + mag_{left}} \tag{1.7}$$

$$if\ x_{dip} > 0\ then\ LI = \frac{\sqrt{P_{S+N}} - \sqrt{P_N}}{\sqrt{P_{S+N}} + \sqrt{P_N}} \tag{1.8}$$

$$if\ x_{dip} < 0\ then\ LI = \frac{\sqrt{P_N} - \sqrt{P_{S+N}}}{\sqrt{P_N} + \sqrt{P_{S+N}}} \tag{1.9}$$

Signal-to-noise ratio

The measured relative response amplitudes, obtained from the square root of the signal power at the frequency of stimulation, and the Signal to Noise Ratios (SNRs) can be calculated from the DSS components. The response amplitudes can be obtained by taking the square root of the signal power. The signal power, P_S, can be then calculated from the Hotelling t-squared statistic, it represents the squared amplitude of the responses mean across all the data trials at the bin of the modulation frequency.

The noise floor amplitude, P_N, required to compute the SNR, may also be estimated from the Hotelling t-squared statistic and would show the standard error of the amplitude responses at the modulation frequency mf across n epochs, being: $\sigma(R_{mf})/\sqrt{n}$. Based on the definition of power response and noise amplitude, the SNR may be defined as the ratio between the power of the response signal and the power of the EEG noise, Equation 1.10.

$$SNR = \frac{P_S}{P_N} = \frac{\|mean(R_{mf})\|^2}{\left(\frac{\sigma(R_{mf})}{\sqrt{n}}\right)^2} \tag{1.10}$$

Where R_{mf} is a complex vector containing the responses at the modulation frequency of all epochs, σ is the standard deviation and n is the number of epochs.

Phase Coherence

Phase coherence represents the inter-trial variability of the phase difference between two signals for a specific frequency and it can be interpreted as a measure for connectivity (Picton et al., 2001).

It can show the synchrony that can be found between two signals through the estimation of how stable the difference between the phase of two signals is. The higher the value for Phase Coherence the higher the synchronisation between the two signals.

The phase of each epoch can be obtained from the complex representation of the neural response in the frequency domain. Phase coherence can be calculated according to Equation 1.11, (Picton et al., 2001).

$$PhCoh = \frac{1}{n}\sqrt{\left(\sum_{i=1}^{n} cos\ \theta_i\right)^2 + \left(\sum_{i=1}^{n} sin\ \theta_i\right)^2} \tag{1.11}$$

Where $\theta(f, i)$ represents the phase difference between two signals, in this case the selected signals would be the first and the second computed DSS component, this can be expressed as: $\phi_1(f, i) - \phi_2(f, i)$. Usually the difference is averaged across n epochs.

1.7 Objectives of the project and thesis outline

In this PhD project we want to combine the methodology of brain source analysis through EEG source modelling together with ASSRs in order to study auditory processing in adolescents and children with developmental dyslexia. More specifically, we aim to investigate how the different levels of auditory neural entrainment between normal readers and readers with dyslexia evolve during childhood and how they are in the adolescence.

To achieve these goals, we developed three studies, each of them represented in one chapter.

Chapter 2 presents the work involved in developing an appropriate methodology for source reconstruction suitable for group comparisons in dyslexia. Chapter 3 explains how we applied the methodology of the first study to analyse the differences in brain activation patterns during auditory temporal processing in adolescents with and without dyslexia. Finally, in chapter 4, we explain our study investigating how differences in the brain activation patterns found in adolescents evolve with age at three important reading stages: at the age of 5, before formal reading instruction; at the age of 7, during formal reading instruction and at the age of 9, after formal reading instruction.

The first step of the project is detailed in chapter 2, and it focuses on the need to reconstruct the activity of the brain source generators involved in auditory temporal processing from EEG data. We aim to obtain the brain source activation pattern and the associated electrical activity through source reconstruction techniques in evoked ASSRs. ASSRs sources despite being a periodical response sustained in time present high correlation and low Signal-to-noise Ratio (SNR). Their periodicity facilitates their detection in the frequency domain in electrode-level analyses. However, their intrinsic low SNR and high correlation are a challenge for source reconstruction techniques, since most of them assume low or no correlation between the signal generators. An average across trials can enhance the effect of noise and enhance the SNR of ASSR, but this would cause the number of epochs to be significantly decreased, and shorter recordings reduce the accuracy of source localisation approaches (Delorme & Makeig, 2004). Techniques that use variance of the signals will not be suitable for our analyses, because the search for the contribution of each generator to the total variance is strongly related to the power contribution to the total signal power. Thus, we want to use an appropriate source reconstruction technique that does not reduce the number of epochs and that is insensitive to baseline shifts as induced by spectral or spatial filtering while preserving anatomical information (De Cheveigné & Parra, 2014). Hence, in chapter 2 we develop and test a methodology by combining ICA and DSS with very low prior assumptions for the characterisation of the most prominent auditory evoked potentials during speech-related modulation frequencies.

In chapter 3, our goal is to study from a source level perspective the differences between readers with and without dyslexia during auditory temporal processing. Part of the data we analyse it has been studied from an electrode-level methodology. However, we want to analyse whether the group differences found in previous electrode level studies were caused

by a different source activation pattern or conversely it was an effect that could be found on the active brain sources. With our methodology developed in chapter 2, we hypothesise that a source reconstruction analysis may provide essential supplementary information because identical events observed at the electrode level may have different causes that could be revealed by a source analysis. Thus, we investigate a dyslexia research question based on an extended brain source analysis of EEG recordings. Through our methodology, a group of adolescents with dyslexia is compared with typically developing adolescents under the stimulation at frequencies modulated to match important aspects of speech perception. We use various measures to evaluate the neural synchronisation and hemispherical preference to the temporal modulation of the stimulation.

In chapter 4, we aim to measure the neural entrainment for auditory stimulation in three different moments of childhood, at the ages of 5, 7 and 9 years old. These age moments also represent important stages for formal reading instruction. In this longitudinal study, we evaluate the brain activation patterns and the hemispherical asymmetries before, during and after formal reading instruction. Our scope is to find what differences are the most critical during reading skills acquisition and how these differences evolved along the years when we recorded the data.

We aim to quantify synchronised neural auditory processing activity based on ASSRs using the methodology tested in chapter 2. The stimulation is again modulated at syllabic and phonemic fluctuation rates present in speech. Our goal is to investigate if we can extract meaningful common oscillatory patterns. The measures we aim to use include (1) estimations of source localisation, (2) hemispherical preferences using a laterality index and measures of neural entrainment, (3) signal-to-noise ratios (SNR) and (4) connectivity using phase coherence measures.

CHAPTER 2

The identification of predominant Auditory Steady-State Response brain sources in Electroencephalography using Denoising Source Separation.

The contents of this chapter have been adapted from the work published in Granados Barbero, et al. (2021): "The identification of predominant auditory steady-state response brain sources in electroencephalography using denoising source separation." European Journal of Neuroscience, 53(11), 3688–3709.

Abstract

Different approaches have been used to extract auditory steady-state responses (ASSRs) from electroencephalography (EEG) recordings, including region-related electrode configurations (electrode level) and the manual placement of equivalent current dipoles (source level). Inherent limitations of these approaches are the assumption of the anatomical origin and the omission of activity generated by secondary sources. Data-driven methods such as independent component analysis (ICA) seem to avoid these limitations but only to face new others such as the presence of ASSRs with similar properties in different components and the manual selection protocol to select and classify the most relevant components carrying ASSRs. We propose the novel approach of applying a spatial filter to these components in order to

extract the most relevant information. We aimed to develop a method based on the reproducibility across trials that performs reliably in low-signal-to-noise ratio (SNR) scenarios using denoising source separation (DSS). DSS combined with ICA successfully reduced the number of components and extracted the most relevant ASSR at 4, 10 and 20 Hz stimulation in group and individual level studies of EEG adolescent data. The anatomical brain location for these low stimulation frequencies showed results in cortical areas with relatively small dispersion. However, for 40 and 80 Hz, results with regard to the number of components and the anatomical origin were less clear. At all stimulation frequencies the outcome measures were consistent with literature, and the partial rejection of inter-subject variability led to more accurate results and higher SNRs. These findings are promising for future applications in group comparison involving pathologies.

2.1 Introduction

Auditory Steady-State Responses (ASSRs) are phase-locked electro-physiological responses from the brain, evoked by a periodically varying continuous auditory signal, typically a sinusoidally modulated sound (Rance, 2008). The responses are a waveform with the same periodicity as the auditory signal we use as stimulation. The responses can be easily detected in the frequency domain at the modulation frequency (Picton et al., 2001) and can be measured in electroencephalography (EEG) and magnetoencephalography (MEG) recordings. By adjusting the stimulation parameters to match important speech-related components, ASSRs allow an objective investigation of auditory temporal processing in the brain and brainstem (Lins & Picton, 1995). Studies using ASSRs have provided novel insights on the impact of hearing impairment (Luts & Wouters, 2004), the ageing auditory system (Goossens et al., 2019), auditory electrical stimulation in cochlear implant users (Hofmann & Wouters, 2012) and the underlying causes of learning disorders such as developmental dyslexia (Van Hirtum et al., 2019a; Vanvooren et al., 2015; De Vos et al., 2020). Furthermore, ASSRs have become of interest in other clinical areas, like the psychopathological domain. ASSRs are used as biomarkers in different mental disorders as Alzheimer's disease (van Deursen et al., 2011) and schizophrenia (O'Donnell et al., 2013). However, the mathematical tools used for ASSRs extraction aiming to ascertain the common characteristics of a group of subjects may be

improved. ASSR require a high signal-to-noise ratio (SNR) in order to perform reliably and some time-consuming underlying manual selection processes might be automatised.

The previously mentioned studies aim to extract brain-generated activity, that is, ASSRs, from electromagnetic signals recorded at the surface level using an array of electrodes or sensors. Each of these electrodes records independently the electric or magnetic amplitudes as a function of time (time series). Each recording experiment will end with a number of time series equal to the number of sensors or electrodes utilised. Depending on the type of analysis, different ways of extracting ASSR have been used. In analyses investigating the presence of ASSR at the electrode level with low density EEG configuration, a selection of averages of electrode pairs situated on top of the regions of interest is used (Poelmans et al., 2012b). In high-density EEG configurations, the responses are typically averaged over two groups of electrodes on both hemispheres and subsequently analysed either in the time domain (De Vos et al., 2017b; Van Hirtum et al., 2019a) or in the frequency domain (Vanvooren et al., 2014). Other techniques try to maximise the SNR of ASSR signals by assuming a simplistic anatomical configuration of the brain. This approach often involves the assumption that the brain activity during auditory processing can be represented by a small amount of sources, generally modelled with equivalent current dipoles and manually placed in regions where ASSR sources are expected (Herdman et al., 2002; Poulsen et al., 2007; Spencer, 2012). In Herdman et al. (2002), two symmetrical source dipoles are placed in left and right superior temporal planes, each consisting of tangential and radial components plus a midline brainstem generator with vertical and lateral components. The location and orientation of these dipoles is determined based on the ASSR recorded by 47 scalp electrodes. All these studies have in common that after processing the data, the remaining number of signals of interest is smaller than the original set of time series measured with the EEG electrodes or the MEG sensors. These analyses aim to extract the strongest ASSR and to accomplish that the original information provided by the electrodes or sensors is "condensed" into region-related electrode averages or equivalent current dipoles. Nonetheless, these approaches become insufficient when the anatomical origin of the ASSR is unknown or secondary source activity is of interest and its information needs to be disentangled from the primary activity. In order to avoid these limitations, data-driven source separation methods are often considered, such as independent component analysis (ICA).

Data-driven methods used to estimate spatial filters, as ICA, assume that the signals measured with the EEG electrodes or MEG sensors are a linear mixture of the activity generated by the different brain sources in the brain. ICA is a known technique for unmixing the signals present in the electrodes using only recorded time course information (Onton et al., 2006). ICA unmixes the input recordings into statistically independent components. These components are often interpreted as the activity produced by individual brain sources based on the presumption that the cortex is organised into compact regions of specialised functions. ICA has been used in previous studies to analyse ASSR from multichannel EEG recordings (Van Dun et al., 2007; Farahani et al., 2017). In methods based on component separation, such as ICA, a manual selection process of the desired components is often used. The number of ICA components equals the number of input channels or electrodes used, and often many of them carry evoked responses, in our case ASSRs. The ASSR information carried by the ICA components is not always generated by different brain sources, residual ASSR produced by the same or close brain generators will induce ASSR with similar properties in different ICA components. High-amplitude generators would be separated first by the ICA, weaker ASSR sources might have their oscillations masked, and sometimes they may leak into the surrounding high-amplitude components obtained through ICA. The independency criterion used by ICA might not be sufficient to extract ASSR in low-SNR scenarios. In previous analyses (Putilov et al., 2013; D'Croz-Baron et al., 2021), the selection procedure of the signals of interest often entailed the estimation of the explained variance, the SNR or their evoked-to-total power ratio. These procedures may be time-consuming in some cases if they are not automatised, and they can lead to misinterpretations since their definition and thresholds may not be the same for all subjects. Furthermore, there is another difficulty that might arise when ICA is used at a group level in the modality of group-ICA. Group-ICA is obtained by concatenating over time multiple subject data to extract common patterns of brain responses from the whole group (Farahani et al., 2019; Vakorin et al., 2010; Huster et al., 2015). In this case, if the inter-subject variability is high, the set of components drawn may show the strongest individual responses from various subjects instead of showing the brain responses that are common to the whole group. This "overlapping" would be difficult to predict, since the reconstructed location and brain activity of the sources for one or a few subjects would be as physiologically plausible as the source brain activity of the whole group. We expect that all

the ASSR produced by different subject generators showing similar properties such as location and time-series activity may be extracted and be "condensed" into one single component. The same would happen for one single generator that is present in several ICA components. This ASSR extraction process would be done by implementing a data-driven approach that would not consider individual ASSR as a group pattern feature, and it would not require a manual rejection of artefactual components. We think the use of the proposed approach might avoid probable misinterpretations of the data or the rejection of useful information. Furthermore, in some cases these processes may be automatised. In other words, we want to find the most optimal configuration for the selection and extraction of ASSR contained in the ICA subspace for both individual and group analyses. This would follow the idea that any subset of selected components defines a subspace of the data in which the activity of interest is concentrated (De Cheveigné & Parra, 2014).

To improve the artefact rejection and ASSR extraction, other data-driven mathematical methods can be used in combination with ICA. Certain data-driven methods can reduce the dimensionality of the data by extracting the most prominent underlying activity shared across different signals. These kinds of methods might be useful to "condense" the ASSR measured at the electrode level without any anatomical constraints. The most widely used are from the same family of ICA, the family of the data-driven methods used to estimate spatial filters. One of the most common techniques utilised for the estimation of spatial filters, apart from ICA, is principal component analysis (PCA), which obtains the direction of maximum variance of the data (Kayser & Tenke, 2003). PCA has been used in clinical applications with ASSR to assess the shared maximum variance between subjects and across conditions as a function of frequency (Hamm et al., 2012). However, the search for the direction of maximum variance is strongly related to the power contribution to the total signal. Hence, the search for the direction of maximum variance will provide with the signal of interest only if it carries more power than any other measured electrical activity, which does not always happen. Our signal of interest is phase-locked ASSR, which has an intrinsic low SNR and as a consequence, the power contribution to the total signal is also low, resulting in a minor contribution to the direction of maximum variance and making PCA unreliable for ASSR analyses. However, a simple average across trials can mitigate the effect of noise and emphasise the presence of ASSR in any EEG recording, but the number of epochs would be dramatically decreased

after computing the average, and shorter recordings reduce the accuracy of source localisation approaches (Delorme & Makeig, 2004). Due to the intrinsic low SNR of ASSR recordings a high number of epochs is also required, since instantaneous detection is extremely complicated.

Therefore, if any reliable physiological information is to be extracted from a source analysis perspective in ASSR experiments, the number of epochs should not be reduced. Denoising source separation (DSS) satisfies the aforesaid condition. DSS is a data-driven method that estimates a spatial filter designed to partition recorded activity into stimulus related and stimulus-unrelated components (de Cheveigne & Simon, 2008). DSS uses as criterion the reproducibility across epochs, which means that DSS maximises the part of the data that is consistently present across trials (signal) and diminishes the data that is not consistently present across trials (noise). Thus, this procedure would retain the phase-locked ASSR as well as the original number of epochs.

The goal of this chapter was to automatise the source selection procedure for physiologically meaningful ICA analyses of ASSR, more specifically for its application in studies of the brain cortical processes related to speech. We aimed to characterise the most representative brain activity that results from ASSR stimulation, focusing on the extraction of the most prominent time series reconstruction across trials and its anatomical origin in the brain at an individual and a group level. We combined the capability of ICA to identify artefactual from non-artefactual sources together with the power of DSS to resample a data set by finding the principal ASSR components considering the reproducibility across epochs as the maximisation factor. We aimed to build a novel approach that was insensitive to baseline shifts as induced by spectral or spatial filtering while preserving anatomical information and that could improve the dimension reduction in ASSR analyses involving the cortical processing of the speech envelope, which contains modulations up to 50 Hz (Rosen, 1992), although the main energy in the modulation spectrum of the speech envelope is situated between 4 Hz and 16 Hz (Drullman et al., 1994a,b). This dimension reduction is based on the consistency of the responses across epochs, which gives a better estimation of the signal of interest than using only the direction of maximum variance (PCA). This technique might be useful when trying to ascertain differences between different population groups by providing reliable data in studies involving the use of phase-locked ASSR. We hypothesise that the application of ICA and DSS will allow the elimination of artefacts from the data and the application of dimensionality data

reduction in an EEG data set, leading to the extraction of the most prominent brain patterns at a group level. First, a group analysis was performed wherein we tried to characterise the main aspects of the group under study, reducing the individual differences that could lead to misinterpretations. Second, an individual subject data analysis was carried out with the aims of understanding the effect of individual differences in the complete method pipeline. To be able to make both, individual and group-based studies comparable, a cluster-based approach was applied to the individual data. This technique will be used to analyse the ASSR sources in a data set of De Vos et al. (2017b).

2.2 Materials and Methods

A general overview of the methodology used in this chapter can be found in Figure 2.1.

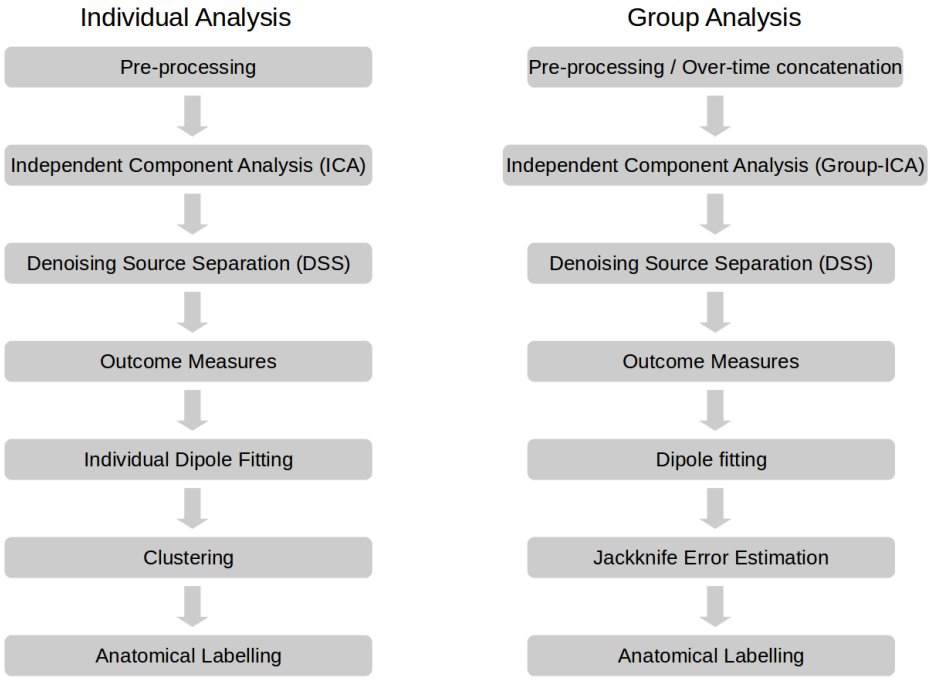


Figure 2.1: General overview of the methodological pipeline used.

2.2.1 Data acquisition

Participants

Twenty-one (10 male, 11 female) normal reading participants joined the study. The total mean age of the group was 14.7 years. All subjects presented bilateral normal hearing, a normal non-verbal intelligence (IQ score $\geq$ 80) and neither history of neurological disorders nor brain injury. Data were adopted from the study of De Vos et al. (2017b).

Stimulation

The stimuli used in the present study consisted of amplitude modulated speech-weighted noise. The carrier noise was adopted from the *Leuven Intelligibility Sentence Test* (LIST) (Van Wieringen & Wouters, 2008). This carrier noise is based on the long-term average speech spectrum of all sentences of the female speaker with LIST readings. The speech-weighted carrier noise was 100% amplitude modulated at approximately 4, 10 and 20 Hz, frequencies representative of the speech envelope, then 40 Hz, which triggers the highest cortical as well as subcortical responses and finally 80 Hz, which mainly triggers responses at the brainstem level. More information about the spectrum (dB/Hz) of the carrier wave, as well as the time signals of the modulated stimuli can be found in De Vos et al. (2017b). All stimuli were presented at 70 dB SPL through insert earphones monaurally to the left and to the right ear. For each subject, a total of 15 EEG measurements (5 modulation frequencies $\times$ 2 stimulation modalities) were collected. Each measurement consisted of a 5-min (300 s) EEG recording. We started recording from the lowest (4 Hz) to the highest modulation frequency (80 Hz), we stimulated the left ear first and the right ear afterwards. We recorded the activity for left and right ear before increasing the modulation frequency. Only monaural stimulation was considered in this study to avoid simultaneous activation of both auditory pathways.

Recording System

EEG data were recorded with the BioSemi ActiveTwo system using 64 active Ag/AgCl electrodes mounted in head caps according to the 10-10 electrode system. Electrode offsets were kept below 30 mV. All recordings were administered in a double-walled soundproof booth with a Faraday cage. Participants were asked to lie down on a bed while watching a soundless

film to warrant the same level of alertness and attention throughout the EEG measurement (Vanvooren et al., 2014; Poelmans et al., 2012b; Goossens et al., 2016).

2.2.2 Pre-processing

A common pre-processing procedure was applied to all data using MATLAB. First, EEG signals were filtered using a zero-phase high-pass filter with a cut-off frequency of 2 Hz and a slope of 12 dB/Octave to exclude distortions caused by skin potentials and the DC component of the amplifier. The filtered signal was segmented into different epochs with a length of 1.024 s, the result of this segmentation was an array of 292 epochs per electrode. Next, the 36 epochs showing the highest peak-to-peak amplitude were rejected, resulting in a total amount of 256 epochs per electrode and per subject, these were the data used for the individual study. After the epoch-based artefact rejection, all the electrodes were referenced to the C_z electrode. This reference was used over the average reference based in previous studies that stated that C_z reference lowers the noise estimates around the stimulation frequency reducing the detection threshold for ASSRs (Van der Reijden et al., 2005; Van Dun et al., 2009; Poelmans et al., 2012b). This pre-processing procedure was applied to each frequency and side of stimulation separately. Two subjects were not considered for further analysis (one male and one female) at the individual level due to their high number of epochs with high-amplitude muscular artefacts. The remaining 19 participants presented enough clean epochs for all stimulation conditions and were included in the individual study.

We prepared the data for the group study from the epochs used in the individual analysis applying the following steps. The aim was to obtain 128 epochs per subject with the lowest amount of artefacts in all the channels for each side of stimulation. To do that, we considered the 128 epochs showing the lowest absolute amplitude. The accepted 128 epochs per subject were concatenated along the time dimension, resulting in a total array of 2,432 epochs for all EEG channels.

2.2.3 ICA

ICA can be applied to identify and extract the brain source activities which are linearly mixed due to volume conduction. ICA decomposes EEG data into an array of maximally

independent components (Onton, 2009). In the present study, ICA was applied to our data in order to remove the components that are not carrying ASSR activity, and to assure that all the activity considered was triggered by selected stimulation, which is known for stimulating speech-related neural regions. The brain source localisation and projection weights were assumed to be spatially stationary for the duration of the experiment (Onton et al., 2006). The Infomax algorithm was utilised in FieldTrip (Oostenveld et al., 2011) due to its fast and reliable performance (Bell & Sejnowski, 1995). Other ICA algorithms, as AMICA or Extended Infomax were discarded due to the very high computation times. For group-ICA, we applied ICA to temporally concatenated data from all the subjects (Delorme & Makeig, 2004). This selection assumes a similar geometrical distribution of the sources since the mixing matrices for all subjects must be identical (Huster et al., 2015). In addition, when topographies of the sources change much across subjects the performance drops (Cong et al., 2013). Nevertheless, this approach aims to extract the common activity shared by a group of subjects. That is the reason we selected this technique over multichannel concatenation. Multichannel concatenation follows the notion that the different participants may produce a diverse set of components (Eichele et al., 2011). This multichannel approach would allow inter-subject variability in the weighting of independent components to the single-subject scalp recordings (Eichele et al., 2011; Huster et al., 2015). However, this model would not directly deliver subject-specific time courses of the components, but rather some aggregate group component time courses that would need a manual multiplication of the original data with the demixing matrix. Furthermore, a data reduction would be a required step due to the extremely high computational load associated with high-density EEG recordings (Huster et al., 2015). Thus, after computing ICA, the number of output components equalled the number of input channels for both, individual and group analysis. There were 63 channels per stimulation condition. After the computation of ICA a one-sample Hotelling t-squared test was performed on the ICA components for the individual and group analysis, see section 2.2.6. Components that did not show significant ASSR were rejected.

2.2.4 DSS

DSS performs a separation of the data into desirable components (signal) and undesirable components (noise), assuming linearity of the coefficients and of the DSS components (Särelä & Valpola, 2005).

The denoising procedure was carried out in different steps. First, a spatial whitening of each channel from the input data was performed. This was carried out through PCA (Kayser & Tenke, 2003) and normalisation. This process created a data set with spherical symmetry. The resulting data were then submitted to a denoising function or bias function, followed by another PCA which specified the orientations that maximised the bias function. This maximisation of the bias function searched for directions that maximised the signals reinforced by the averaging across trials. In our case, the expected reinforced signal was phase-locked ASSR. The second PCA created a transformation matrix that was the one finally applied to the result of the first PCA, the whitened data. This bias function was chosen to be the *proportion of epoch-averaged (evoked) activity* (de Cheveigne & Simon, 2008). This bias function represented the total-power reproducibility across trials. It allows the ranking of the DSS components according to the most consistent activity along trials, the components ranked first will have a higher amount of activity that is present along all the trials while the last components will carry activity that is only present in a few epochs. Since the stimulation during the experiment was periodical and consistent across trials we expect the activity of the main ASSR phase-locked generator to be ranked first.

We input the accepted ICA components obtained from our EEG data into the DSS algorithm and the result is an array of components sorted by decreasing total-power reproducibility across trials. In order to determine whether these DSS components were carrying ASSR, a one-sample Hotelling t-squared test was computed, see the section 2.2.6.

2.2.5 Outcome Measures

Relative response amplitudes and SNRs were extracted from the DSS components containing significant ASSR for all the stimulation frequencies and for both sides of stimulation separately, an example of these results at individual level may be found in Figure 2.2.

The response amplitudes were obtained by taking the square root of the signal power.

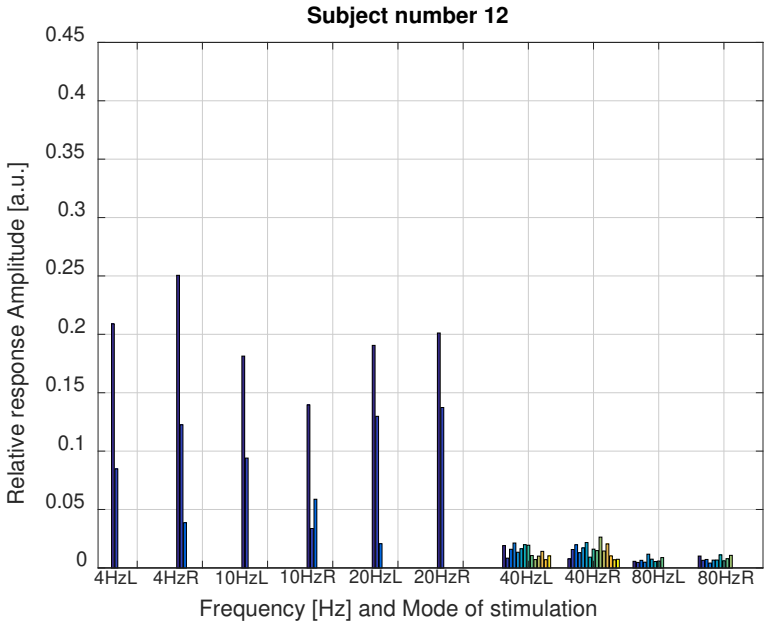


Figure 2.2: Bar graph representing the total number of DSS components carrying ASSR and their relative response amplitudes for an example subject, the bar colours have been selected for representation purposes.

The signal power, P_S, was calculated from the Hotelling t-squared statistic, it represents the squared amplitude of the responses mean across all the data trials at the bin of the modulation frequency.

The noise floor amplitude, P_N, required to compute the SNR, was also estimated from the Hotelling t-squared statistic and shows the standard error of the amplitude responses at the modulation frequency across epochs, being: $\sigma(R_{mf})/\sqrt{n}$. Based on the definition of power response and noise amplitude, the SNR may be defined as the ratio between the power of the response signal and the power of the EEG noise, Equation 2.1.

$$SNR = \frac{P_S}{P_N} = \frac{\|mean(R_{mf})\|^2}{\left(\frac{\sigma(R_{mf})}{\sqrt{n}}\right)^2} \tag{2.1}$$

Where P_S is the power of the signal at the stimulation frequency and P_N is an estimation of the noise power. R_{mf} is a complex vector containing the responses at the modulation frequency of all epochs, σ is the standard deviation and n is the number of epochs.

2.2.6 Detecting significant ASSR responses

To determine whether the ICA or the DSS components were carrying ASSR or not, the one-sample Hotelling t-squared test was performed in the frequency spectrum of the components (Hotelling, 1931). These spectra were obtained by means of a Discrete Fourier Transformation. The statistical test compared the complex responses at the modulation frequency bin across n different epochs, Equation 2.1.

Obtained components were considered to have ASSR activity when the Hotelling t-squared test showed a significant difference ($\alpha \geq 0.05$) between the squared mean of the response, numerator of the Equation 2.1, and the squared Standard Error of the R_{mf} distribution, denominator of the Equation 2.1 (Hofmann & Wouters, 2012).

2.2.7 Error estimation for group analysis

In order to estimate bias and variance (σ_{JK}) for the group analysis, the Quenouille and Tukey jackknifing approach was utilised (Miller, 1974). The standard deviation from the mean value, the value including all M subjects, was estimated from the jackknife estimate of variance (Efron & Stein, 1981), see Equation 2.2.

$$\sigma_{JK} = \sqrt{\frac{M-1}{M}\sum_{m=1}^{M}[\zeta_m - \zeta_{all}]^2} \tag{2.2}$$

Where ζ_{all} represents the over-time concatenated data with the epochs of all subjects and ζ_m represents the epochs of an individual subject.

2.2.8 Dipole fitting

The projection weights of the first component obtained through DSS and ICA analyses were fitted to equivalent current dipoles for the individual and group data. These projection weights were obtained through the product of the mixing matrices of the ICA and DSS decompositions, this procedure is equivalent to first project back the ICA components to the sensor space and then compute the DSS in the new formed sensor space. The maximum number of obtained DSS components can be again the number of channels. However, we only fitted the first DSS component because the projection weights of the rest of the DSS not

always have an interpretable spatial pattern (Haufe et al., 2014). This dipole fitting procedure was performed using a Boundary Element Method (BEM) as a head model (Meijs et al., 1989; Hämäläinen & Sarvas, 1989). This BEM conductivity model was created in FieldTrip from 14 year-old averaged MRI images (Richards et al., 2016; Sanchez et al., 2012). The BEM model, Figure 2.3, described the electrical properties of the scalp, skull and brain as well as their conductivity values, which were chosen to be 0.3300, 0.0042 and 0.3300 S/m respectively (Gabriel et al., 1996). After creating the mesh, the EEG electrode position was rescaled and manually aligned with the three fiducial points: nasion, left and right pre-auricle.

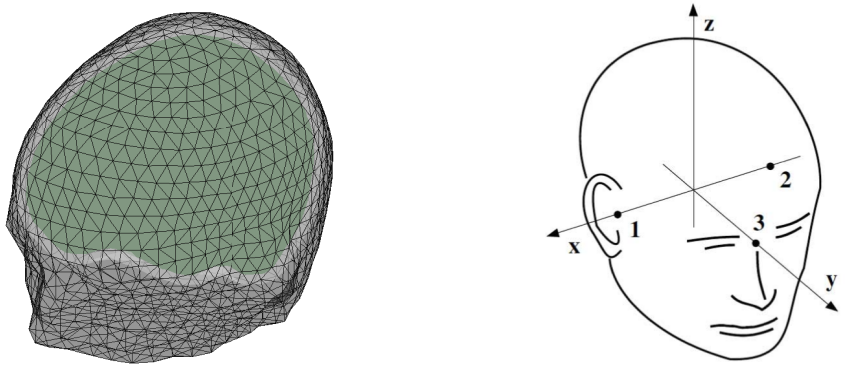


Figure 2.3: Left panel: BEM mesh surface with three different layers: brain (green), skull (clear grey), scalp and skin (dark grey). **Right panel:** Neuromag coordinate system.

Once the head model was ready, a coarse three-dimensional grid was drawn. This grid was created by projecting the electrode positions on the skin surface of the head model, excluding the grid positions that were outside the head. Then, the grid was scanned in order to determine adequate starting positions for each component. Once the best grid positions were determined, the programme ran a non-linear algorithm to determine the exact position of the dipoles. This location was selected based on the goodness of fit (residual variance) obtained after the fitting (Delorme & Makeig, 2004), the position with the best fit score (the least residual variance) was chosen as the final location. This procedure was applied in the first DSS component twice, one for one dipole and the second one for two symmetrical dipoles along the x-axis in neuromag coordinates, Figure 2.3. Since two dipoles will always have a lower residual variance, that is, a better goodness of fit, than only one dipole, it is required to add a restriction to the distance between them. Auditory electrophysiological signals can be symmetric, thus two symmetrical dipoles along the x-axis was the default configuration as

long as the distance between them was more than 20 mm, the one dipole configuration was selected otherwise. The position of the dipole or dipoles was then projected on the original MRI used to create the head model for visualisation. The dipoles were plotted following the MRI orientations showed in Figure 2.4.

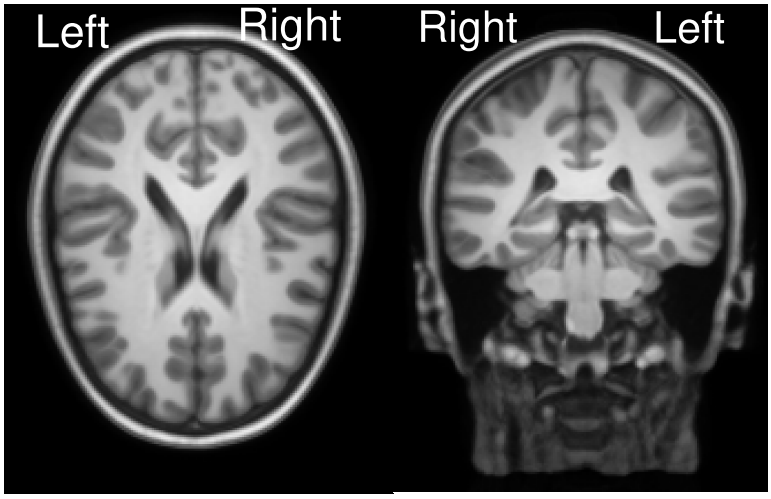


Figure 2.4: MRI orientations used for the visualisation of the dipoles fitted.

2.2.9 Clustering

A clustering algorithm was applied in the individual analysis in order to gather the individual dipole locations of the brain responses. This clustering algorithm was developed by Farahani et al. (2017) for its use in ASSR source localisation with ICA.

The phase plays an important role in the generation of auditory brain responses. The neural processing centres along the auditory pathways create responses with apparent latencies or phase delays (Herdman et al., 2002; Picton et al., 2003). These delays are considered in the clustering method by utilising the phase angle at the modulation frequency: $Arg(mean(R_{mf}))$ obtained through the Fourier transformation. Since the phase angle is a circular quantity it could not be used directly with the dipole location data. All phase data were converted from polar units to Cartesian coordinates by means of Euler's expression: $e^{i\phi} = cos(\phi) + i\ sin(\phi)$. The real and imaginary part of $e^{i\phi}$ together with the location data were the input for the clustering algorithm. Dipole location and phase angle data were normalised and weighted by 3 and 1, respectively, in order to emphasise the spatial compactness of clusters (Farahani

et al., 2017).

Clustering of the dipole locations of the first DSS component was computed based on a Gaussian Mixture Model (GMM) (Bouveyron & Brunet-Saumard, 2014). The k-means algorithm with the criteria of three standard deviations for outlier detection implemented in EEGLAB (Delorme & Makeig, 2004) was used for the initialisation procedure of the GMM. After fitting the GMM model, clusters were assigned to each data point by selecting the component that maximised the posterior probability. The posterior probability of each data point indicates the probability of belonging to a specific cluster.

The final number of GMM clusters was selected based on the Bayesian Information Criterion (BIC) (Schwarz, 1978). The GMM was computed using a number of clusters from 2 to 5, the configuration that showed the lowest BIC was preferred.

2.2.10 Anatomical labels

Anatomical labels were assigned to the mean values of the dipole locations in the group analysis, and to the cluster centres in the individual study. These labels were obtained from an age-related atlas derived from LPBA40 (Shattuck et al., 2008) and the MRI used to create the volume head model (Richards et al., 2016; Sanchez et al., 2012). This atlas was loaded into the software 3D Slicer (Fedorov et al., 2012) and the cluster centres were assigned a label by visual inspection. This label referred to the anatomical region that was the closest to the mean dipole location in group analysis or the cluster centre in the individual study.

2.3 Results

We applied the method individually for each subject. To complete the individual analysis, source localisation results were clustered to make them comparable to the group analysis. The group analysis was obtained by concatenating over time the channel data and treating each stimulation condition separately. The error estimation was derived from the Jackknifing approach mentioned in the methods section.

This section is structured as follows: First, the subsection Number of components summarises the results acquired in the study of the ASSR extraction and source selection from the ICA subspace using DSS. As an example of how the frequency spectrum of a DSS component

carrying ASSR looks like we plotted the Fourier transformation of one DSS component in Figure 2.5. Second, the outcome measures subsection reviews the physiological plausibility of the method by analysing the physiological information retained. Lastly, the source localisation subsection contains the results of the anatomical locations obtained for the different sources considered.

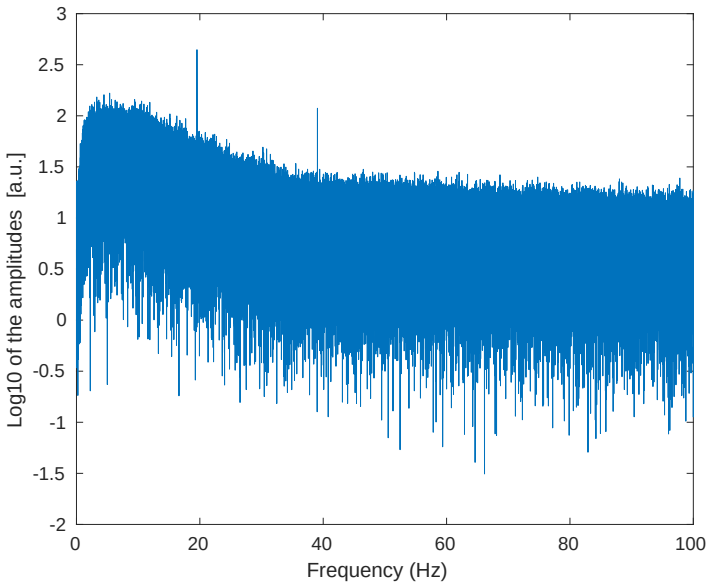


Figure 2.5: Frequency spectrum of a DSS first component for 20 Hz left ear stimulation in the group analysis data. ASSR main response can be observed at 20 Hz together with the first harmonic at 40 Hz. The amplitudes are shown in a logarithmic scale for representation purposes, amplitudes obtained from DSS or ICA do not retain units.

2.3.1 Number of components

Figure 2.6 shows the number of reconstructed time-series carrying ASSR information after performing only ICA and after computing DSS on the Independent components. For low frequency stimulation conditions, i.e., 4 Hz, 10 Hz and 20 Hz, the number of reconstructed time-series carrying ASSR is strongly reduced after the application of DSS to the Independent components. While there is a less clear effect at 40 Hz and 80 Hz, more information can be found in the Appendix A.

In the group analysis, all the frequencies used for stimulation present the highest SNR at the modulation frequency in the first DSS component. This effect is not found in the individual analysis, where some subjects do not show the highest SNR in the first DSS component,

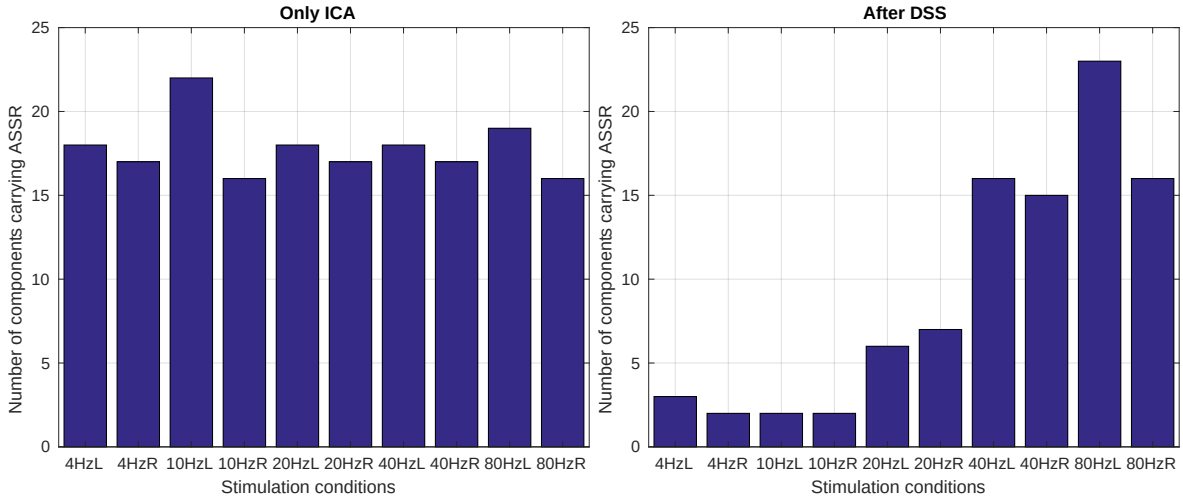


Figure 2.6: Number of reconstructed time-series carrying ASSR obtained from the group analysis after the computation of only ICA (**left panel**) and after the application of DSS to the Independent components (**right panel**).

as Table 2.1 shows. These results are an improvement compared to the percentage of subjects whose first ICA component containing ASSR carries the highest SNR at the stimulation frequency, as it can be seen in Table 2.2, where results shown were calculated before the application of DSS. Furthermore, we have included the first ICA component carrying ASSR and compared it with the ICA component carrying the highest SNR at the modulation frequency despite the first ICA component that carried ASSR was never ranked among the first ones. This means no ICA component carrying ASSR had the highest mean projected variance in contrast with the DSS components, where for all the modulation frequencies the first ranked DSS component carried ASSR.

Table 2.1: Number of subjects whose first DSS component is showing the highest SNR at the modulation frequency.

Frequency	**4 Hz**		**10 Hz**		**20 Hz**		**40 Hz**		**80 Hz**	
Ear	**L**	**R**	**L**	**R**	**L**	**R**	**L**	**R**	**L**	**R**
n	19	18	18	18	12	16	11	7	5	3
$n/n\text{total} \times 100$	100%	95%	95%	95%	63%	84%	58%	37%	26%	16%

Table 2.2: Number of subjects whose first ICA component carrying ASSR is showing the highest SNR at the modulation frequency.

Frequency	**4 Hz**		**10 Hz**		**20 Hz**		**40 Hz**		**80 Hz**	
Ear	**L**	**R**	**L**	**R**	**L**	**R**	**L**	**R**	**L**	**R**
n	2	1	3	1	5	1	4	2	3	2
$n/n\text{total} \times 100$	10%	5%	15%	5%	26%	5%	21%	10%	15%	10%

2.3.2 Outcome measures

Individual analysis

DSS components calculated for the individual analysis were compared with the ICA components computed before the application of DSS. The application of DSS significantly increased the SNR, as Figure 2.7 shows. The difference is more noticeable for low modulation frequencies and non-existent for 80 Hz right ear stimulation, where the SNR is comparable.

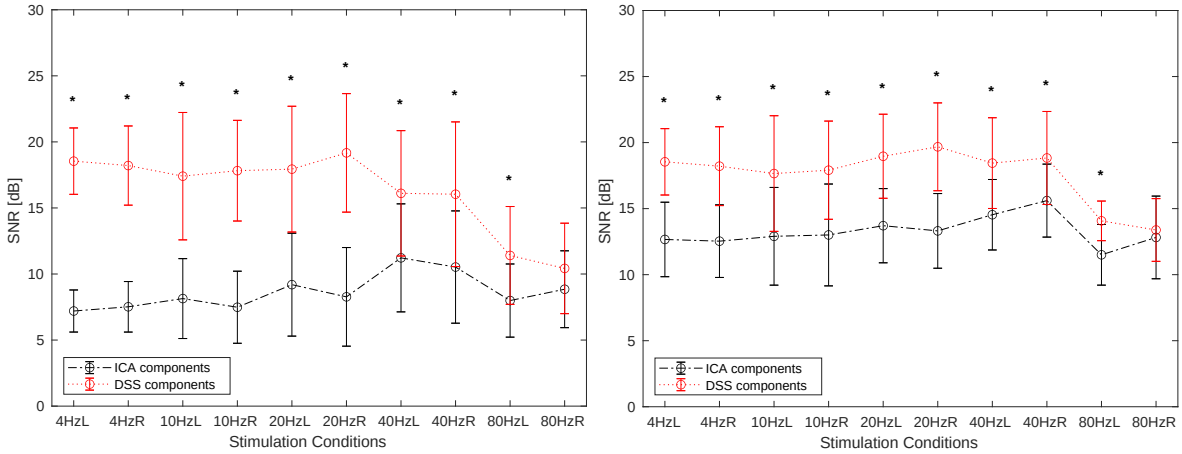


Figure 2.7: Comparison between the SNR levels of the first ICA component carrying ASSR and the first DSS component for all the stimulation frequencies and subjects, in **left panel**; and the ICA and DSS component carrying the highest SNR for all the subjects and all the modulation frequencies, in **right panel**. Bonferroni-Holm corrected p-values below a significant threshold of 0.01 are marked with an $\star$ for all figures.

Group analysis

Figure 2.8 shows the relative response amplitudes, the noise level and SNR estimates at the modulation frequency of the first DSS component calculated for all the jackknifing conditions in the group data. The relative response amplitudes decrease with the stimulation frequency,

being maximum for the lower frequencies and reaching a minimum at 80 Hz stimulation. The SNRs are more evenly distributed, reaching maximum values at 40 Hz stimulation frequency. The noise level amplitudes also decrease with the stimulation frequency, meaning that the noise level is lower at higher frequencies.

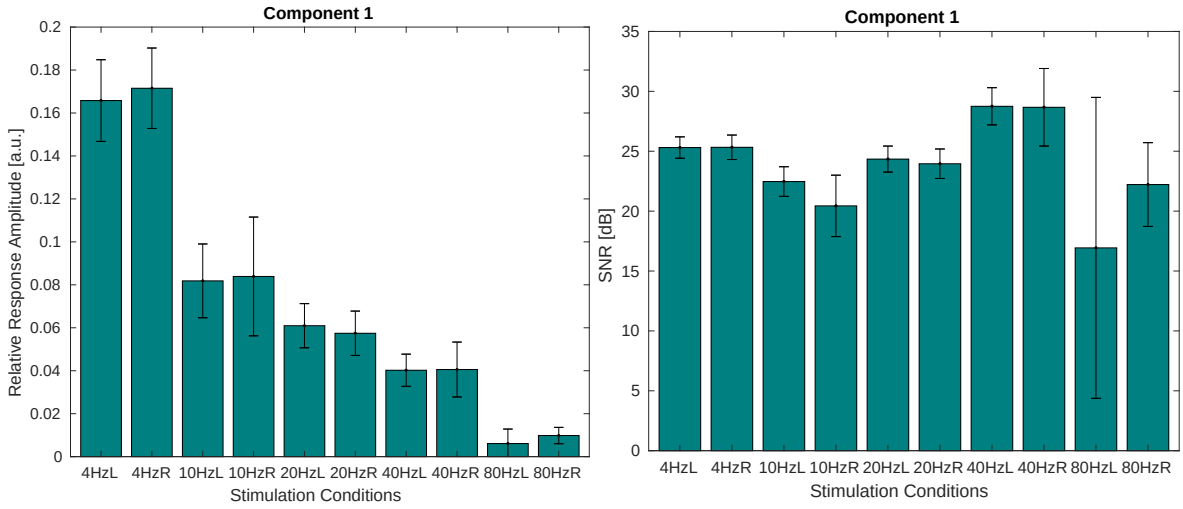


Figure 2.8: Mean values and standard deviations obtained from the group analysis for: the relative amplitudes, in **left panel**, and the SNR estimates, in **right panel**, of the first DSS component for all stimulation frequencies.

Individual analysis and group analysis comparison

Figure 2.9 shows the noise level and SNR at the modulation frequency calculated separately for the first DSS component. The values for the individual data, in red, show larger error bars than the group analysis for the response amplitudes and the SNR estimates. In addition, individual results show higher mean relative response amplitudes than group results except for 40 Hz, though none of these differences is statistically significant. These differences are due to the presence of a higher noise level as it is shown in the bottom panel of Figure 2.9, where the individual results show statistically higher Noise Level Amplitudes for all modulation frequencies except for 80 Hz left ear. A smaller noise level makes the SNR to be higher for group analysis, as the right panel of the Figure 2.9 shows, where statistically significant differences are found for all the modulation frequencies except for 10 Hz and 80 Hz left ear stimulation. The SNR differences between the means can be found in Table 2.3.

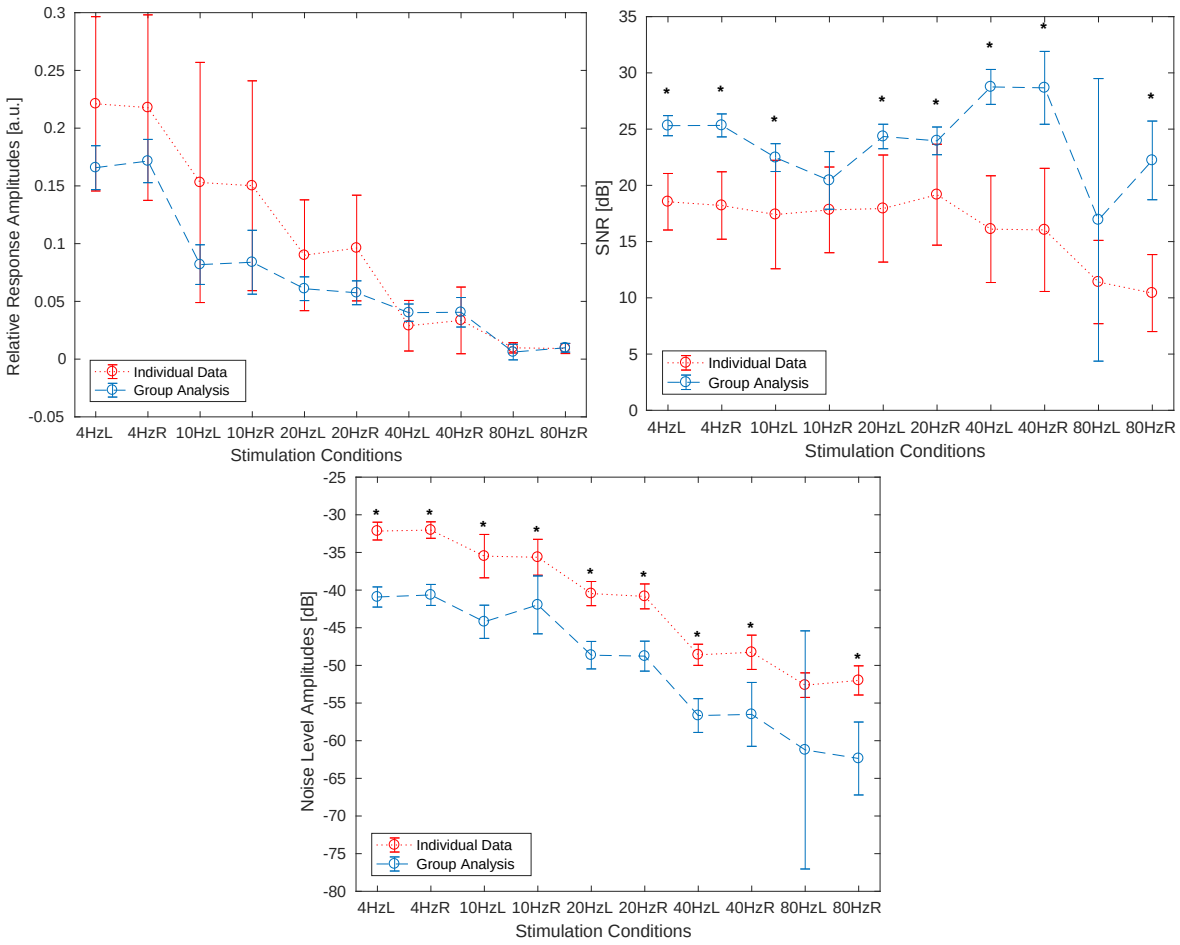


Figure 2.9: Comparison between group and individual results of the first component estimates of the relative response amplitudes, in **top left panel**; the SNR, in **top right panel**; and the noise level amplitudes, in **bottom panel.** Bonferroni-Holm corrected p-values below a significant threshold of 0.01 are marked with an $\star$ for all figures.

Table 2.3: SNR differences between the means of group and individual data measured at the stimulation frequency. A double paired t-test was performed to evaluate any differences between the individual and the over-time concatenated data. A two-tailed Bonferroni-Holm correction was applied to the p-values (Holm, 1979). Differences below a corrected chance level of 0.01 are marked with an *.

Frequency	**4 Hz**		**10 Hz**		**20 Hz**		**40 Hz**		**80 Hz**	
Ear	**L**	**R**	**L**	**R**	**L**	**R**	**L**	**R**	**L**	**R**
SNR difference in dB	6.8 (*)	7.1*	5.1*	2.6	6.4*	4.8*	12.6*	12.6*	5.5	11.8*

2.4 Discussion

We used real EEG data to evaluate the performance of the approach proposed in this chapter and its physiological plausibility. We studied the ASSR extraction from ICA components

using DSS and its dimension reduction as well as the physiological information contained in the extracted DSS components, the outcome measures and the anatomical origin. We opted for the combination of ICA and DSS and not for beamformers or other signal-space projection. Typical beamformers, which scan the brain using a single equivalent current dipole as the underlying source model, will fail to yield reliable results. This happens as a result of the violation of the underlying assumption that for any source-of-interest there are no other temporally correlated sources (Popov et al., 2018). Therefore, in ASSR analyses, where bilateral areas can show zero-lag correlated activity, a bilateral region suppression technique is required (Dalal et al., 2006). Furthermore, the use of beamformers would have forced us to a high level of approximation due to the lack of individual head models, while ICA and DSS estimate the lead-field matrix independently of the head model utilised.

2.4.1 Dimension reduction and number of sources.

The first aim of this study was to automatise the signal separation processes based on ICA component selection in ASSR analyses and to ensure that the activity extracted in group analyses represented the group pattern. When only ICA is used, the selection procedure of the signal of interest often entails the estimation of the explained variance and the subsequent selection of components is based on this criterion. Furthermore, this criterion is not always reliable since only a few subjects had an ICA component carrying ASSR ranked first. Sometimes in place of the explained variance the components are selected or rejected based on their SNR or on their evoked-to-total power ratio. In either case, the application of these criteria might lead to the rejection of components that still contain ASSRs. We propose that more information can be retained if the search for maximum variance is replaced by the search for the direction that is maximised across trials, as DSS does. With this procedure all ASSR information may be "condensed" in the first obtained DSS components, and it can be easily detected by using a statistical test. These DSS components with detected significant ASSR would be considered as signal and the rest would be discarded as noise. The reduction of the final number of components sharing similar information leads to an easy understanding of the global population behaviour in comparison analyses, due to the extraction of the main representative activity of the group under study.

The application of DSS to ICA could gather all the ASSR present in the channel data into a few DSS components. This dimension reduction worked especially well with cortical generators in low modulation frequencies: 4 Hz, 10 Hz and 20 Hz for both, individual and group analysis. For these stimulation frequencies, all the ASSR activity was extracted into the first DSS components. This means that different ICA components exhibited ASSR information that could be gathered by the application of DSS. Equivalent generators from different subjects at the group level were condensed into the same components after the application of DSS, leading to a more reduced number of sources without losing ASSR information. This was achieved as a result of using DSS bias function, allowing the method to search and rank the components with a higher reproducibility across trials regardless of their power and variance. The capability of the method to find ASSRs independently of the shared variance and power has been shown to be an improvement against the traditional PCA method, which is very sensitive to those factors (Abdi & Williams, 2010; Kayser & Tenke, 2003; Hyvärinen et al., 2001, Chapter 6). Conversely, for 40 Hz and 80 Hz the number of DSS components carrying ASSR compared to the number of ICA components carrying ASSR either does not decrease to the same extent as in the low frequencies, or it even increases. This might happen because for 40 Hz and 80 Hz stimulation cortical and deep sources such as the brainstem fire together, leading to overlapping fields produced by the multiple generators, which are simultaneously detected by the EEG electrodes in the scalp. Since the latency between the activation at brainstem level and at cortical level is approximately equal to one cycle of the 40 Hz stimulus, the responses of the brainstem and cortical sources interfere constructively (Bohórquez & Özdamar, 2008; Herdman et al., 2002). In addition, as an explanation for the over-time concatenated group results, it might have happened that latency differences between subjects together with the differences in geometry would have made DSS less sensitive at those high modulation frequencies, since latency differences between subjects have a higher impact at responses evoked by faster modulation frequencies. Another possible description for the large number of DSS components detected is that the neural structures underlying ASSR exhibit an oscillatory behaviour with a fundamental resonance frequency around 40 Hz (Hari et al., 1989; Rance, 2008). An oscillation at the fundamental frequency causes the system to oscillate with larger amplitude than when the stimulation is applied at other frequencies (Halliday et al., 2013, Chapter 15).

Either way, the simultaneous activation of multiple generators per individual creates a multiple ASSR pattern indiscernible by the DSS algorithm because all the sources are similarly sustained in time. Thus, the preferred direction, easily found at low modulation rates, is not as consistent across subjects in 40 Hz and 80 Hz modulation frequencies preventing the DSS to find the predominant brain generator. At the individual level, this effect causes the first DSS components to not always carry the highest SNR, especially for high modulation frequencies. In addition, the lack of a high number of trials causes the DSS bias function to worse estimate the data direction maximised by the trial average. The bias function SNR increases proportionally to $\sqrt{N}$ (De Cheveigné & Parra, 2014). At group level the inability of DSS to find a preferred direction for the data adds with the sensitivity of the ICA to high inter-subject variabilities in over-time concatenated EEG analyses (Huster et al., 2015).

We considered the idea of using a band pass filter to mathematically force the method to reduce even more the number of sources. However, this band pass filter would be centred in the frequency of interest and applied to the ICs before performing DSS. By removing all non-interest activity, DSS will be imposed to only find activity in the frequency band of the filter. This will lead to an underestimation of the noise present and therefore to an overestimation of the obtained responses amplitudes, above all in 80 Hz modulation, where the SNR is intrinsically very low. This approach has been used to estimate the covariance matrices for ASSR detection with GEVD in Biesmans et al. (2015). A very narrow band pass filter was applied around the modulation frequency to estimate the signal of interest covariance matrix. To estimate the noise covariance matrix 12 Hz below and 12 Hz above, the stimulation frequency were extracted by low and high pass filters, respectively. This estimation needs a high bandwidth of the noise spectrum around the stimulation frequency, which becomes unsuitable at low modulation frequencies. The application of a band pass filter was suitable for ASSR detection at 40 Hz. However, if the source reconstruction and the retainment of anatomical information are relevant, this approach would obscure the physiological interpretation of the amplitudes obtained from the components, and furthermore it will entail the loss of temporal resolution and distortion of the waveforms (De Cheveigné & Parra, 2014).

2.4.2 SNR and relative response amplitudes.

The second goal of this study was to prove that this method retains the physiological relevance of the ASSR components determined for a specific group, which is useful for posterior analyses. That is the motivation to measure the SNR and the relative response amplitudes at all stimulation frequencies. In comparison with ICA alone, the application of DSS improves ASSR detection by increasing the SNR. It also simplifies the selection procedure, since DSS components having the highest SNR appear ranked first in most of the subjects at the individual level for low modulation frequencies and for the group analysis the DSS component having the highest SNR is ranked first in all subjects.

Group analysis

For group analysis, the relative response amplitudes were maximal at 4 Hz and decreased with the increase of the modulation frequency. This behaviour has also been observed in adults and children, where the effect was stronger (Vanvooren et al., 2015) and in this data set at the electrode level (De Vos et al., 2017b). The SNR for group analysis was maximal at the modulation frequency of 40 Hz, as the literature suggests (Rance, 2008).

Individual analysis

This contrasts with the individual analysis, where this cannot be observed. The smaller SNR and bigger error bars for the individual analysis demonstrates that the reduction of the inter-subject variability leads to cleaner signals for the first component, since some individual effects weaken the ASSR activity.

Group and individual analysis comparison

The response amplitudes for the group analysis were smaller than for the individual analysis, although these differences were not statistically significant due to the big error bars produced by the higher inter-subject variability of the individual study. Differences in SNR and the error dispersion prove, as it has been mentioned before, that the method is sensitive to the number of the trials used, meaning that there is a better performance in the group analysis due to the higher number of trials, as it has been proven with the use of Group-ICA that is known

to extract robust and reproducible patterns of brain responses from a group of participants (Farahani et al., 2019; Vakorin et al., 2010; Huster et al., 2015).

After the application of the mathematical method the general properties known of the ASSRs are still present (Picton et al., 2003), which demonstrates that the physiological information is retained.

2.4.3 Source localisation

Cortical sources of ASSRs are mainly located bilaterally in the auditory cortex, more exactly in the supra temporal plane. This has been detected in numerous studies (Luke et al., 2017; Poulsen et al., 2007; Reyes et al., 2005; Steinmann & Gutschalk, 2011; Teale et al., 2008).

Low modulation frequencies (4 Hz, 10 Hz & 20 Hz)

Individual analysis: Figure 2.10 and Figure 2.11 show the anatomical regions of the clusters calculated for the ICA components carrying the highest SNR. For low modulation frequencies, similar behaviour was observed, the clusters were located in symmetrical anatomical regions along the x-axis, as it can be seen in the Table 2.4, which shows a summary of the anatomical brain locations of the clusters. At 4 Hz right ear stimulation, in addition to the cortical clusters, a third cluster with a lower SNR was also found in the cerebellum. Although the existence of brain activity during slow modulation (<40 Hz) stimulation in deep regions has been found in previous studies (Herdman et al., 2002), the presence of the third deep cluster was not found while stimulating the left ear. Deep sources are normally hard to detect, especially at low modulation frequencies when cortical sources activate with high amplitudes at the same time and can hide the activity from the deep generator (Lucka et al., 2012). That reason might explain the absence of a deep source in left ear stimulation while for right ear that source is present, located in the cerebellum. The presence of activity in the cerebellum has been suggested in previous studies (Pastor et al., 2008, 2002), where they found neuro-metabolic activity as a response to 40 Hz clicks using techniques of PET and fMRI.

Group analysis: Dipole location of the brain sources together with the jackknifing standard deviation estimates can be found in Figure 2.12 for left ear stimulation and in Figure 2.13 for

Table 2.4: Table with source information for group analysis.

f_{Stim}	SN	Anatomical region of the cluster's centre
4 Hz L	S1	Left middle temporal gyrus
	S2	Right middle temporal gyrus
4 Hz R	S1	Left middle temporal gyrus
	S2	Right middle temporal gyrus
10 Hz L	S1	Right inferior temporal gyrus
	S2	Left middle temporal gyrus
10 Hz R	S1	Left middle temporal gyrus
	S2	Right middle temporal gyrus
20 Hz L	S1	Left middle temporal gyrus
	S2	Right superior temporal gyrus
20 Hz R	S1	Left middle temporal gyrus
	S2	Right parahippocampal gyrus
40 Hz L	S1	Left fusiform gyrus
	S2	Right fusiform gyrus
40 Hz R	S1	Brainstem
80 Hz L	S1	Right supramarginal gyrus
80 Hz R	S1	Right middle temporal gyrus
	S2	Left middle temporal gyrus

right ear stimulation. The anatomical brain coordinates were transformed into brain regions by using the anatomical labels. These locations are summarised in the Table 2.5. The sources found for the first component were symmetric, cortical and located in the vicinities of the auditory cortex. The obtained anatomical brain regions for the first component were located either in the right and left temporal gyrus for all stimulation conditions, except for 20 Hz

right, where one dipole was located in the right parahippocampal gyrus, an adjacent region of the temporal gyrus. The position of the source dipoles collected the expected cortical nature of the brain responses for the first component. They were located in the temporal gyrus or in neighbouring areas, in agreement with what was found in previous studies where the cortical sources of ASSRs were reported to be located specifically in the superior temporal gyrus (Herdman et al., 2002; Reyes et al., 2004). The absence of deep sources in low modulation frequencies in comparison to the individual study might be due to a higher inter-subject variability. This variability can also affect the detection of deep sources, since it is known that high inter-subject variability decreases the probability of detecting a source in over-time concatenated ICA analyses (Farahani et al., 2017; Huster et al., 2015).

High modulation frequencies (40 Hz & 80 Hz)

Individual analysis: There was no symmetry along the x-axis for 40 Hz, the cluster centres were located in the brainstem and in the right cingulate gyrus for left ear, see Table 2.4; the first cluster collected the cortical responses and the second one the deep responses. The size of the first cluster was bigger than the average sizes found for the same stimulation frequency in Farahani et al. (2017). This was due to the different cluster criteria used. In this study, we clustered the sources of the first DSS component separately from the rest, instead of clustering all the brain sources obtained for all the components together, which would have given to the clustering algorithm much more flexibility to group the sources into smaller and more compact clusters (Bouveyron & Brunet-Saumard, 2014). For right ear 40 Hz stimulation, the clusters collected the activity generated in deep regions. In addition, they had comparable SNR levels, a phenomenon also observed in Farahani et al. (2017). The collected brainstem activity was not observed in the group analysis. That means that the regions showing the most reproducible ASSRs across trials in the group analysis for that modulation frequency were cortical. The opposite happens when stimulating the right ear, where the regions detected were located in the brainstem. This presence of ASSR activity in deep brain regions at 40 Hz stimulation has been reported previously in literature (Picton et al., 2003; Giraud et al., 2000; Herdman et al., 2002).

Table 2.5: Table with cluster information for individual analysis.

f_{Stim}	CN	Anatomical region of the cluster's centre	SNR (dB)
4 Hz L	C1	Left superior temporal gyrus	18.5
	C2	Right superior temporal gyrus	18.5
4 Hz R	C1	Left superior temporal gyrus	19.4
	C2	Right superior temporal gyrus	19.6
	C3	Cerebellum	16.8
10 Hz L	C1	Right middle temporal gyrus	18.8
	C2	Left middle temporal gyrus	18.8
10 Hz R	C1	Left middle temporal gyrus	18.1
	C2	Right inferior temporal gyrus	18.2
20 Hz L	C1	Left insular cortex	17.4
	C2	Right insular cortex	19.0
20 Hz R	C1	Left middle temporal gyrus	19.3
	C2	Right middle temporal gyrus	20.2
40 Hz L	C1	Brainstem	14.1
	C2	Right cingulate gyrus	17.4
40 Hz R	C1	Left superior temporal gyrus	13.8
	C2	Right superior parietal gyrus	15.1
	C3	Brainstem	18.5
80 Hz L	C1	Left lingual gyrus	11.2
	C2	Right cingulate gyrus	11.5
80 Hz R	C1	Right cingulate gyrus	12.2
	C2	Left gyrus rectus	7.7

Group analysis: The mean value for the sources obtained at 40 Hz left ear stimulation is located in the fusiform gyrus, which is a neighbouring area of the temporal gyrus and has also shown important contributions to the phase synchronisation in memory processes (Fell & Axmacher, 2011). However, the error bars include different brain regions due to their size, including the auditory cortex. Similar behaviour was found at 40 Hz in Luke et al. (2017), where the estimate of the source to noise variance was found higher at 40 Hz than in lower modulation frequencies in grand averaged data. For 40 Hz right side stimulation, one dipole is found in the brainstem.

The jackknifing estimates drew very big error bars for 80 Hz modulation frequency. Some sources were detected in cortical regions, cortical activity at 80 Hz has also been found in other fMRI (Giraud et al., 2000) and MEG studies (Coffey et al., 2016; Schoonhoven et al., 2003).

Individual and group analysis discussion: Checks have been performed in other EEG studies (Luke et al., 2017; Farahani et al., 2017) to compare the obtained source coordinates with the coordinates defined in literature for the auditory cortex in adult populations (Poulsen et al., 2007). In our case, this was not possible due to the use of a different, age-related, MRI template and head model. Thus, the comparison with literature and other studies has been done with the anatomical regions obtained through the LPBA40 atlas (Shattuck et al., 2008) mentioned in the methods section. More information can be found in the Appendix B, where we computed the only ICA dipole locations and compared it with the DSS dipole location at an individual level.

We determined the variability of the source locations in the group analysis utilising the jackknifing estimates of the standard deviation of the dipole coordinates calculated, as mentioned in the methods section. The ellipsoids and the error bars obtained for the cortical ASSR sources were much larger than the active regions normally encountered in fMRI studies (Harms & Melcher, 2002; Steinmann & Gutschalk, 2011; Giraud et al., 2000) especially for 40 Hz and 80 Hz.

We do not know how to interpret the cortical dipoles of the 80 Hz data. Stimulation at 40 Hz and 80 Hz is known to generate subcortical responses. The high dispersion might be an effect of forcing the dipoles to be symmetrical along the x-axis. Cortical responses are

produced in symmetrical locations i.e., both auditory cortices are active during stimulation. However, subcortical responses do not necessarily present symmetry along the x-axis, symmetry could exist along a different axis or there could be a complete lack of symmetry. The restrictions added to the localisation might have increased the dispersion in the localisation accuracy at these modulation frequencies.

The obtained locations at 40 Hz and 80 Hz led to a lower precision in the localisation compared to 4 Hz, 10 Hz and 20 Hz due to the big inter-subject variability reflected in the big error bars and the big size of the clusters. The ASSR activity contained in the ICA components is produced by a numerous amount of brain sources (Reyes et al., 2005; Farahani et al., 2017). This prevented the DSS method from finding a predominant direction to extract the ASSR information. This reduction of localisation accuracy is especially noticeable for deep sources due to the depth bias present in the inverse models (De Peralta et al., 2009; Lucka et al., 2012; Fuchs et al., 1999), when the response amplitudes are intrinsically low, as for 80 Hz (Vanvooren et al., 2015). It is the same problem addressed in the section 2.4.1. Intrinsic low response amplitudes represent another obstacle that may lead to an even bigger decrease in the localisation accuracy. In low modulation frequencies, the different ICA components carrying ASSR were extracted into a few components by the DSS algorithm, representing plausibly the anatomical origin of the ASSR activity and reliably extracting the group pattern.

This analysis presents a high inter-subject variability despite the intrinsic lower spatial resolution of EEG compared to fMRI. Furthermore, it is also possible that the absence of an individual head model together with the individual electrode position information contributed to increase the source localisation variability. In addition, the position of the electrodes was rescaled manually from an adult template, considering only changes in size not in shape. Thus, the application of an age-related head model was limited by the rescaled adult geometry of the electrode position. A better estimation of the adolescent geometry also in the electrode location might lead to an improvement in the localisation accuracy. All the novel EEG techniques that aim at high precision source localisation results should consider all the limitations already mentioned. Individual head models together with the electrode geometry can increase the precision in the localisation independently of the mathematical approach used, but BEM can only be created from individual MRIs if they have an outstanding quality, which is rarely the case, normally they are obtained from averaged MRIs. Other methods

used to create head models, such as the Finite Element Method (FEM), can generate head models from individual MRIs independently of its quality and resolution. However, FEM needs much more computational resources than the BEM.

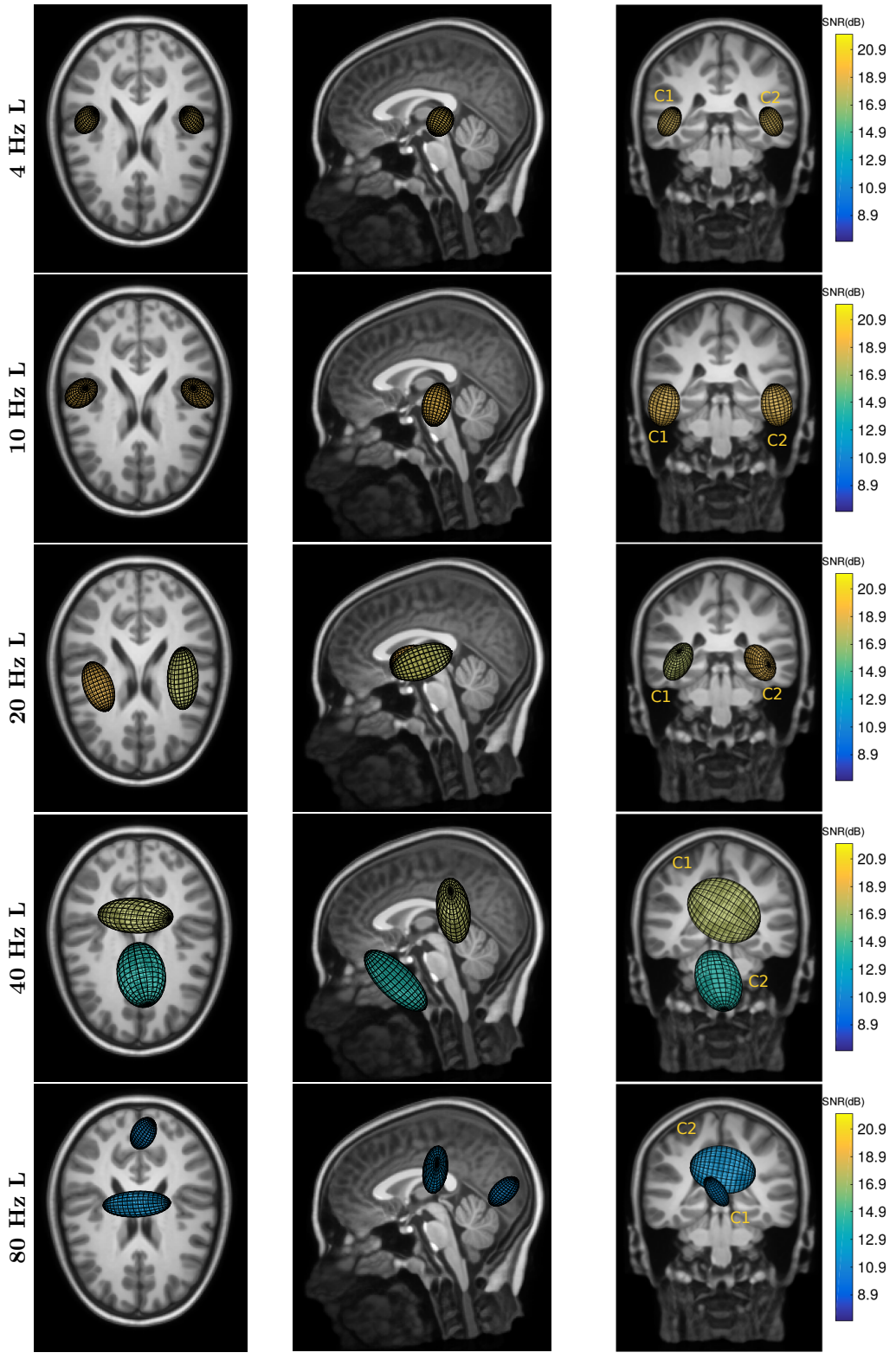


Figure 2.10: First Component cluster location for different modulation frequencies in left ear stimulation.

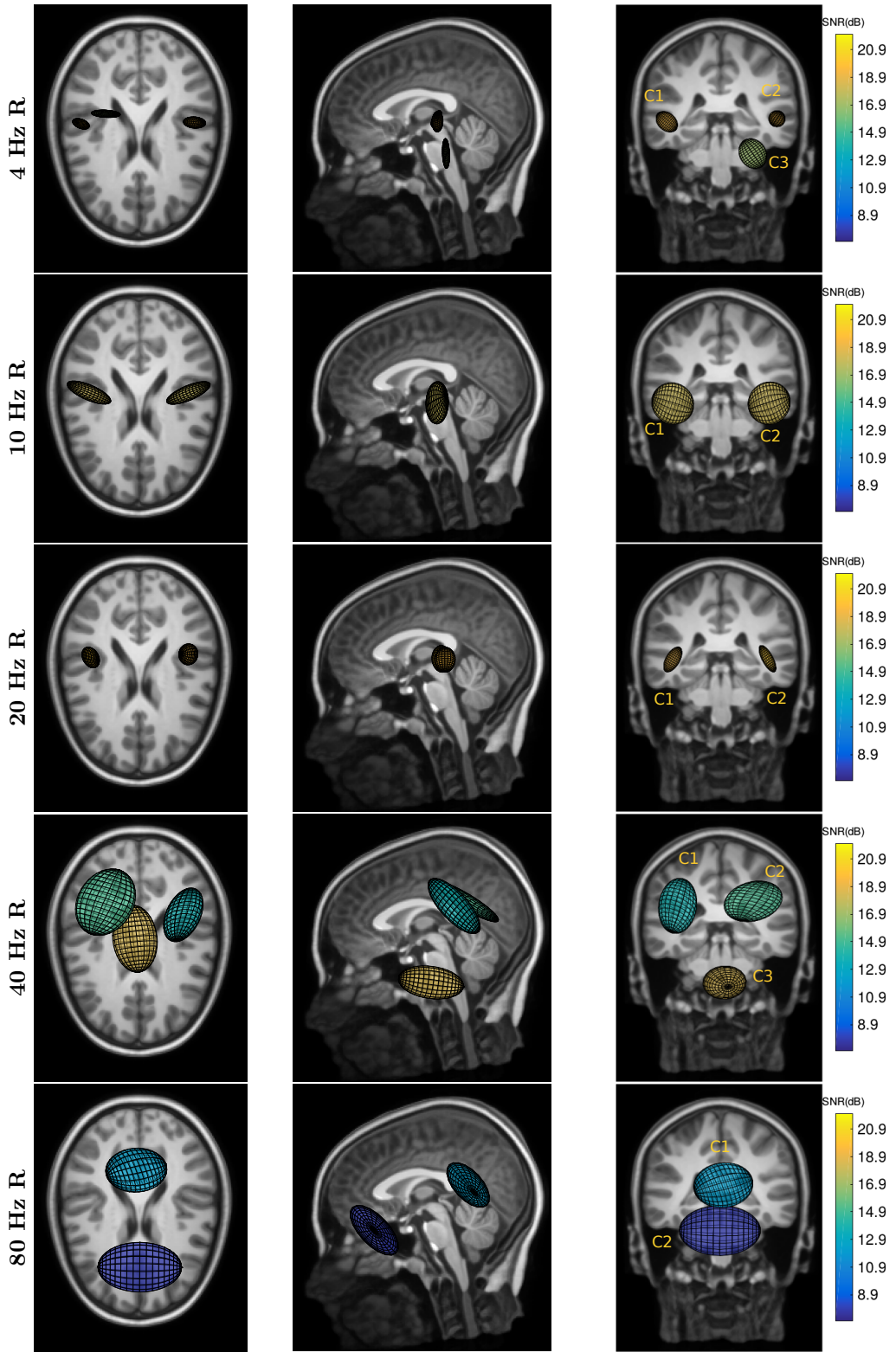


Figure 2.11: First Component cluster location for different modulation frequencies in right ear stimulation.

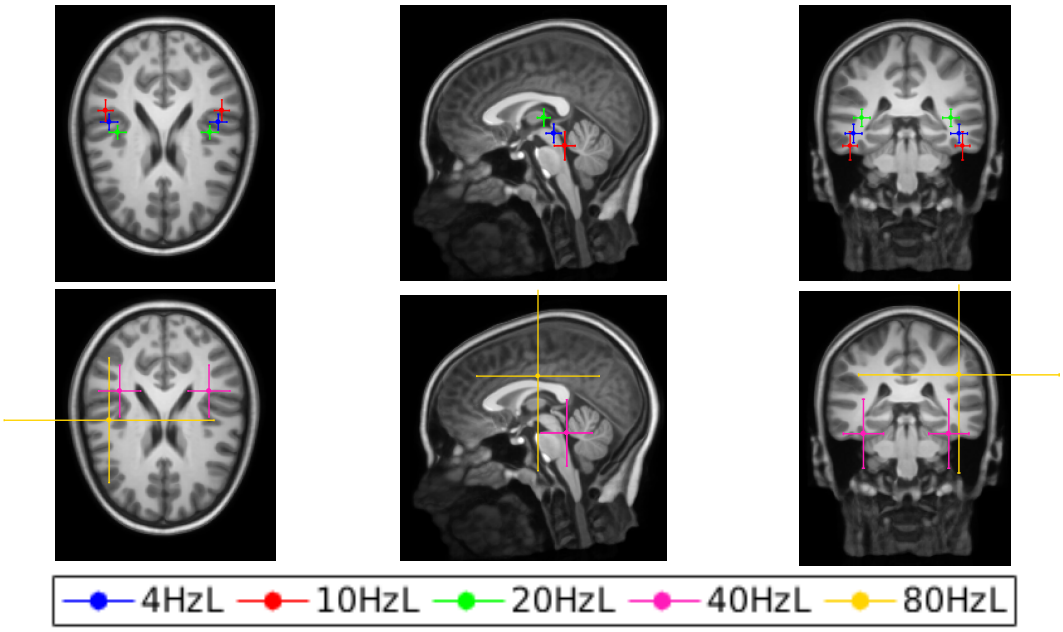


Figure 2.12: Brain coordinates of the first DSS component. Dipole locations were obtained together with the standard deviation estimates for left ear stimulation. The **top** three images represent slow modulation frequencies, 4 Hz, 10 Hz and 20 Hz while the **bottom** three were obtained for 40 Hz and 80 Hz modulation rates.

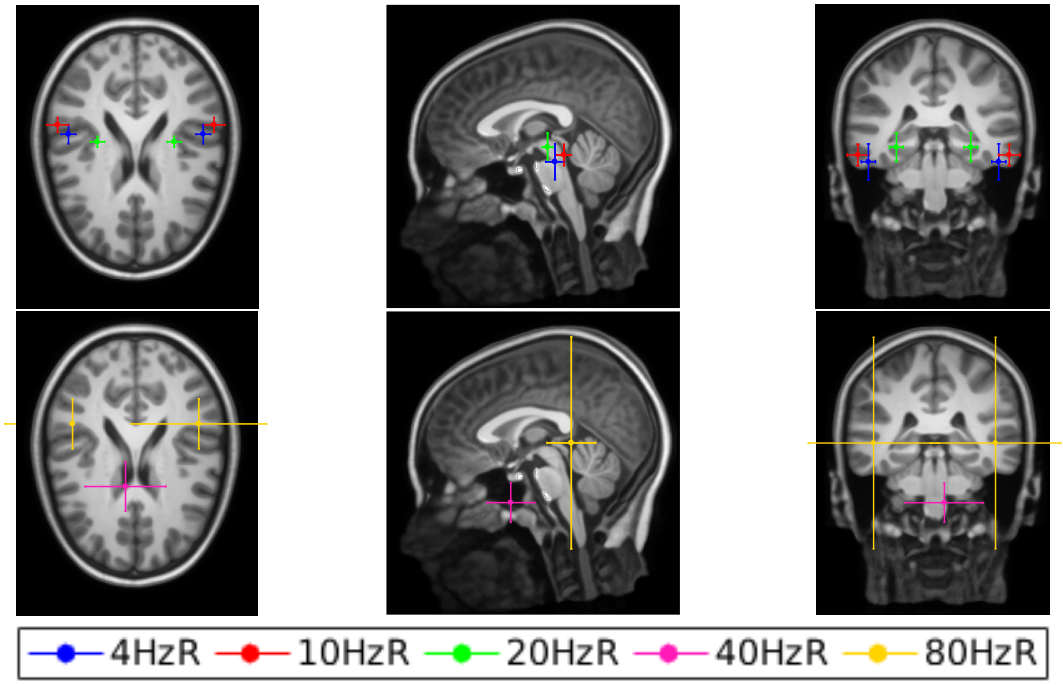


Figure 2.13: Brain coordinates of the first DSS component. Dipole locations were obtained together with the standard deviation estimates for right ear stimulation. The **top** three images represent slow modulation frequencies, 4 Hz, 10 Hz and 20 Hz while the **bottom** three were obtained for 40 Hz and 80 Hz modulation rate.

2.5 Conclusion

This chapter reports an investigation aiming at a better extraction of the most representative features that arise from ASSR stimulation as well as the reconstruction of its anatomical origin in the brain. Our approach, using DSS combined with ICA was developed for the application in studies using stimulation that is representative of the speech envelope modulations, where the main energy in the modulation spectrum of the speech envelope is situated between 4 Hz and 16 Hz (Drullman et al., 1994a,b; Shannon et al., 1995). The proposed algorithm can extract the reproducible patterns of brain activity at low modulation rates. Those rates lay within the stimulation frequency range of the speech envelope. This proposed method might replace, in ASSR studies, the search for maximum variance with a more reliable technique that involves the maximisation of reproducible activity across trials. The bias function used by DSS was based on the average across trials, it was expected that a higher number of epochs would mean a better estimation of that average. This bias function was selected due to the nature of the ASSRs, which are sustained across epochs. Any mathematical method aiming at detection of ASSRs must be able to minimise the noise using the ASSRs property of being sustained across trials. Furthermore, the method should be compatible with source localisation techniques and able to manage correlated sinusoidal sources while preserving the anatomical and physiological information. With this method we expected to "condense" the ASSR activity present in the ICA subspace into a limited number of components. Hence, the process would allow us to automatically reduce the number of components carrying ASSR to be used in further analysis. ASSR activities coming from nearby regions in the brain or equivalent generators across subjects in the ICA subspace would be merged into the DSS components. Note that this procedure will not be very useful in studies that require a very high level of detail or where the assumption that the obtained brain sources are uncorrelated cannot be accepted. However, this feature will facilitate studies based on the general trend or behaviour of a population. We first applied this technique at an individual level to study its performance in high-variability scenarios with low amounts of data. We know that by concatenating over time we are providing more samples to the whole method, something that can improve the detection and source localisation in data-driven methods. However, it is possible that by only using ICA we might be detecting not the most prominent sources in

the whole group but the most prominent sources of single subjects, each of them with region specific locations. To avoid that, we proposed the inclusion of DSS and its bias function, to ensure that the extracted waveform and related brain locations were the ones representative of the group features.

The application of DSS to ICA components consisted of the extraction of the direction maximising the evoked signal across epochs in the ICA subspace. In low stimulation frequencies, where the number of brain generators is low, ASSR is present in many ICA components. However, they are being generated in the same or in neighbouring brain regions. The high amount of properties shared as well as the low variability across subjects makes possible for the DSS to find a predominant direction in the ICA subspace and to extract those common features into a few components with good enough anatomical accuracy and relatively good precision. This extraction allows the gathering of all relevant ASSR into a few components, facilitating any further physiological interpretation of the results. When the number of independent brain sources is high, there is not one predominant direction. DSS cannot condense the ASSR activity present in the ICA responses since they are not sharing similar properties and the full oscillation pattern is very complex, all of this reduces the source localisation accuracy.

The properties shown by the outcome measures extracted from the DSS components are in line with what is known from literature in both, group and individual studies. Localisation results were restricted by the inherent limitations of EEG as well as by the scarce number of age-related head models available, which forced us to manually implement our age-related head models. However, the critical factor for the source localisation accuracy was the multiple generator problem at 40 Hz and 80 Hz. The general performance for 4 Hz, 10 Hz and 20 Hz modulation frequency showed a successful extraction of the ASSR present in ICA components and its physiological properties at the individual but more importantly at the group level that was in line with literature. The obtained results for these frequencies showed ASSR sources near the expected auditory cortex region without making any prior assumption regarding its anatomical origin as well as good SNR at the stimulation frequencies in the reconstructed time series. The results observed at high modulation frequencies invite to consider other methods that impose stricter constraints in order to successfully detect and extract all the relevant ASSR information. Since the high number of sources active, the effects of resonance

and intrinsic low-SNR signals are a challenge for all the mathematical methods eligible for ASSR studies.

2.6 Appendix

2.6.1 Appendix A

As it is shown in the Table 2.1 in the main text, the percentage of subjects with the first DSS component at the highest SNR decreases with the stimulation frequency. In the supplementary Table 2.6 below, we represent which DSS component number is carrying the highest SNR per subject for the high modulation frequencies 40 Hz and 80 Hz. A high number for more than a few subjects shows the difficulties of the method used to reliably extract ASSR information for high modulation frequencies at the individual level.

Table 2.6: DSS component number with the highest SNR at the stimulation frequency for the individual analysis.

Subjects	Stimulation Conditions			
	40 Hz L	40 Hz R	80 Hz L	80 Hz R
S1	1	3	3	5
S2	1	4	2	2
S3	2	1	1	4
S4	2	1	3	7
S5	1	1	1	8
S6	1	1	20	3
S7	1	4	11	1
S8	1	2	17	15
S9	1	1	1	5
S10	2	5	2	11
S11	1	2	10	6
S12	2	2	1	2
S13	4	3	4	21
S14	1	5	12	14
S15	2	4	1	4
S16	1	17	5	6
S17	1	1	5	4
S18	5	1	9	1
S19	5	6	3	1

2.6.2 Appendix B

In order to compare the locations provided by ICA mixing matrix with the results obtained by DSS we computed the clusters for the dipole locations of the ICA components with the highest SNR at an individual level. Results are presented in Figure 2.14 and Figure 2.15. Those clusters were calculated for the ICA components carrying the highest SNR using the same dipole fitting procedure utilised for the DSS components. By looking at the figures and comparing the clusters extracted for the ICA with the DSS clusters we can see that the cluster sizes for the ICA are bigger than DSS clusters, which are more compact. At 4 Hz left ear stimulation the components were clustered around similar regions. At 10 Hz left ear stimulation ICA components were clustered in four clusters while DSS components were only clustered in two cortical and symmetrical clusters. The two cortical clusters for ICA were located in neighbouring regions of the auditory cortex, as well as the two clusters found for DSS. For 20 Hz left ear stimulation ICA dipole location showed an extra deep cluster that cannot be found for DSS analysis. However, the cortical clusters were in both analyses, ICA and DSS, found in regions near the auditory cortex. At 40 Hz left ear the number of clusters was the same, but the configuration was different. ICA components were clustered in two cortical clusters while DSS components were located in one cortical cluster and another deep cluster. For 80 Hz left ear, two clusters were found for ICA and DSS, but ICA components had the two clusters in symmetrical and cortical regions. For 4 Hz right ear stimulation, there is one more cluster located deeply for the DSS components, the cortical clusters are located in similar cortical and symmetrical regions. For 10 Hz and 20 Hz right ear, despite the difference in size of the clusters, the number of clusters and their configuration is similar between ICA and DSS dipole configurations. For 40 Hz right ear stimulation, there are two clusters for both ICA and DSS components, but the configuration is different. ICA has one cortical cluster and two clusters located deeply while DSS produced two cortical clusters and one deep. For 80 Hz right ear, the same number of clusters was found, however, ICA components were clustered symmetrically near cortical regions. In summary, DSS can improve the SNR of the components and automatises the component selection procedure. Dipole locations, especially for low modulation frequencies, do not show large differences, except the presence of extra clusters for some conditions in ICA dipole fitting configuration. Also, more compact

clusters were found after DSS. We can conclude then that the application of DSS improves the detection of ASSR by enhancing the SNR and finding a ranking criterion that allows DSS components carrying ASSR to be ranked first. However, the application of DSS after the computation of ICA increases the compactness of the location results. This means that the search for the most reproducible activity across trials diminishes the inter-subject variability, making this technique more suitable for the search of common patterns among subjects in a group under study and less suitable for analyses that have the study of individual features as the main goal.

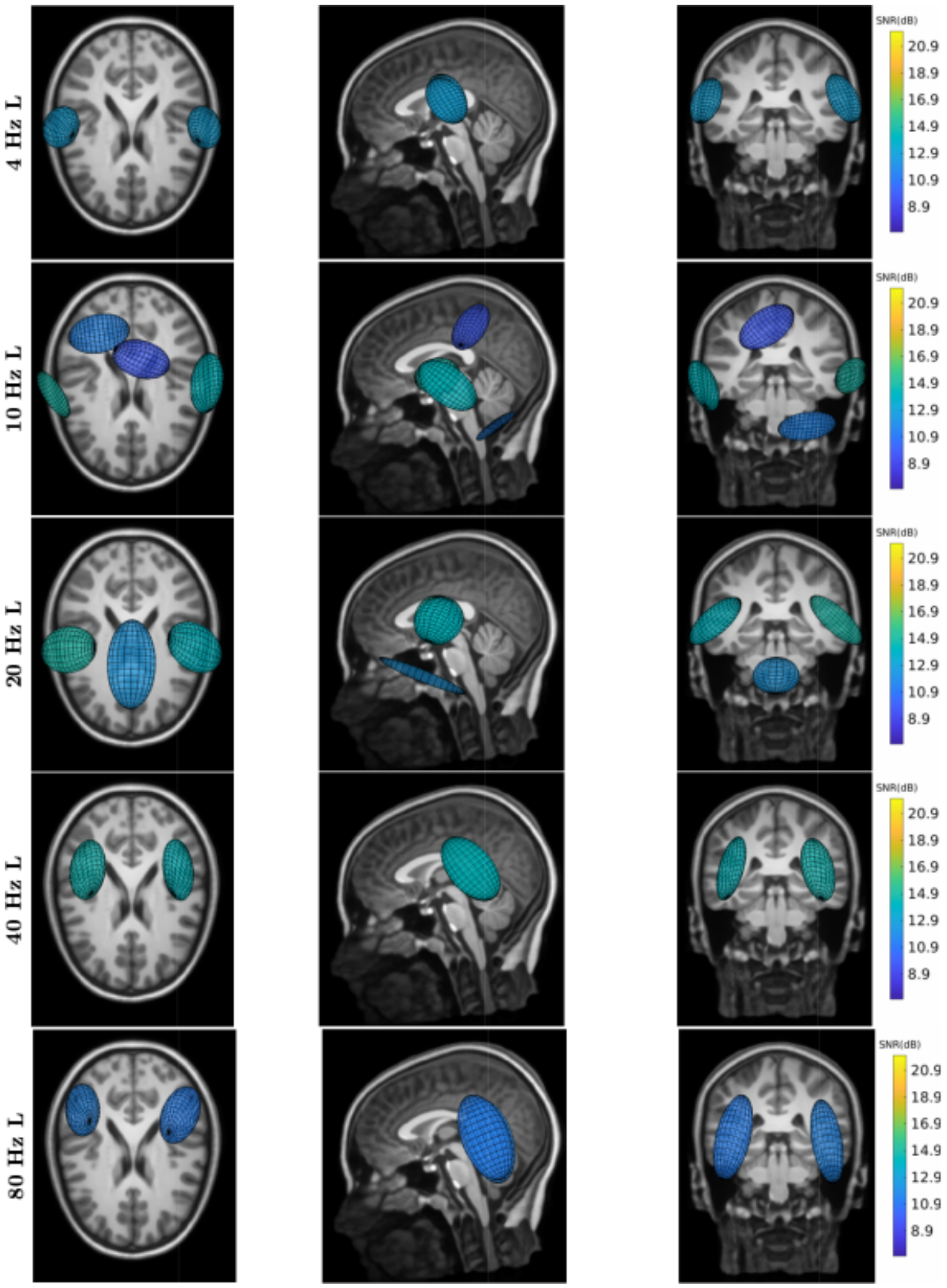


Figure 2.14: Cluster locations of ICA components with the highest SNR obtained from ICA mixing matrix at an individual level for left ear stimulation

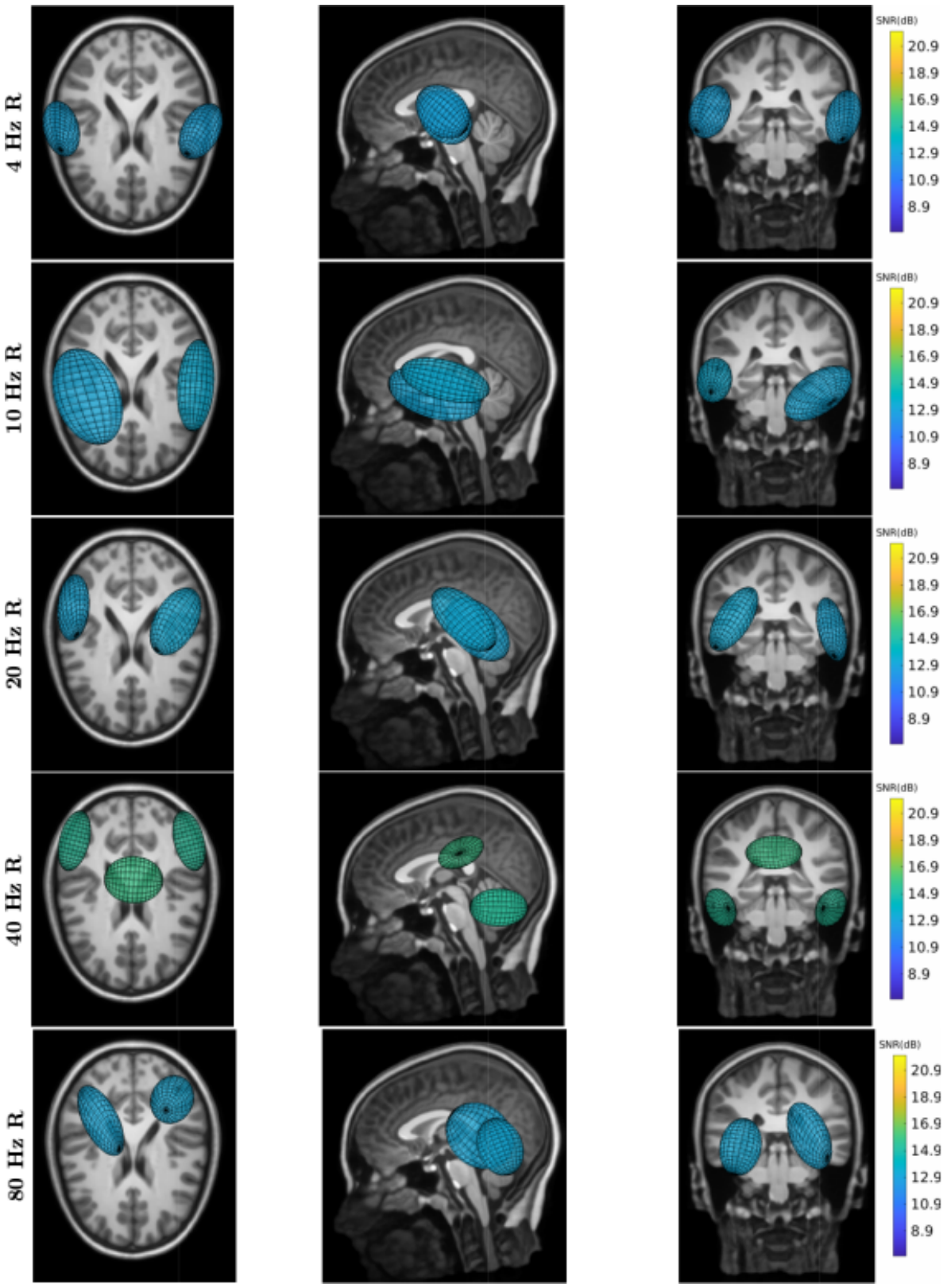


Figure 2.15: Cluster locations of ICA components with the highest SNR obtained from ICA mixing matrix at an individual level for right ear stimulation

CHAPTER 3

Atypical processing in neural source analysis of speech envelope modulations in adolescents with dyslexia.

The contents of this chapter have been adapted from the work published in Granados Barbero, et al. (2021): "Atypical processing in neural source analysis of speech envelope modulations in adolescents with dyslexia." European Journal of Neuroscience, (October), 1–21.

Abstract

Different studies have suggested that language and developmental disorders such as dyslexia are associated with a disturbance of auditory entrainment and of the functional hemispheric asymmetries during speech processing. These disorders typically result from an issue in the phonological component of language that causes problems to represent and manipulate the phonological structure of words at the syllable and/or phoneme level. We used Auditory Steady-State Responses (ASSRs) in EEG recordings to investigate the brain activation and hemisphere asymmetry of theta, alpha, beta and low-gamma range oscillations in typical readers and readers with dyslexia. The aim was to analyse whether the group differences found in previous electrode level studies were caused by a different source activation pattern or conversely was an effect that could be found on the active brain sources. We could not

find differences in the brain locations of the main active brain sources. However, we observed differences in the extracted waveforms. The group average of the first DSS component of all signal-to-noise ratios of ASSR at source level was higher than the group averages at the electrode level. These analyses included a lower alpha synchronisation in adolescents with dyslexia and the possibility of compensatory mechanisms in theta, beta and low-gamma frequency bands. The main brain auditory sources were located in cortical regions around the auditory cortex. Thus, the differences observed in auditory EEG experiments would, according to our findings, have their origin in the intrinsic oscillatory mechanisms of the brain cortical sources related to speech perception.

3.1 Introduction

Neural temporal coding is essential for speech processing, and it is key for the development of phonological representations. A phonological representation is the mental representation of the sounds and combinations of sounds that comprise words in a particular spoken language (Goswami, 2012). In phase-locked stimulation experiments, entrainment is an important characteristic of interactions between brain rhythms and refers to the coupling of two independent oscillatory systems in such a way that their periods of oscillation become related by virtue of phase alignment (Cummins, 2009). The word synchronisation can be used sometimes instead of entrainment since it also shows how the brain rhythms respond to external oscillatory activity. A higher entrainment or synchronisation of the brain to external oscillatory stimulation usually means higher brain responses at the frequencies of stimulation. With neural entrainment, we refer to evoked oscillatory activity at the same frequency as the stimulation frequency; higher entrainment means higher oscillatory activity at the stimulation frequency. In this way, we use the wording neural entrainment in the broad sense as it was defined in Obleser & Kayser (2019). The process of neural entrainment to the temporal modulations of speech is believed to make temporal coding possible (Giraud & Poeppel, 2012). The temporal information of the speech envelope is in essence a form of amplitude modulation, principally between 2 Hz and 50 Hz (Rosen, 1992). Syllabic pattern information is contained between 2 Hz and 12 Hz (Edwards & Chang, 2013), and phonemic pattern information lays in the frequency range between 12 Hz and 50 Hz (Chait et al., 2015). Theories about speech perception suggest

that speech-related modulation frequencies are processed asymmetrically in the auditory cortices, with a right hemispheric preference to process those syllabic rate modulations (Boemio et al., 2005; Poeppel, 2003), whereas a symmetrical pattern is found during the processing of phoneme rate modulations (Jamison et al., 2006; Obleser et al., 2008). In the last years, different studies have suggested that a disturbance of this functional hemispheric asymmetries and of the auditory entrainment during speech processing can be observed for language and reading disorders such as dyslexia (Giraud & Poeppel, 2012; Goswami, 2011). Developmental dyslexia is a neurological and hereditary disorder characterised by difficulties with accurate and fluent word reading and by poor spelling and decoding abilities (Eden et al., 2016). These difficulties typically result from a difference in the phonological component of language that causes problems to represent and manipulate the phonological structure of words at the syllable and/or phoneme level (Vandermosten et al., 2020; Vellutino et al., 2004). To assess the relationship of differences in the synchronisation of speech-related neural oscillations with dyslexia, prior studies have investigated different oscillatory ranges. Modulations around 4 Hz are the most prominent for syllable rate processing, and they also are key for accurate speech perception (Drullman et al., 1994a,b). Studies using this modulation frequency did not find differences in neural synchronisation of theta rhythms in pre-reading children with a genetic risk for dyslexia (De Vos et al., 2017a; Vanvooren et al., 2014) neither in adults (Hämäläinen et al., 2012; Lehongre et al., 2013; Poelmans et al., 2012a). On the other hand, to evaluate the phoneme rate, processing modulations of 20 Hz and higher have been used. It has been proposed that readers with dyslexia might present a lower neural entrainment in the gamma band, which might limit the representation of phonemic units (Giraud & Poeppel, 2012). However, inconsistent conclusions can be found in studies using beta and low-gamma stimulation. In some studies, participants with dyslexia showed reduced synchronisation in the left hemisphere (Lehongre et al., 2011; Poelmans et al., 2012a), higher synchronisation in the right hemisphere (Lizarazu et al., 2015), no overall synchronisation differences (Hämäläinen et al., 2012) or an overall lower synchronisation (McAnally & Stein, 1997; Menell et al., 1999). All the presented findings might lead to the conclusion that a dyslectic brain could present atypical synchronisation behaviour in beta and low gamma while no clear differences would be expected in theta stimulation. Although it has been hypothesised that alpha rhythms play an important role in neurophysiological mechanisms of speech segmentation, sometimes even

a more important role than theta oscillations (Dimitrijevic et al., 2017; Shahin & Pitt, 2012), only a few studies are reported about auditory neural synchronisation of alpha rates (8 Hz-13 Hz) within the dyslexia research field. Furthermore, syllable rate information can be encoded within these alpha rates, in frequencies up to 12 Hz, in the speech envelope.

Amongst other measures, neural entrainment to speech-related temporal modulations can be measured from the amplitudes of the Auditory Steady-State Responses (ASSR) as recorded using EEG or MEG. ASSRs are phase-locked neural responses to periodic auditory stimulation (Picton et al., 2003). Large amplitudes at the modulation frequency are considered a result of high neural entrainment (Alaerts et al., 2009; Van Hirtum et al., 2019a; Vanvooren et al., 2014) and have been used in studies in dyslexia research (De Vos et al., 2017b; Lehongre et al., 2011; Poelmans et al., 2012a). These studies analysed the information at the scalp level and involved the measurement of the response amplitudes, the noise level and the overall signal-to-noise ratio at the modulation frequency, and they also added some information regarding the neural entrainment. However, the activity recorded at the electrode level is a combined potential of multiple brain sources being active simultaneously at different loci in the brain. Although some differences between groups that can be found at the electrode level might not be detectable at a source level, identical events observed at the electrode level may have different causes that could be revealed by a source analysis. We hypothesise that a source level analysis will provide essential supplementary information and will reveal different underlying causes and interpretations of effects observed at the electrode level. More specifically in this study, we will investigate a dyslexia research question based on extended brain source activity analyses of electrode level EEG recordings. A group of adolescents with dyslexia will be compared with typically developing adolescents by stimulating at modulation frequencies related to speech perception and taking various measures of the neural synchronisation to the temporal modulation of the stimulation. We will use the method introduced in chapter 2 to investigate whether the group differences found in previous electrode level analyses are caused by a different source activation pattern or conversely it is an effect that can be found on the activity of the ASSR brain sources. In case the latter applies, that would mean an inherent alteration of the neural entrainment. To this end, with a source level method, we will re-analyse the data used in De Vos et al. (2017b), in which no group differences were found when stimulating with frequencies contained in theta and low-gamma rhythms. However, atypical

alpha and beta range synchronisation were found. At electrode level that study revealed that readers with dyslexia present significantly reduced neural synchronisation responding to a stimulation whose modulation frequency lies in the alpha oscillation range. It was also found that the readers with dyslexia presented significantly enhanced neural synchronisation when stimulated with a frequency contained in the beta rhythm. As an addition of measuring the SNR, a measure for connectivity between the main ASSR brain generators might provide with some additional information about the level of synchrony of the main activity evoked by our stimulation, as it was performed in Thiede et al. (2020), where connectivity was used in combination with MEG.

The present study explores the origin of these effects at the level of the brain sources. This will be achieved (1) through source localisation, (2) through the estimation of the hemispherical preference of the ASSR sources using a Laterality Index and through the measure of neural entrainment combining the results provided by the (3) SNRs and the (4) Phase Coherence. These two last methods will provide information of the main ASSR generators oscillatory activity. One will measure the evoked responses compared to the background noise, and the second will quantify the connectivity by measuring the phase difference variability of the main ASSR brain generators. We also calculated the SNR for the individual data to clarify the effect of performing a group analysis based on concatenated data versus computing it based on the superposition of the individual data. We aim to illustrate how the concatenation of data attenuates individual differences affecting variance and, thus, the final result.

3.2 Materials and Methods

3.2.1 Data acquisition

Participants

Fifty-four adolescents participated in this study, 22 (10 male and 12 female) typical reading adolescents (TR) and 32 (15 male and 17 female) adolescents with dyslexia (DR). Participants of both groups were matched in age. The mean age of the typical reading participants was 14.75 years, and for the participants with dyslexia, the mean age was 14.66 years old. All subjects presented bilateral normal hearing, a normal non-verbal intelligence (IQ score $\geq$ 80)

and neither history of neurological disorders nor brain injury.

Participants were classified as typical readers or readers with dyslexia based on their history of reading problems and their current reading performance. For more details on the participants and the informed consent, we refer to De Vos et al. (2017b). This study was approved by the Medical Ethical Committee of the University Hospitals of Leuven. All participants and their parents gave written informed consent.

Auditory steady-state responses

Auditory Steady-State Responses (ASSRs) are phase-locked electro-physiological responses from the brain, evoked by a periodically varying continuous auditory signal, typically a sinusoidally modulated sound (Rance, 2008). The responses are a waveform with the same periodicity as the auditory signal that appear in the frequency domain at the modulation frequency (Picton et al., 2001) and can be measured in the electroencephalography (EEG) and magneto-encephalography (MEG) recordings.

ASSRs allow an objective investigation of auditory temporal processing in the brain and brainstem by adjusting the stimulation parameters to match important speech-related components (Lins & Picton, 1995). Because of that reason ASSRs have been suggested to provide an objective measure for the ability of the auditory system to encode the different time scales represented in the speech envelope (Miyazaki et al., 2013; Tang et al., 2016a,b). A number of studies have indeed demonstrated significant correlations between ASSRs and speech perception (Alaerts et al., 2009; Dimitrijevic et al., 2004; Manju et al., 2014; Poelmans et al., 2012a), thereby consolidating the link between low-level auditory temporal processing and speech perception.

Stimulation

The stimuli used in the present study consisted of amplitude modulated speech-weighted noise. The carrier noise was adopted from the *Leuven Intelligibility Sentence Test* (LIST) (Van Wieringen & Wouters, 2008). This carrier noise represents the long-term average speech spectrum of all sentences of the female speaker with LIST readings. The speech-weighted carrier noise was 100% amplitude modulated at approximately 4 Hz, 10 Hz, 20 Hz, frequencies

representative of the speech envelope, then 40 Hz, which triggers the highest cortical as well as subcortical responses and finally 80 Hz, which mainly triggers responses at the brainstem level. The spectrum (dB/Hz) of the carrier wave, as well as the time signals of the modulated stimuli are shown in figure 3.1. All stimuli were presented at 70 dB SPL through insert earphones monaurally to the left or to the right ear.

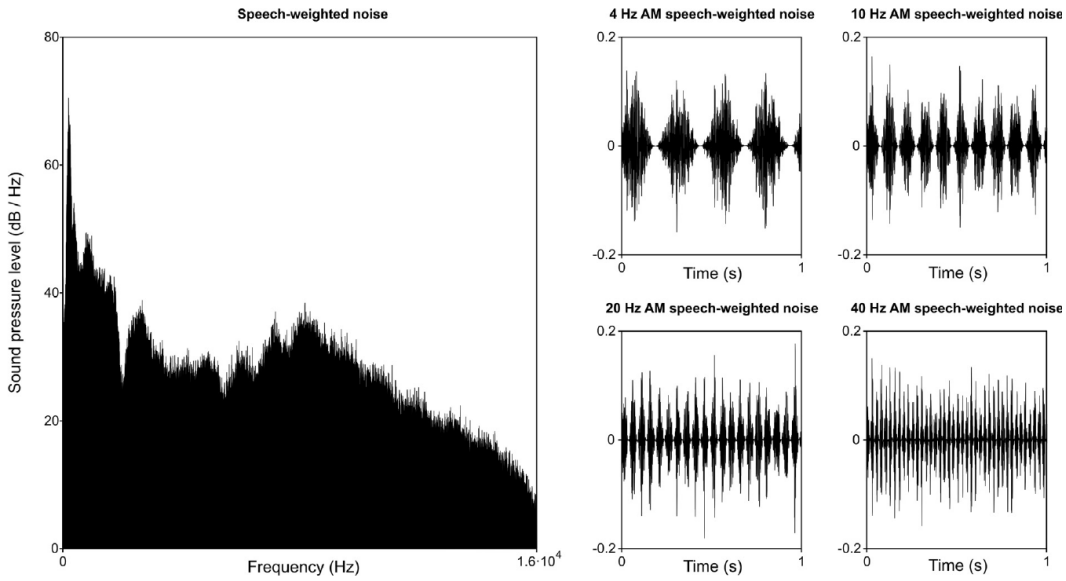


Figure 3.1: Stimulus parameters. The **panel on the left** shows the spectrum of the speech-weighted carrier noise adopted from LIST. The **panels on the right** show a 1 s time signal of different frequencies of the amplitude modulated stimuli. Syllabic rate modulation (4 Hz & 10 Hz) at the top, and phonemic rate modulations (20 Hz & 40 Hz) at the bottom, (De Vos et al., 2017b).

Recording System

EEG data were recorded with the BioSemi ActiveTwo system using 64 active Ag/AgCl electrodes mounted in head caps according to the 10–10 electrode system with a sampling frequency of 8,192 Hz. Electrode offsets were kept below 30 mV. All recordings were administered in a double-walled soundproof booth with a Faraday cage. Participants were asked to lie down on a bed while watching a soundless film to warrant the same level of alertness and attention throughout the EEG measurement (Vanvooren et al., 2014; Poelmans et al., 2012b; Goossens et al., 2016). For each subject, a total of 8 EEG measurements (4 modulation frequencies $\times$ 2 stimulation modalities) were collected. Each measurement consisted of a 5-min (300 s) EEG recording. In the present study, bilateral stimulation was not considered to avoid simultane-

ous activation of both auditory pathways. Thus, monaural stimulation to the left and right ears separately was considered for this study.

3.2.2 Pre-processing

A common pre-processing procedure was applied to all data using MATLAB. First, EEG signals were filtered using a zero-phase high-pass Butterworth filter with a cut-off frequency of 2 Hz and a slope of 12 dB/Octave to exclude distortions caused by skin potentials and the DC component of the amplifier. The filtered signal was segmented into different epochs with a length of 1.024 s; the result of this segmentation was an array that ranged of 292 epochs per electrode. Next, 10% of the epochs showing the highest peak-to-peak amplitude as well as incomplete and very artefactual epochs were rejected, resulting in a total amount of 256 epochs per electrode and per subject. From these 256 epochs, we applied the following steps: The mean Peak to Peak (PtoP) amplitude was calculated for each channel separately. Any channel with a mean PtoP four times greater than the median PtoP of all the channels was rejected; any subject with rejected channels was discarded. The aim was to obtain 128 epochs with the lowest amount of artefacts in all the channels. To do that, we considered the 128 epochs showing the lowest absolute amplitude. If one of these selected epochs had reached a maximum threshold of 120 μV, the subject was discarded. Seven subjects, four with dyslexia and three without dyslexia were not considered for further analysis due to their high number of epochs with high-amplitude artefacts. The remaining 47 participants (19TR, 28DR) presented enough clean epochs for all stimulation conditions and were included in the study. Thus, the accepted 128 epochs per subject were concatenated along the time dimension separately for the two groups, resulting in a total array of 2,432 epochs for the typical readers group and 3,584 epochs per EEG electrode for the adolescents with dyslexia. After the epoch-based artefact rejection, all the electrodes were referenced to the C_z electrode. This reference was used over the average reference based in previous studies that stated that C_z reference lowers the noise estimates around the stimulation frequency reducing the detection threshold for ASSRs (Van der Reijden et al., 2005; Van Dun et al., 2009; Poelmans et al., 2012b).

3.2.3 Source Activity Reconstruction

To extract the most prominent ASSR source activity from the concatenated data, we used a combination of Independent Component Analysis (ICA) and Denoising Source Separation (DSS) applied to temporally concatenated data of the two different groups: adolescents with and without dyslexia, for all the stimulation conditions separately, as was suggested in chapter 2. With this combination, we aimed to extract the most reproducible ASSR across epochs for the whole group. ICA decomposes EEG data, which are linearly mixed due to volume conduction, into an array of maximally independent components (Onton, 2009). The brain source localisation and projection weights were assumed to be spatially stationary for the duration of the experiment (Onton et al., 2006). The Infomax algorithm was utilised in FieldTrip (Oostenveld et al., 2011) due to its fast and reliable performance (Bell & Sejnowski, 1995). Since we applied ICA to temporally concatenated data, we were performing what it is known as group-ICA. For group-ICA, we applied ICA to temporally concatenated data from all the subjects (Delorme & Makeig, 2004). This selection assumes a similar geometrical distribution of the sources since the mixing matrices for all subjects must be identical (Huster et al., 2015). The number of output components equalled the number of input channels, which were 63 per stimulation condition. After computing the ICA a one-sample Hotelling $t-$squared test was performed; see section 3.2.5. Components that did not show significant ASSR were rejected.

After computing ICA we input the accepted components into the DSS algorithm. DSS performs a separation of the data into desirable components (signal) and undesirable components (noise), assuming linearity of the coefficients and of the DSS components (Särelä & Valpola, 2005).

To increase the sensitivity of DSS towards phase-locked ASSR, we used a bias function. This bias function was chosen to be the *proportion of epoch-averaged (evoked) activity* (de Cheveigne & Simon, 2008). This bias function represented the total-power reproducibility across epochs. It allows ranking the DSS components according to the most consistent activity along epochs. Since the stimulation during the experiment was periodical and consistent across epochs, we expected the activity of the main ASSR phase-locked generator to be ranked first. The result obtained from the DSS algorithm is an array of components sorted

by decreasing total-power reproducibility across epochs. In order to determine whether these DSS components were carrying ASSR, a one-sample Hotelling $t-$squared test was performed; see section 3.2.5.

The projection weights of the components obtained through DSS and ICA analyses were fitted to equivalent current dipoles using the neuromag coordinates, see figure 3.2. Two symmetrical dipoles along the x axis was the default configuration as long as the distance between them was more than 20 mm; the one dipole configuration was selected otherwise. This dipole fitting procedure was performed using a Boundary Element Method (BEM) as a head model (Meijs et al., 1989; Hämäläinen & Sarvas, 1989). This BEM conductivity model was created in FieldTrip from 14-year-old adolescents averaged MRI images (Richards et al., 2016; Sanchez et al., 2012). The BEM model described the electrical properties of the scalp, skull and brain and the conductivity values chosen for these tissues, which were 0.3300, 0.0042 and 0.3300 S/m respectively (Gabriel et al., 1996).

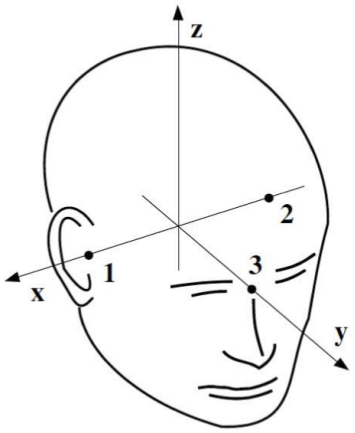


Figure 3.2: Neuromag coordinate system.

In order to estimate bias and variance for all the dipole directions (x, y, z), first, for the mean value of the distribution, we calculated the location of the sources, per DSS component, per stimulation condition and per group separately using all concatenated data. Then, we estimated the variance applying the jackknife approach; see section 3.2.5 for more information, separately for each direction. This gave us an estimation of the deviation from the mean of the whole group for each direction (x, y, z).

3.2.4 Outcome Measures

In this study, we investigated response strength, Phase Coherence (for quantifying connectivity) and Laterality Index (for lateralisation) as main outcome measures.

Response SNR

The measured relative response amplitudes, obtained from the square root of the signal power at the frequency of stimulation, and the Signal to Noise Ratios (SNRs) were calculated from the DSS components carrying significant ASSR. We obtained these responses and SNR from the concatenated data for all the stimulation conditions and all frequencies. We also calculated the SNR at the individual level to show how the concatenation of data attenuates individual differences (individual variance) affecting the final result. The response amplitudes were obtained by taking the square root of the signal power. The signal power, P_S, was calculated from the Hotelling t-squared statistic. It represents the squared amplitude of the responses mean across all the data epochs at the bin of the modulation frequency. We selected the Hotelling t-squared statistic because it uses a similar criterion to find significant activity as the DSS bias function does: Brain activity that appears consistently across the trials is maximised. The noise floor amplitude, P_N, required to compute the signal to noise ratio, was estimated from the Hotelling t-squared statistic and shows the standard error of the amplitude responses at the modulation frequency mf across n epochs, being: $\sigma(R_{mf})/\sqrt{n}$. Based on the definition of power response and noise amplitude, the SNR may be defined as the ratio between the power of the response signal and the power P_N of the EEG noise, equation 3.1.

$$SNR = \frac{P_S}{P_N} = \frac{\|mean(R_{mf})\|^2}{\left(\frac{\sigma(R_{mf})}{\sqrt{n}}\right)^2} \tag{3.1}$$

Where R_{mf} is a complex vector containing the responses at the modulation frequency of all epochs, σ is the standard deviation of R_{mf} and n is the number of epochs.

Phase Coherence

Phase coherence is a measure for connectivity and represents the inter-trial variability of the phase difference between two signals for a specific frequency (Picton et al., 2001). Phase

coherence shows how stable the difference between the phase of two signals is. It can describe the phase-locking capability of a neural source (Koerner & Zhang, 2015). We will measure the phase coherence between the first two DSS components. Components 1 and 2 carry the highest SNR of all the components as well as the highest reproducibility power ratios. This means those two components will give us an overall model or estimation of most of the ASSR activity (in terms of energy/amplitude) triggered by our stimuli. The phase coherence would measure the neural interaction of the activity generated during stimulation. Higher values would imply a higher synchronisation or joint effort towards 'decoding' or processing the stimulus. The phase coherence was computed after averaging segments of data into 32 epochs, as suggested in Picton et al. (2001). The phase of each epoch was obtained from the complex representation of the neural response in the frequency domain. Phase coherence was calculated according to equation 3.2, (Picton et al., 2001).

$$PhCoh = \frac{1}{n}\sqrt{\left(\sum_{i=1}^{n} cos\ \theta_i\right)^2 + \left(\sum_{i=1}^{n} sin\ \theta_i\right)^2} \tag{3.2}$$

Where $\theta(f, i)$ represents the phase difference between the two signals; in our case, these signals would be the first and the second DSS component; this can be expressed as $\phi_1(f, i) - \phi_2(f, i)$. This difference will be averaged across n epochs.

Laterality Index

To estimate the lateralisation of the extracted sources, the Laterality Index (LI) was computed. The dipole fitting procedure estimated the neural origin for the DSS components. This neural origin could be modelled by one or two symmetrical dipoles, as it was mentioned in the dipole fitting section. For components whose origin was modelled by two symmetrical dipoles, we defined the LI based on the dipole magnitudes as it is shown in Equation 3.3. For components modelled by only one dipole, we calculated the LI based on the obtained responses and the noise level of the extracted component. If the dipole was in the right hemisphere ($x_{dip} > 0$), the noise floor was used to estimate the neural response of the left hemisphere, see equation 3.4. If the dipole was in the left hemisphere ($x_{dip} < 0$), the noise floor was used to estimate the neural response of the right hemisphere, see equation 3.5. Either with one or two dipoles an LI of +1 represents a response completely lateralised to the right hemisphere and an LI of

-1 represents a response completely lateralised to the left hemisphere.

$$LI = \frac{mag_{right} - mag_{left}}{mag_{right} + mag_{left}} \tag{3.3}$$

$$if\ x_{dip} > 0\ then\ LI = \frac{\sqrt{P_{S+N}} - \sqrt{P_N}}{\sqrt{P_{S+N}} + \sqrt{P_N}} \tag{3.4}$$

$$if\ x_{dip} < 0\ then\ LI = \frac{\sqrt{P_N} - \sqrt{P_{S+N}}}{\sqrt{P_N} + \sqrt{P_{S+N}}} \tag{3.5}$$

3.2.5 Statistical methodology

Detecting significant ASSR responses

To determine whether the ICA or the DSS components were carrying ASSR or not, the one-sample t-squared Hotelling test was performed in the frequency spectrum of the components (Hotelling, 1931). These spectra were obtained by means of a Discrete Fourier Transformation. The statistical test compared the complex responses at the modulation frequency bin across n different epochs, see equation 3.1.

Obtained components were considered to have ASSR activity when the Hotelling t-squared test showed a significant difference ($\alpha \geq 0.05$) between the squared mean of the response, numerator of the equation 3.1, and the squared Standard Error of the R_{mf} distribution, denominator of the equation 3.1 (Hofmann & Wouters, 2012).

Error estimation for group analysis

Since we concatenated all subject's data per condition, we would obtain only one data point for each of these conditions. In order to estimate the dispersion of the obtained data, we used the Quenouille and Tukey jackknife approach (Miller, 1974). This procedure creates a distribution based on performing the same analysis as many times as subjects plus one. The first data point is obtained by removing the corresponding epochs of sub- ject one, the second data point by removing the epochs of subject two and so on. This approach provides us with an estimation for the dispersion of a measurement. This means that for each measurement, we will have a distribution associated that would express how good that measurement represents a feature that is common to the whole group. The estimation of bias and variance (σ_{JK})

for the group analysis is calculated as follows. The standard deviation from the mean value, which is the value including all M subjects, was estimated from the jackknife estimate of variance; see equation 3.6. This jackknife statistic estimation is assumed to have a normal distribution (Efron & Stein, 1981).

$$\sigma_{JK} = \sqrt{\frac{M-1}{M}\sum_{m=1}^{M}[\zeta_m - \zeta_{all}]^2} \tag{3.6}$$

Where ζ_{all} represents the data of all subjects and ζ_m represents the data for one subject; M is the total number of subjects.

Two tailed t test

Based on the mean and standard deviations extracted using the jackknife procedure for all the outcome measures, we calculated the significance of the differ- ences between the control group (TR) and the group with dyslexia (DR) as follows. First, we calculated the degrees of freedom based on the samples available for each group:

$$d = M_{TR} + M_{DR} - 2 \tag{3.7}$$

With M_{TR} and M_{DR} being the total number of typical readers and readers with dyslexia, respectively. Second, we calculated the T-statistic using the means, μ, and the standard deviations, σ:

$$T = \frac{\mu_{TR} - \mu DR}{\sqrt{\frac{\sigma^2_{TR}}{M_{TR}} + \frac{\sigma^2_{DR}}{M_{DR}}}} \tag{3.8}$$

In order to calculate the two-tailed statistical test, first, the probability distribution was created based on the parameters of the samples. To calculate it, the incomplete beta function $I_X(z, w)$ was used, defined in Equation 3.9:

$$I_X(z, w) = \frac{1}{B(z, w)}\int_0^x t^{z-1}(1-t)^{w-1}dt \tag{3.9}$$

where $B(z, w)$ is the beta function, and it is defined as Equation 3.10 shows:

$$B(z,w) = \int_0^1 t^{z-1}(1-t)^{w-1}dt = \frac{\Gamma(z)\Gamma(w)}{\Gamma(z+w)} \tag{3.10}$$

with $\Gamma(z)$ is the gamma function.

The p values are then the result of using Equations 3.9 and 3.10 together with the following parameters:

$$x = \frac{d}{T^2}; \quad z = \frac{d}{2}; \quad w = 0.5 \tag{3.11}$$

These parameters allowed to define the Equation 3.9 as a normal probability distribution based on the joint means and standard deviations obtained from the jackknife estimates, Equation 3.6 of all the outcome measures. Thus, the combination of these parameters and the joint means and standard deviations would show through Equation 3.9 the probability of the outcome measures to be significantly different between the two groups. The Bonferroni-Holm (Holm, 1979) correction was applied to all stimulation conditions every time we performed a multiple comparison.

3.3 Results

3.3.1 Source Localisation

The dipole locations obtained for the first component in both population groups can be found in figure 3.3 for left ear stimulation and in figure 3.4 for right ear stimulation. The group of readers with dyslexia shows a higher dispersion at 10 Hz represented by the noticeable bigger error bars in left and right ear stimulation. However, the averaged location for all the subjects obtained for all the stimulation frequencies were in the temporal gyrus for both groups. There were some exceptions: For the typical readers, 40 Hz left ear stimulation had its sources located in the right and left fusiform gyrus, 40 Hz right ear stimulation presented one source in the brainstem. For the group with dyslexia, one source near the brainstem was found at 40 Hz left and right ear stimulation; for 10 Hz left ear, the centre of the sources was found near the brainstem as well.

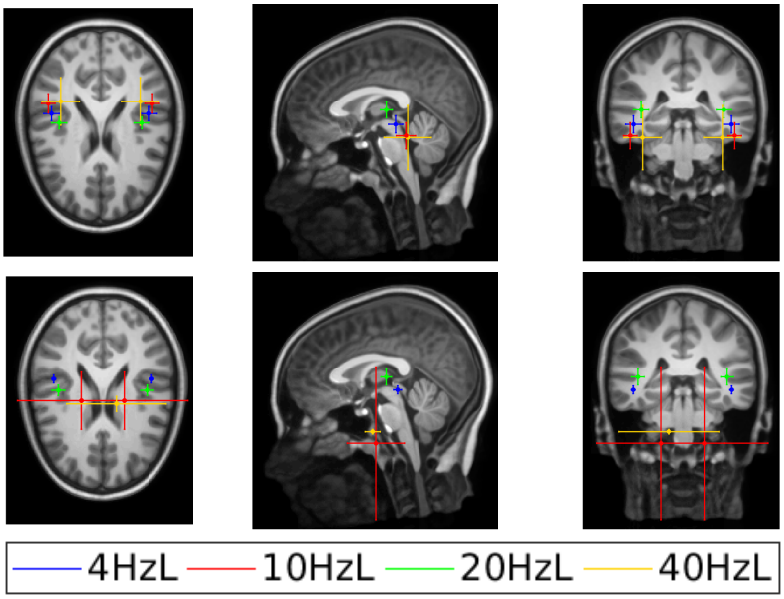


Figure 3.3: Brain coordinates of the first DSS component. Dipole locations were obtained together with the standard deviation estimates for left ear stimulation. The **top row** shows the dipole locations for the group of typical readers. While the **bottom row** shows the dipole locations obtained for the group of readers with dyslexia.

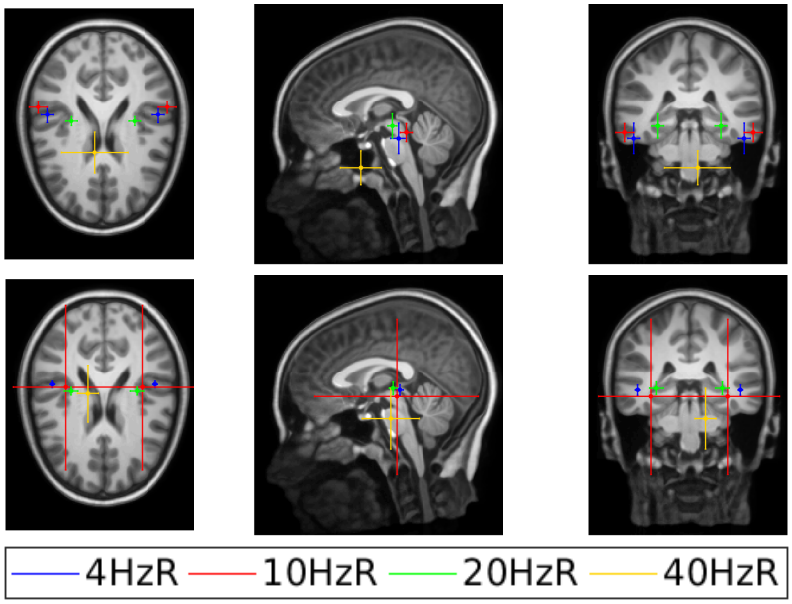


Figure 3.4: Brain coordinates of the first DSS component. Dipole locations were obtained together with the standard deviation estimates for right ear stimulation. The **top row** shows the dipole locations for the group of typical readers. While the **bottom row** shows the dipole locations obtained for the group of readers with dyslexia.

3.3.2 Signal-to-noise ratio

In Figures 3.5 and 3.6, the SNRs at the modulation frequencies are represented for components 1 and 2, respectively. The SNR of the first components is higher than the SNR of the second component, except at the modulation frequency of 10 Hz for the group with dyslexia, where there is no significant difference between the first and the second component, as it can be seen in Table 3.1 When comparing the two groups, we can find for the first component, Figure 3.5, a significantly higher SNR for the readers with dyslexia at the modulation frequencies of 4 Hz (theta, $p < 0.001$ for left and right ear), 20 Hz (beta, $p < 0.01$ for left and $p < 0.001$ for right ear) and 40 Hz (low-gamma, $p < 0.01$ for left ear and $p < 0.05$ for right ear), while the typical readers present higher SNR at 10 Hz (alpha), statistically significant $p < 0.05$ for left ear stimulation. For the second component, Figure 6, the group with dyslexia has a significant higher SNR at 4 Hz ($p < 0.01$, for left and right ears) and 20 Hz ($p < 0.01$ for left ear and $p < 0.05$ for right ear), agreeing with the first component SNR. The SNR for typical readers is not statistically significant for 10 Hz L. There is more dispersion for the second component, especially at 40 Hz, as the error bars in Figure 3.6 show.

Table 3.1: First and second DSS component signal-to-noise ratios and p values of a two-sample t test comparing the means of the two DSS components. The p values were corrected using the Bonferroni-Holm approach. Bolden numbers are below significance threshold.

Frequency		**4 Hz**		**10 Hz**		**20 Hz**		**40 Hz**	
Ear		**L**	**R**	**L**	**R**	**L**	**R**	**L**	**R**
TR SNR (dB)	Comp. 1	25.307	25.329	22.468	20.439	24.344	23.956	28.751	28.669
	Comp. 2	19.247	18.176	18.366	18.395	19.235	6.000	20.384	20.944
Corrected p-values		**<0.001**	**<0.001**	**<0.001**	**0.017**	**<0.001**	**<0.001**	**<0.001**	**0.016**
DR SNR [dB]	Comp. 1	28.809	27.713	17.962	18.856	27.133	28.806	31.694	31.716
	Comp. 2	20.624	19.938	17.961	18.313	22.360	21.191	24.922	22.965
Corrected p values		**<0.001**	**<0.001**	0.99	0.93	**<0.001**	**<0.001**	**<0.001**	**<0.001**

For the individual analysis, the same procedure was used, we applied the methodology subject by subject. This created two distributions per stimulation condition, one for the group with dyslexia and another one for the group without it, as it can be seen in Figure 3.7 for the low modulation frequencies and in Figure 3.8 for the high modulation frequencies. In Table 3.2, a comparison of the distributions of the two groups can be found. For the individual results, the group with dyslexia presented statistically higher SNR levels at 4 Hz left ear stimulation, 20 Hz right ear stimulation and 40 Hz left ear stimulation.

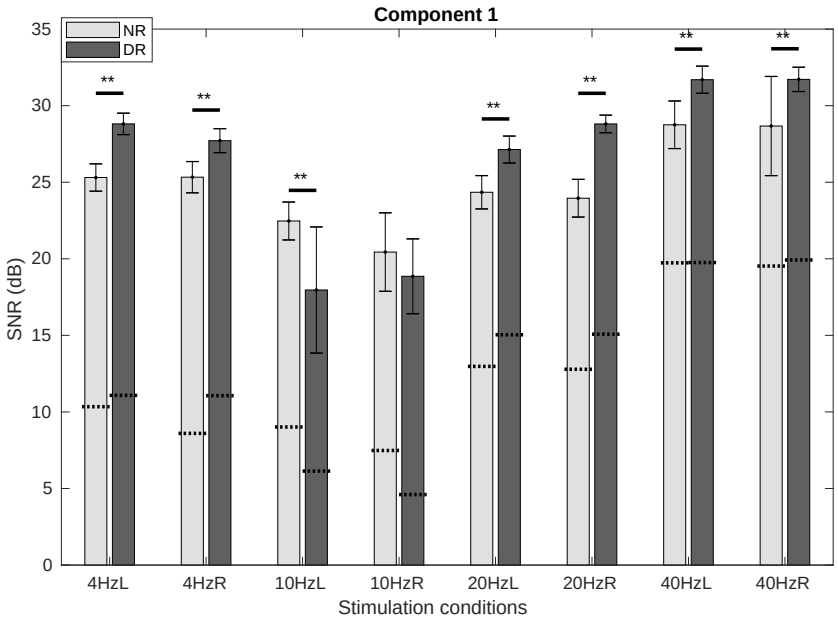


Figure 3.5: Comparison of the obtained SNR of the first component at the stimulation frequency. Statistically significant differences for typical readers and readers with dyslexia are marked with a $\star$ for p-values lower than 0.05 and with $\star\star$ for p-values lower than 0.01. P-values were corrected using the Bonferroni-Holm correction test.

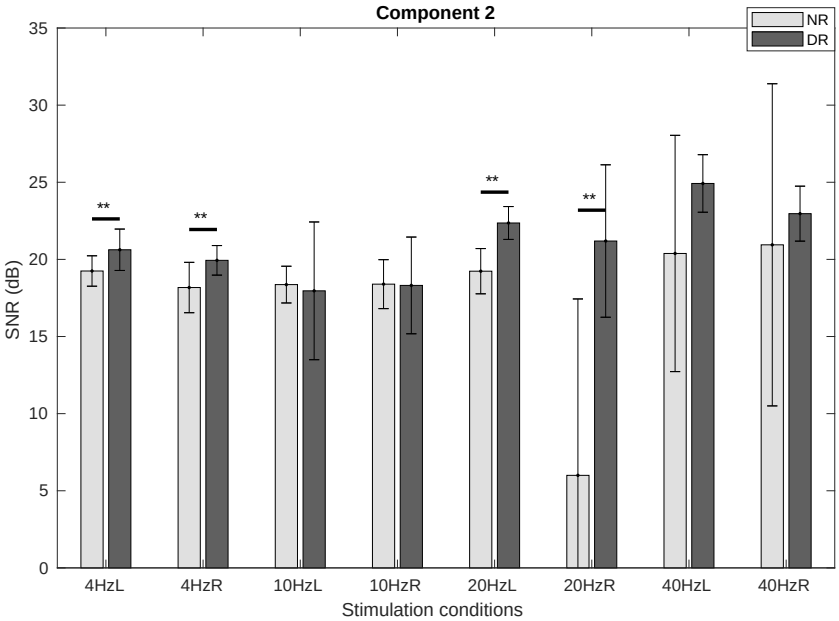


Figure 3.6: Comparison of the obtained SNR of the second component at the stimulation frequency. Statistically significant differences for typical readers and readers with dyslexia are marked with a $\star$ for p-values lower than 0.05 and with $\star\star$ for p-values lower than 0.01. P-values were corrected using the Bonferroni-Holm correction test.

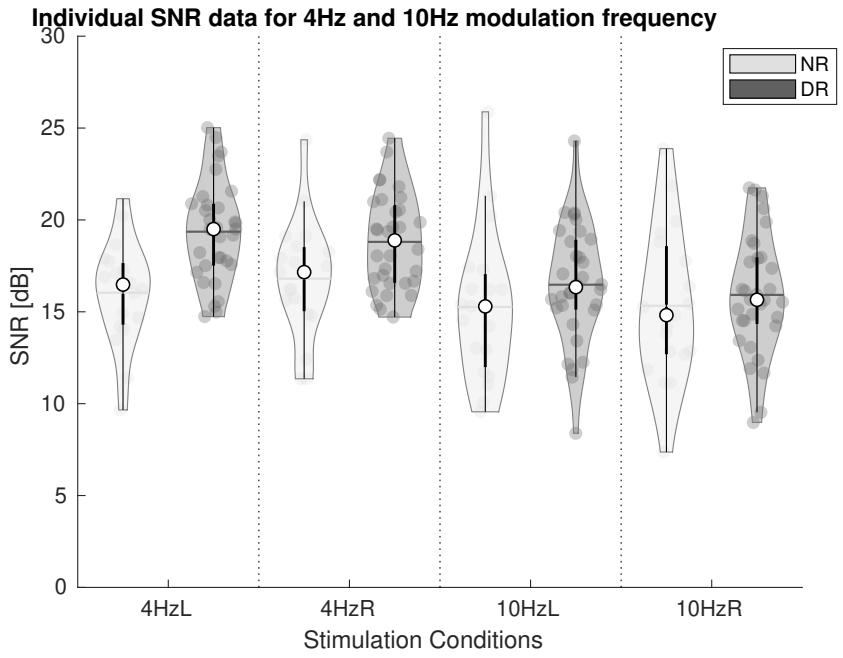


Figure 3.7: Violin plots showing the SNR distribution, mean and variance for the individual subject analysis for both groups at 4 and 10 Hz

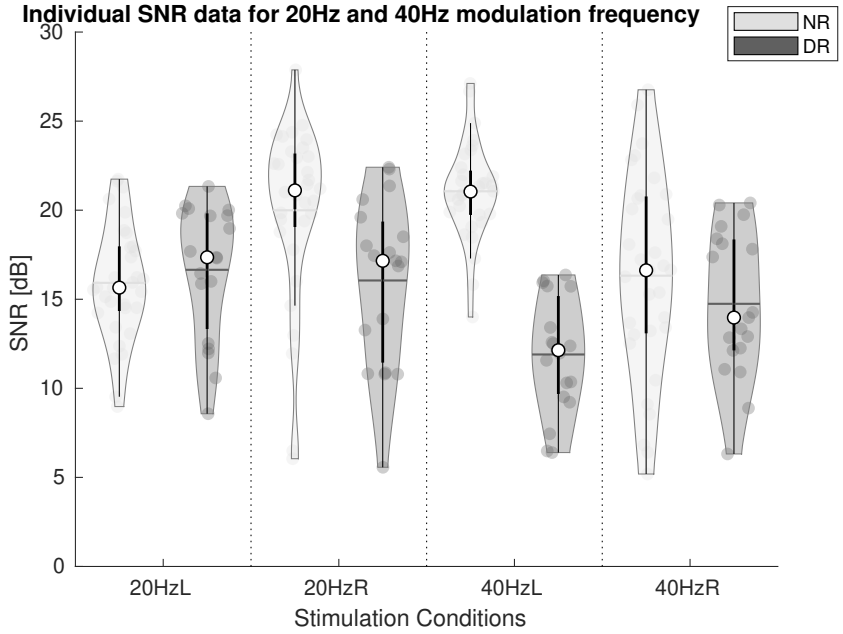


Figure 3.8: Violin plots showing the SNR distribution, mean and variance for the individual subject analysis for both groups at 20 and 40 Hz

Table 3.2: Comparison of signal-to-noise ratios distribution obtained after an individual analysis of both groups. The p values represent the results of a two-sample t test between the two groups, and they were corrected using the Bonferroni-Holm method. Kolmogorov–Smirnov tests granted normality for all the distributions at a chance level of 5%. Bolden numbers are below significance threshold.

Frequency		**4 Hz**		**10 Hz**		**20 Hz**		**40 Hz**	
Ear		**L**	**R**	**L**	**R**	**L**	**R**	**L**	**R**
Avg (SNR) [dB]	TR	16.038	16.804	15.264	15.327	16.653	16.054	11.900	14.744
	DR	19.360	18.805	16.474	15.920	19.995	21.062	16.323	16.582
Corrected p-values		**0.0008**	0.0738	0.6550	0.5703	0.0738	**0.0001**	**0.0176**	0.6550

3.3.3 Phase coherence

In figure 3.9, the Phase Coherence between the first two components is represented. As the figure shows, the group with dyslexia displays significantly higher connectivity values ($p < 0.01$) at 4 and 10 Hz right ear stimulation as well as at 20 Hz, both conditions and 40 Hz left ear. The group of typical readers only shows a higher connectivity level at 10 Hz left ear stimulation ($p < 0 : 05$). No differences are observed for 4 Hz left ear and 40 Hz right ear. These results show that the group of readers with dyslexia have a higher level of neural synchrony except at the modulation frequency of 10 Hz in left ear, where the typical readers show higher levels of neural connectivity. As figure 3.10 shows, typical readers consistently present lower phase coherence values when the right ear is stimulated at speech related modulation frequencies, relative to left ear stimulation and relative to readers with dyslexia.

As a summary, phase coherence results show a higher capability for phase locking in the group diagnosed with dyslexia except at the modulation frequency of 10 Hz. For 10 Hz presented in left ear, the typical readers show higher levels of neural connectivity between the two main sources. This level of connectivity displayed by the two main brain ASSR sources is in line with what can be seen when measuring the SNR.

3.3.4 Laterality Index

We computed the Laterality Index for the first component at 4 Hz and 20 Hz modulation frequencies; see figure 3.11. Both groups, with and without dyslexia, presented statistically significant ipsilateral responses when the modulation frequency was 20 Hz for all conditions, meaning right lateralised responses were detected during right ear stimulation and vice versa.

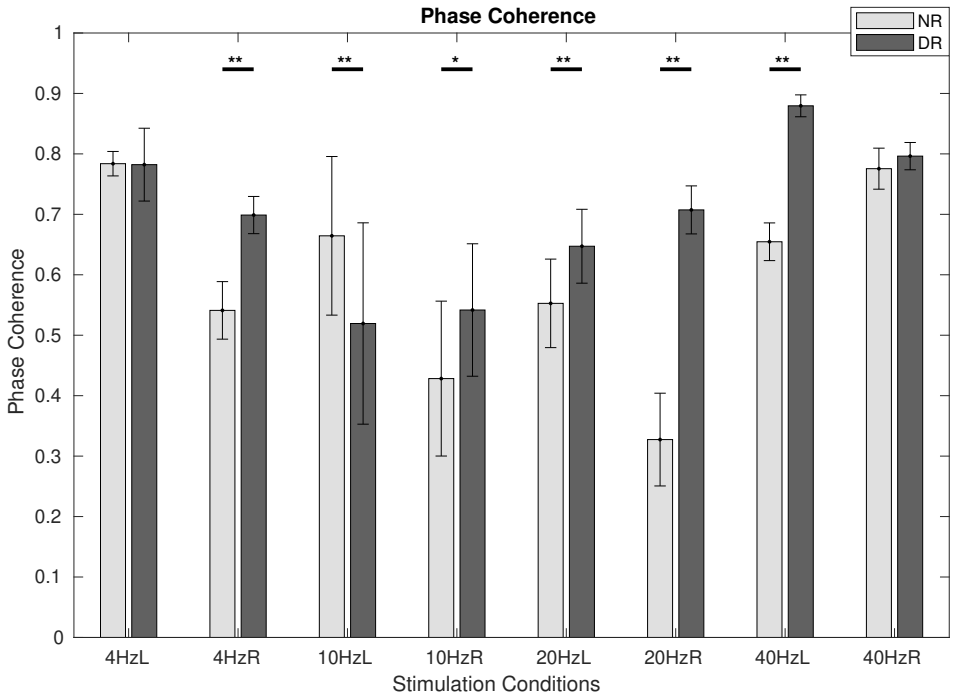


Figure 3.9: Phase Coherence of the first and second component at the stimulation frequencies. Statistically significant differences for typical readers and readers with dyslexia are marked with a $\star$ for p-values lower than 0.05 and with $\star\star$ for p-values lower than 0.01. P-values were corrected using the Bonferroni-Holm correction test.

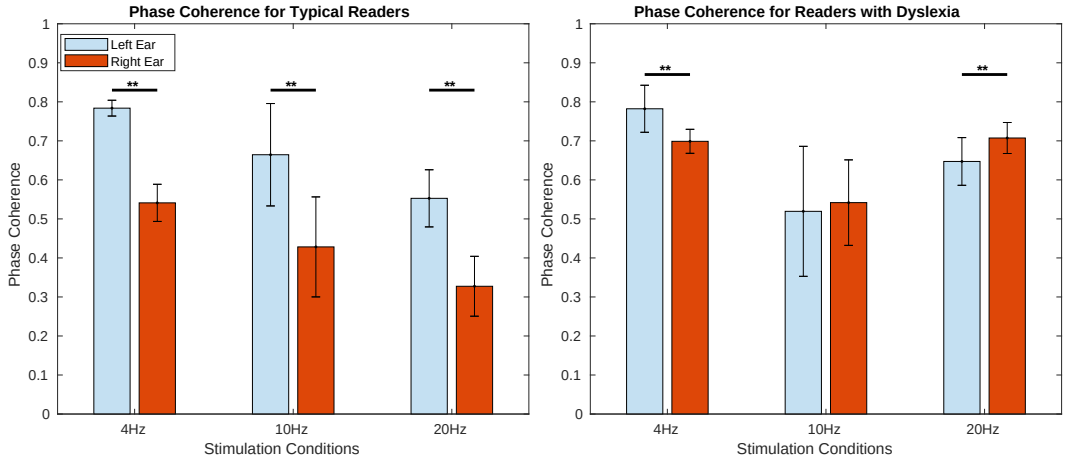


Figure 3.10: Left panel: Comparison of left and right ear stimulation effect in the phase coherence of the first and second component for the typical readers. **Right panel:** Comparison of left and right ear stimulation effect in the phase coherence of the first and second component for the readers with dyslexia. Statistically significant differences are marked with $\star\star$ for p-values lower than 0.01. P-values were corrected using the Bonferroni-Holm correction test.

During 4 Hz modulation right lateralisation significant responses were found for both groups for all conditions except typical readers and right ear stimulation. During right ear stimu-

lation, the group of controls did not present lateralisation statistically distinguishable from zero.

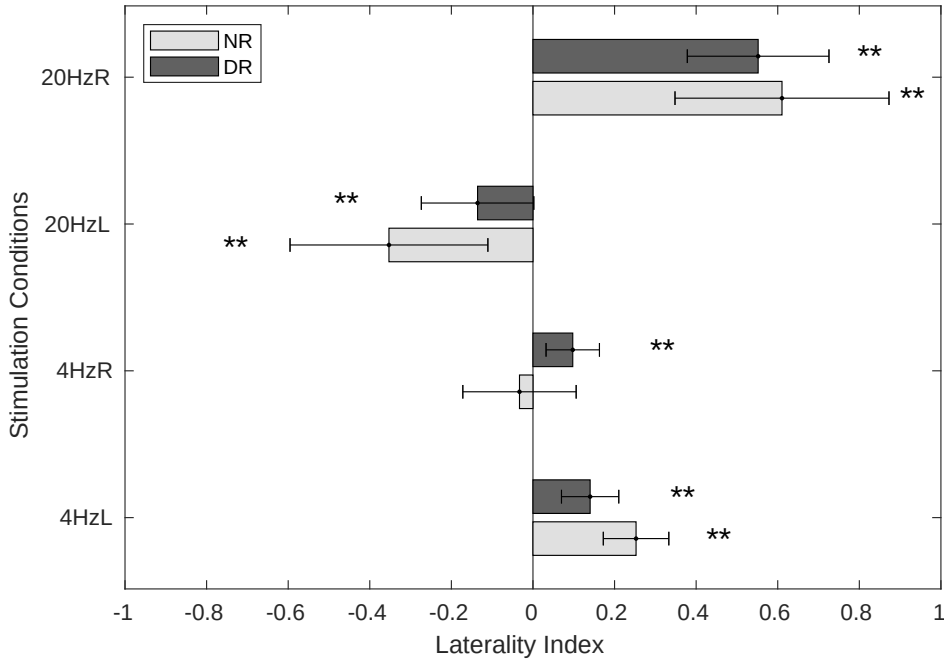


Figure 3.11: Laterality Index measures for the first component at 4 Hz and 20 Hz modulation frequencies. Laterality Indices significantly different ($p < 0.01$) from zero are marked with $\star\star$. P-values were corrected using the Bonferroni-Holm correction test.

3.4 Discussion

Although the authors are inclined to think that the type of stimulation used reflects speech perception patterns inherent to the groups, we would like to remark that the dataset used belongs to a larger longitudinal database where participants were only matched in age, not in reading skills. This creates a situation where we cannot claim that the effects we found were solely linked to the specific causal deficits at the basis of dyslexia, because we cannot measure the consequences of the less reading experience of the group with dyslexia.

3.4.1 Source localisation

For 4, 10 and 20 Hz, we could not find differences between the group of typical readers and readers with dyslexia in the location of the sources. Although the error bars included

in Figures 3.3 and 3.4 showed dispersion around the mean, the low spatial resolution of EEG in addition with the lack of individual head models produced a decrease of the source localisation accuracy that was not reflected in the length of these error bars. Thus, we cannot assess whether there are differences in the source localisation for the two groups under study due to their proximity and the spatial resolution issues. This localisation results were restricted by the inherent limitations of EEG as well as by the scarce number of age-related head models available, which forced us to manually implement our age-related head models. The absence of an individual head model together with the individual electrode position information contributed to increase the source localisation variability. In addition, the position of the electrodes was rescaled manually from an adult template, considering only changes in size not in shape. Thus, the application of an age-related head model was limited by the rescaled adult geometry of the electrode position. What we could find it was that, with a few exceptions, all dipole centres (average values) were located in the temporal gyrus, the region of the brain where the auditory cortex is. At 10 Hz for the group with dyslexia, the centres were in deep regions, but their high dispersion around the mean represented by their big error bars makes this result almost irrelevant. Other exceptions happened at 40 Hz modulation, we know the localisation performance drops at these high modulation frequencies compared to 4, 10 and 20 Hz when using this methodology. This issue was discussed in chapter 2.

Structural differences found with other methods with a higher spatial resolution, such as structural MRI, reported significant differences between subjects with and without dyslexia of a few voxels, (Adrián-Ventura et al., 2020; Im et al., 2015; Raschle et al., 2011). These small differences cannot be detected in EEG measurements.

A higher subject variability of stimulus-driven cortical responses in children with dyslexia has been suggested by Centanni et al. (2018). In that study, the group of children with dyslexia showed higher variability than the controls under syllabic stimulation, consonant-vowel- consonant words. The upper limit of the temporal rates at which syllables occur in speech have been situated around 10 Hz (Edwards & Chang, 2013; Greenberg et al., 2003), which is the same modulation frequency where we found a higher variability in the source localisation of the first component for readers with dyslexia compared to control readers.

3.4.2 Signal-to-noise ratio

Activity in 4 Hz and 10 Hz (theta and alpha rhythm)

If neural oscillations encode temporal information in a rate-dependent manner, alpha oscillations are responsible for encoding information in the corresponding 8-16 Hz frequency range. As described by Drullman et al. (1994a,b) and Shannon et al. (1995), the most important modulation frequencies for accurate speech perception are situated below 16 Hz. In addition, modulation rates around 10 Hz have been associated with (the upper limit of) temporal rates at which syllables occur in speech (Edwards & Chang, 2013; Greenberg et al., 2003).

Although a lower entrainment in the syllabic rate processing for the group with dyslexia has been suggested to occur in the theta band (Goswami, 2011), we found a higher entrainment for the group with dyslexia at 4 Hz stimulation compared to the controls. This agrees with the results obtained at the electrode level for the right ear stimulation (De Vos et al., 2017b) and with other EEG studies (Arns et al., 2007; Marosi et al., 1995) as well as with the MEG study of Lizarazu et al. (2015). Moreover, other studies have never been able to show a theta rate synchronisation difference in adults with dyslexia (Hämäläinen et al., 2012; Poelmans et al., 2012a) nor in pre-reading children with a hereditary risk for dyslexia (Vanvooren et al., 2014).

The non-existence of a difference at 4 Hz stimulation might suggest that the encoding of frequency ranges other than the theta range may be more important for accurate syllabic processing. According to the current results and the ones found in De Vos et al. (2017b), the underlying neural differences leading to syllabic encoding problems seem to be an alpha, not a theta, related issue. Since these results demonstrate that participants with dyslexia exhibit a significant difference in the neural synchronisation during alpha-related stimulation, we are inclined to hypothesise that this inability to enhance alpha activity might be related to the speech- in-noise perception differences that have been shown in dyslexia (Boets et al., 2007; Dole et al., 2012; Poelmans et al., 2011; Ziegler et al., 2009). In addition, the fact that the first two components did not show significant differences during 10 Hz stimulation in the group with dyslexia suggests two possibilities. Either the presence of a higher variance in this group or the inability of the method to find a predominant ASSR source due to a weaker neural entrainment of these subjects at this alpha-related modulation frequency.

Activity at 20 Hz stimulation frequency (beta rhythm)

We found a higher neural synchronisation in the group with dyslexia at 20 Hz stimulation, which belongs to the oscillations in the beta range. This effect was also found at the electrode level in De Vos et al. (2017b) where no lower neural synchronisation was found for the group with dyslexia. In adults with dyslexia, MEG studies did not find lower synchronisation in the beta range for the group diagnosed with dyslexia (Hämäläinen et al., 2012; Lehongre et al., 2011). Also, a study that involved 5-year-old preschoolers revealed no group differences in beta synchronisation between children with and without a hereditary risk for dyslexia (Vanvooren et al., 2012). In De Vos et al. (2017b), no lateralisation differences were found. It was also suggested that beta range synchronisation differences might still emerge in later stages of reading development, being reflective of an atypical maturation of beta oscillations, in line with the results observed in pre-readers (Vanvooren et al., 2014, 2015) and in school-aged children (Lizarazu et al., 2015). De Vos et al. (2017b) also proposed that enhanced beta synchronisation could be the manifestation of a compensatory mechanism, by which the dyslectic brain attempts to improve phonemic rate processing, in line with a series of ERP studies that showed enhanced responses to phonemic rate alterations in speech and non-speech stimuli in school-aged children and adults with dyslexia (Helenius et al., 2002; Lohvansuu et al., 2014).

Activity at 40 Hz (low-gamma rhythm)

Regarding low-gamma neural synchronisation, stimulation with a modulation frequency of 40 Hz induced higher responses in the group with dyslexia compared to the controls. These results differ with what was found at the electrode level in De Vos et al. (2017b), where no group differences between typical reading and adolescents with dyslexia were observed. One reason for this effect might be the high number of ASSR sources that appear at this modulation frequency (Farahani et al., 2019), see also chapter 2. The superposition of the electrophysiological activity produced by all the sources that is measured at the electrode level may obscure any significant differences that could have been found in the first component at the modulation frequency. However, although the speech envelope supposedly contains modulations up to 50 Hz (Rosen, 1992), the main energy in the modulation spectrum of the

speech envelope is situated between 4 and 16 Hz (Drullman et al., 1994a,b; Shannon et al., 1995).

Effect of the main source in global results

The individual results for the SNR showed a higher inter subject variability, represented by a higher variance. This higher variance affected the results, showing only statistical differences between the two groups in three stimulation conditions, while concatenated analysis showed statistically significant differences in all the stimulation conditions, except at 10 Hz right ear stimulation. This higher variance present in the individual analysis was reduced by using the concatenated methodology, where individual differences are attenuated, and this allows for the extraction of the most common bran activity pattern. We have found that the results in adolescents with dyslexia point to lower SNRs in phonemic rates, specifically in the alpha band, and higher SNRs at other frequency bands, meaning the electrode level results are reproduced in the first and most predominant component at the source level. The presence of a phonemic rate lower responses in cortical oscillatory processes during low-frequency stimulation was also described in Di Liberto et al. (2018). Since there were no differences in the brain location and the outcome measures of the time domain delivered similar results, we may suggest that what causes the deficit at the alpha rhythm and tries to overcompensate at the other frequency bands is within the nature of the main ASSR generator. It is this intrinsic way of oscillating that causes the differences between the groups that are observable at the electrode level. Similar mechanisms of overcompensation were found in ageing studies, where the elder people despite their overall poorer audiometric thresholds presented higher neural responses than the younger subjects when stimulated at certain modulation frequencies (Berlingeri et al., 2013; Goossens et al., 2019, 2018, 2017)

3.4.3 Connectivity

The group with dyslexia shows higher phase coherence levels as well as higher SNR in theta, beta and low-gamma modulations. Similar results were found while stimulating with continuous natural speech (Thiede et al., 2020). These authors did not find any differences in the alpha rhythm. However, we found significantly higher differences for the control group in left

ear stimulation and for the participants with dyslexia in right ear stimulation. The effects we found while stimulating monaurally might cancel while stimulating binaurally. This may explain the lack of differences in the alpha rhythm (Thiede et al., 2020), where the stimulation was binaural. In addition, we did not find any differences between the preferred hemispherical lateralisation between groups, suggesting that those differences may arise at older ages. Based on our results, we may say that a high neural level of connectivity of the two main brain generators would be reflected in a high SNR level of the brain response at the modulation frequency and vice versa. Thus, both aspects would be intrinsically related to each other. For example, at 10 Hz left ear stimulation, the control group shows higher phase coherence values as well as significantly higher SNR. The existence of a lower phase coherence between the two main generators in the typical readers might indicate a high level of specialisation in the right hemisphere to process speech modulated sounds. This specialisation level would not require a high phase locking or interaction between the two main generators to process speech related sounds when the right ear is stimulated. This effect can be observed in the group of typical readers but does not exist in the group diagnosed with dyslexia. It seems that the overcompensation mechanisms mentioned in the previous section might be playing a role here, too. The higher phase coherence levels of the group with dyslexia compared with the typical readers were reflected on the SNR levels as well, showing the relationship between the neural entrainment, measured through the SNR, and the phase locking mechanisms, measured through the phase coherence, happening during phase-locked stimulation.

3.4.4 Laterality index

We investigated the lateralisation of the responses in theta and beta rhythms through the Laterality Index (LI). The preference for right lateralisation of the brain synchronisation in readers with dyslexia was also reported in Lizarazu et al. (2015). The stimulation used in that study was binaural, while we used monaural stimulation. That might suggest the existence of a lateralisation preference in the right hemisphere in the control group that only exists when the left ear is stimulated. No preference for lateralisation would exist in the controls when the right ear is stimulated, as opposed to the participants with dyslexia, where there was always a right hemisphere lateralisation at the modulation frequency of 4 Hz. Nevertheless, it is known

that the right hemisphere prefers to process syllabic rate modulations (Boemio et al., 2005; Poeppel, 2003), thus, the subjects with dyslexia in our study did not show any deviances in that respect. LI values found at 20 Hz showed that the lateralisation for brain synchronisation is similar between participants with dyslexia and controls. Furthermore, for both groups, the LI showed that the responses to the stimulation at 20 Hz were ipsilateral, following the results that suggested a symmetrical pattern to process phoneme rate modulations (Jamison et al., 2006; Obleser et al., 2008). A hemispheric lateralisation preference, typically ipsilateral, during beta stimulation is a behaviour more commonly found in adults than in children (Vanvooren et al., 2015). In addition, we found that the group with dyslexia presented a right hemisphere lateralisation. A preference for right hemispheric lateralisation during right ear or bilateral stimulation in theta rhythms is a feature found in children (Abrams et al., 2008; Vanvooren et al., 2015) as well as in adults (Bidelman & Howell, 2016; Boemio et al., 2005).

3.5 Conclusion

It is known that there is a preference for heterogeneity during developmental stages, especially in dyslexia. However, despite the existence of higher heterogeneity, there are still common patterns of oscillatory activity that could be found within the two groups. This work focused on the differences between the common features of each group present during developmental ages. The higher number of adolescents with dyslexia in this study reinforced the capability of the methodology of finding common patterns of activity within the groups. Also, the higher number of subjects in the group with dyslexia might have compensated the higher heterogeneity in comparison with the typically developing group. In this study, we investigated at source level neural synchronisation of theta, alpha, beta and low-gamma range oscillations in typical readers and readers with dyslexia. We could not find differences between subjects with dyslexia and controls in the brain locations of the main ASSR generators. Variations between the groups were observed in the source signal waveforms and in the overall SNR. The main ASSR generators in the brain were located in the temporal gyrus, around the auditory cortex. Thus, the differences observed in EEG auditory experiments would, according to our findings, have their origin in the intrinsic oscillatory mechanisms of the brain cortical sources related to speech perception. We also observed that the main brain source carries the highest

SNR and the characteristics observed at the electrode level are mainly driven by this main generator. We observed a significant difference at 10 Hz in the participants with dyslexia, meaning that readers with dyslexia exhibited significantly reduced neural synchronisation during alpha-related stimulation. These findings at a source level follow the results found at the electrode level. However, these findings contrast with recent models suggesting that speech perception and phonological problems in dyslexia are caused by an atypical neural synchronisation during theta and low-gamma range stimulation. As it was stated in De Vos et al. (2017b), those results suggest that this neural difference could be related to syllabic rate speech and phonological processing problems in dyslexia through bottom-up neural encoding as well as top-down inhibitory processes associated with selective attention. Moreover, we also detected in the adolescents with dyslexia significantly enhanced neural synchronisation during the stimulation with frequencies contained in the theta, beta and low-gamma rhythms, suggesting the presence of compensatory mechanisms to improve processing of the phonemic rate information. This has equally been observed in ageing studies.

To conclude, this study has provided descriptive evidence that at a source level higher SNR means can be expected in the component that best represents the group behaviour, that is, the first DSS component, when compared to the SNR means at the electrode level in this type of ASSR studies. Also, we have shown proof that the presence of lower alpha synchronisation in adolescents with dyslexia and the possibility of compensatory mechanisms in theta, beta and low-gamma frequency bands can be explored at a source level. This study on neural synchronisation in dyslexia using EEG provides interesting information about the intrinsic differences in adolescents with and without dyslexia.

CHAPTER 4

Development of atypical reading at ages 5 to 9 years and processing of speech envelope modulations in the brain.

The contents of this chapter have been adapted from the work published in Granados Barbero, et al. (2022) as "Development of atypical reading at ages 5 to 9 years and processing of speech envelope modulations in the brain." Frontiers of Computational Neuroscience, 16.

Abstract

Different studies have suggested that during speech processing readers with dyslexia present atypical levels of neural entrainment as well as atypical functional hemispherical asymmetries in comparison with typical readers. In this study, we evaluated these differences in children and the variation with age before and after starting with formal reading instruction. Synchronised neural auditory processing activity was quantified based on Auditory Steady-State Responses (ASSRs) from EEG recordings. The stimulation was modulated at syllabic and phonemic fluctuation rates present in speech. We measured the brain activation patterns and the hemispherical asymmetries in children at three age points (5, 7 and 9 years old). Despite the well-known heterogeneity during developmental stages, especially in children and in dyslexia, we could extract meaningful common oscillatory patterns. The analyses included (1)

estimations of source localization, (2) hemispherical preferences using a laterality index, measures of neural entrainment, (3) signal-to-noise ratios (SNR) and (4) connectivity using phase coherence measures. In this longitudinal study, we confirmed that the existence of atypical levels of neural entrainment and connectivity already exists at pre-reading stages. Overall, these measures reflected a lower ability of the dyslectic brain to synchronise with syllabic-rate stimulation. In addition, our findings reinforced the hypothesis of a later maturation of the processing of beta rhythms in dyslexia. This investigation emphasizes the importance of longitudinal studies in dyslexia, especially in children, where neural oscillatory patterns as well as differences between typical and atypical developing children can vary in the span of a year.

4.1 Introduction

Developmental dyslexia is a neurobiological and hereditary disorder characterised by severe and persistent difficulties with accurate and fluent word recognition and by poor spelling and decoding abilities (Eden et al., 2016), despite normal intelligence and sufficient educational opportunity (Stoodley, 2016). Different studies have proven that individuals with dyslexia present deficits or atypical responses in the phonological components of language that causes problems to represent and manipulate the phonological structure of words at the syllable and/or phoneme level (Ziegler & Goswami, 2005; Vandermosten et al., 2020; Vellutino et al., 2004). However, the neural dysfunction behind these effects remains unknown. As it was stated in Share (2021) about the phonological deficit theory: phonemic awareness is only the "tip of the phonological iceberg" and that "deeper" spoken-language phonological impairments among people with dyslexia appear well before the onset of reading and even at birth (Guttorm et al., 2005).

Atypical development has been observed for persons with dyslexia. One of the experimental techniques to measure brain electrical responses is electroencephalography (EEG). EEG can measure the electrical impulses of the brain (responses) at the scalp level. EEG can allow us to measure the neural entrainment of the brain to sensory stimulation.

Neural entrainment or neural synchronisation is an important characteristic of interactions between brain rhythms or between brain activity and sensory stimulation. It refers to the coupling of two independent oscillatory systems in the brain or to the coupling of brain

activity to the oscillatory properties of sensory stimulation in such a way that their periods of oscillation at specific frequencies become related by virtue of phase alignment (Cummins, 2009). A higher entrainment or synchronisation of the brain to sensory oscillatory stimulation usually means higher brain responses at the frequencies of stimulation. Thus, we used the broader definition of neural entrainment or synchronisation in the broad sense presented in Obleser et al. (2008).

A number of studies have tested this hypothesis in different age populations, with different methodologies and different oscillatory ranges (McAnally & Stein, 1997; Menell et al., 1999; Lehongre et al., 2011; Poelmans et al., 2012b; Hämäläinen et al., 2012; Lehongre et al., 2013; Vanvooren et al., 2014; De Vos et al., 2017a; Granados Barbero et al., 2021).

These previous findings confirmed that a dyslectic brain could present atypical synchronisation behaviour in beta and low gamma rhythms. Despite being suggested that dyslexia should be a theta related issue (Goswami, 2011) no consensus was found in the results regarding differences during theta stimulation.

However, we cannot say which of these atypical neural effects observed in these previous studies are causally related to the development of dyslexia. An important shortcoming of these studies is that the observed neural deviances might reflect the resulting effects of the reading difficulties. Longitudinal studies in dyslexia aim to reduce the impact of those limitations, that is why they are now considered essential in order to improve our knowledge about dyslexia (Goswami, 2015).

The main objective of this study was to evaluate the relationship of the neural synchronisation with speech envelope modulation rates during reading development. We embarked upon a longitudinal study to analyse the neural entrainment during auditory stimulation in typically developing children and children with dyslexia at the ages of 5, 7 and 9 years old. We believe this age selection is representative for different reading stages: Before formal reading instruction at the age of 5, during the first years of formal reading training at the age of 7 and at the age of 9, after receiving formal reading instructions for a long period of time.

Part of these data were used in De Vos et al. (2017b). However, we will use an extended source analysis methodology firstly developed in chapter 2. We hypothesised that this approach will provide us with essential information about how neural processing during speech related modulations evolves with age as well as its impact in children with dyslexia.

We selected a brain source analysis to avoid defining regions of interest at the scalp level, furthermore with our method selection we could analyse our outcome measures the most prominent brain generators in the same group with no prior assumptions of our data. It is true that we are neglecting the role that inter-subject variability plays in phase difference, however our main goal was to extract information maximally shared by all the subjects in a group. Source analyses have been used widely in literature for their ability to provide with physiologically plausible results with no prior assumption in the location of the sources. Almost no assumption is also taken regarding the relationship between the reconstructed signals. This approach offers the flexibility to look for specific signals in the brain without taking any important prior assumptions.

We considered the use of multivariate regression models. However, we decided to use a method with input parameters well-defined (EEG channel data). Multivariate methodology bases its use in machine learning algorithms that can lead to excellent predictions, but sometimes to not very useful interpretations in terms of brain function (Hebart & Baker, 2018). To avoid this, normally big parts of data are used for training, regions of interest are defined within the brain or other constrictions are applied to the reconstructed data, such as predefining the number of sources. In addition, common multiple regression models used in EEG analyses aim to extract signal predictors based on the spectral properties of a complex signal. They need as an input the temporal and the spectral (frequency) information of the signal. They are mostly used with Event-Related Potentials, which contain information widespread in the frequency domain. Since we aimed to stimulate at certain modulation frequencies to resemble specific parts of human speech, we do not have such a rich frequency spectrum. Therefore, we aimed to have a methodology that could work with oscillatory signals happening in a narrow frequency window as well as having the minimum number of assumptions regarding our data.

The analyses performed in the EEG recorded brain responses included: (1) source localisation, (2) the estimation of the hemispherical preference of the ASSR sources using a Laterality Index and the measure of neural entrainment combining the results provided by the (3) SNRs and the (4) Phase Coherence at the modulation frequencies. The SNR and the Phase Coherence provided information of the main ASSR generators' oscillatory activity. The SNR measured the evoked responses compared to the background noise, and Phase Coherence

quantified the connectivity by measuring the phase difference variability of the main ASSR brain generators.

4.2 Materials and Methods

4.2.1 Data acquisition

Participants

The original sample consisted of 87 children with bilateral normal hearing, normal non-verbal IQ, and no history of brain injury or neurological disorders (for a detailed description of the original sample, see Vanvooren et al. (2014). Fourteen children did not continue their participation in the study, one child was excluded following a diagnosis of general learning difficulties, and EEG data of four children were considered unusable because of overall too high noise levels. Consequently, we were able to retain a longitudinal sample of 68 children for the data presented here. The division in the two groups for the study: readers with and without dyslexia was done retrospectively. Participants were classified as typical readers (TR) or readers with dyslexia (DR) based on their history of reading problems and their reading performance at the age of 9 as well as their spelling history and their spelling performance at the age of 9. More specifically, children diagnosed with dyslexia demonstrated (1) severe and persistent reading problems, implemented as a score below the 10th percentile on the same standardised word reading test (Brus & Voeten, 1973) or pseudoword reading (Van den Bos et al., 1994) at each measurement point, or (2) severe and persistent problems (below 10th percentile) in spelling tasks that were administered at the start of second and third grade. Additionally, participants were required to have adequate non-verbal intelligence, defined by an IQ score of > 85 on the Raven Coloured Progressive Matrices (Raven & Court, 1996) measured at kindergarten age. More details about this classification as well as the reading and spelling performance can be found in De Vos et al. (2017a). Since the number of readers with dyslexia was much smaller than the typical readers, we selected the best readers from the control group in order to have a matched number of participants in each group based on the word recognition test (Brus & Voeten, 1973). We selected the best readers because dyslexia is mostly defined as a reading impairment. Therefore, for the diagnosis of dyslexia

children fulfilling the second criterion (severe and persistent spelling problems) were additionally required to demonstrate reading scores below the 25th percentile at each measurement point. Some of the poor readers not diagnosed with dyslexia belonged to this percentile, we did not want to have overlapped samples in reading performance. We were aware that there might be better choices to separate effects inherent to dyslexia from effects derived simply by poor reading or spelling performance. However, since dyslexia has been widely defined as a reading impairment, the diagnosis of children is mostly based on reading performance. A more appropriate selection of the control group would only try to minimise the difference between observing effects caused by dyslexia or by reading performance. Thus, based on our selection method the total number of participants was 21 for each group. EEG data were recorded from the same group of children in different stages: the first stage corresponded to a pre-reading stage where the participants mean age was five years old; in the second stage, the children were in a beginning reading state and were 7 years of age on average; the third stage corresponded to an advanced reading state where the mean age of the group was 9 years.

Auditory steady-state responses

Auditory Steady-State Responses (ASSRs) are phase-locked electro-physiological responses from the brain, evoked by a periodically varying continuous auditory signal (Rance, 2008; Picton et al., 2001). ASSRs allow an objective investigation of auditory temporal processing in the brain and brainstem by adjusting the stimulation parameters to match important speech-related components (Lins & Picton, 1995).

The stimuli used to evoke these responses consisted of amplitude modulated speech-weighted noise. The carrier noise was adopted from the *Leuven Intelligibility Sentence Test* (LIST) (Van Wieringen & Wouters, 2008). This carrier noise represents the long-term average speech spectrum of all sentences of the female speaker with LIST readings. The speech-weighted carrier noise was 100% amplitude modulated at approximately 4 Hz and 20 Hz rounded to the epoch frequency of 1/1.024 Hz (exact frequencies were 3.91 and 19.53 Hz), representing syllable- and phoneme-rate modulations, respectively. With this stimulation we aimed to measure synchronisation of neural oscillations in the auditory cortex. All stimuli were presented at 70 dB SPL using the Etymotic Research ER-3A insert earphones monaurally to the right ear. This was done for a matter of time since the participants were children

and to avoid the simultaneous activation of both auditory pathways.

Recording System

EEG data were recorded with the BioSemi ActiveTwo system using 64 active Ag/AgCl electrodes mounted in head caps according to the 10-10 electrode system. Electrode offsets were kept below 30 mV. All recordings were administered in a double-walled soundproof booth with a Faraday cage. Participants were asked to lie down on a bed while watching a soundless film to warrant the same level of alertness and attention throughout the EEG measurement (Vanvooren et al., 2014; Poelmans et al., 2012b; Goossens et al., 2016). Each measurement consisted of a 10-min EEG recording, and they were presented randomly to avoid any influence of the stimulation order.

4.2.2 Pre-processing

All data were pre-processed using MATLAB®. First, EEG signals were filtered using a zero-phase high-pass filter with a cut-off frequency of 2 Hz and a slope of 12 dB/Octave. The filtered signal was segmented into different epochs with a length of 1.024 s. From these segmented epochs we applied the following steps: the mean Peak to Peak (PtoP) amplitude was calculated for each channel separately. Any channel with a mean PtoP four times greater than the median PtoP of all the channels was rejected, any subject with rejected channels was discarded. The aim was to obtain 128 epochs with the lowest amount of artefacts in all the channels. To do that, we considered the 128 epochs showing the lowest absolute amplitude. If one of these selected epochs had reached a maximum threshold of 120 νV the subject was discarded. As it was mentioned in the 4.2.1 subsection 4 participants were discarded due to the high noise levels. The accepted 128 epochs per subject were concatenated along the time dimension, resulting in a total array of 2560 epochs per EEG electrode for each group of children. After the epoch-based artefact rejection, all the electrodes were referenced to the C_z electrode. This reference was used over the average reference based in previous studies that stated that C_z reference lowers the noise estimates around the stimulation frequency reducing the detection threshold for ASSRs (Van der Reijden et al., 2005; Van Dun et al., 2009; Poelmans et al., 2012b).

4.2.3 Source Activity Reconstruction

To extract ASSR brain source activity, we combined Independent Component Analysis (ICA) and Denoising Source Separation (DSS), as described in chapter 2. We aimed to extract the most reproducible ASSR across trials and to identify patterns within the whole group for each age. Time-concatenated EEG data was decomposed by ICA into an array of maximally independent components (Onton, 2009). The brain source localisation and projection weights were assumed to be spatially stationary for the duration of the experiment (Onton et al., 2006). The Infomax algorithm was utilised in FieldTrip (Oostenveld et al., 2011) due to its fast and reliable performance (Bell & Sejnowski, 1995). Since we applied ICA to temporally concatenated data, we were performing what is known as group-ICA (Delorme & Makeig, 2004). For group-ICA, we applied ICA to temporally concatenated data from all the subjects in each group and for each age separately. The number of output components equalled the number of input channels, which were 63 per stimulation condition. After computing ICA a one-sample Hotelling t-squared test was performed, see section 4.2.5. Components that did not show significant ASSR were rejected.

The non-rejected ICA components were input into the DSS algorithm. DSS performs a separation of the data into desirable components (signal) and undesirable components (noise), assuming linearity of the coefficients and of the DSS components (Särelä & Valpola, 2005).

DSS can use a bias function to enhance its sensitivity towards phase-locked ASSR. This bias function was chosen to be the *proportion of epoch-averaged (evoked) activity* (de Cheveigne & Simon, 2008). This bias function represented the total-power reproducibility across trials. It allows ranking the DSS components according to the most consistent activity along trials. Since the stimulation during the experiment was periodical and consistent across trials we expected the activity of the main ASSR phase-locked generator to be ranked first.

After computing the DSS algorithm we obtained an array of components sorted by decreasing total-power reproducibility across trials. In order to determine whether these DSS components were carrying ASSR, a one-sample Hotelling t-squared test was computed, see the section 4.2.5.

The projection weights of the components obtained through DSS and ICA analyses were fitted to equivalent current dipoles using the neuromag coordinates, see Figure 4.1. Two

symmetrical dipoles along the x-axis was the default configuration as long as the distance between them was more than 20 mm, the one dipole configuration was selected otherwise. This dipole fitting procedure was performed using a Boundary Element Method (BEM) as a head model (Meijs et al., 1989; Hämäläinen & Sarvas, 1989). We tried to create age-related (5, 7 and 9 years old) BEM head models from averaged MRIs. However, the tissues were so thin, especially in the parietal areas, that they created distortions in the surface boundaries. These distortions led to the creation of unusable BEM head models for the three ages involved in the experiment. The limitations encountered while trying to create an age-related model were solved by using an template based on older subjects. This BEM conductivity model was created in FieldTrip from 14-year-old adolescents averaged MRI images (Richards et al., 2016; Sanchez et al., 2012). The BEM model described the electrical properties of the scalp, skull and brain and the conductivity values chosen for these tissues, which were 0.3300, 0.0042 and 0.3300 S/m respectively (Gabriel et al., 1996).

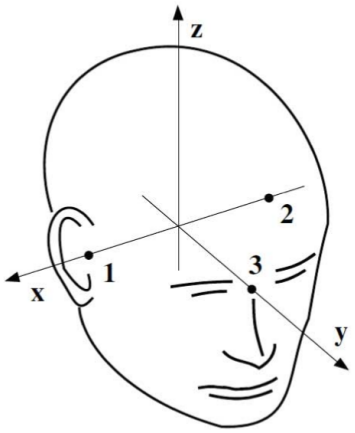


Figure 4.1: Neuromag coordinate system.

4.2.4 Outcome Measures

In this study, our main outcome measures were response strength (SNR), connectivity (Phase Coherence) and lateralisation (Laterality Index).

Signal-to-noise ratio

The measured relative response amplitudes, obtained from the square root of the signal power at the frequency of stimulation, and the Signal to Noise Ratios (SNRs) were calculated from the DSS components carrying significant ASSR. We obtained these responses and SNRs from the concatenated data for both stimulation conditions, in both groups and for all ages. The response amplitudes were obtained by taking the square root of the signal power. The signal power, P_S, was calculated from the Hotelling t-squared statistic, it represents the squared amplitude of the responses mean across all the data trials at the bin of the modulation frequency.

The noise floor amplitude, P_N, required to compute the SNR, was also estimated from the Hotelling t-squared statistic and shows the standard error of the amplitude responses at the modulation frequency mf across n epochs, being: $\sigma(R_{mf})/\sqrt{n}$. Based on the definition of power response and noise amplitude, the SNR may be defined as the ratio between the power of the response signal and the power of the EEG noise, Equation 4.1.

$$SNR = \frac{P_S}{P_N} = \frac{\|mean(R_{mf})\|^2}{\left(\frac{\sigma(R_{mf})}{\sqrt{n}}\right)^2} \tag{4.1}$$

Where R_{mf} is a complex vector containing the responses at the modulation frequency of all epochs, σ is the standard deviation and n is the number of epochs.

Phase Coherence

Phase coherence represents the inter-trial variability of the phase difference between two signals for a specific frequency, and it can be interpreted as a measure for connectivity (Picton et al., 2001).

We measured the phase coherence between the first two DSS components. The first and the second DSS component carry the highest SNR of all the components as well as the highest reproducibility power ratios. We did not include following DSS components because we cannot guarantee the presence of a dipolar pattern. From the third and following DSS component the field spread may represent or contain a superposition of neural activity as well as noise sources (chapter 2). This means that those two components gave us an overall

model or estimation of most of the ASSR activity (in terms of energy/amplitude) triggered by our auditory stimulation. Through the Phase Coherence we obtained an estimation of how the two main ASSR generators oscillate with each other. A higher capability for phase locking means a higher level of synchrony, or in other words, it means a stable phase difference between the two main ASSR generators. The Phase Coherence showed the synchrony that can be found between two signals. This was made by estimating how stable the difference between the phase of two signals is.

In summary, the phase coherence measured the neural interaction of the activity generated during this stimulation. Higher values meant a higher synchronisation or joint effort towards "decoding" or processing the stimulus. The phase coherence was computed after averaging segments of data into 32 epochs, as suggested in Picton et al. (2001). The phase of each epoch was obtained from the complex representation of the neural response in the frequency domain. Phase coherence was calculated according to Equation 4.2, (Picton et al., 2001).

$$PhCoh = \frac{1}{n}\sqrt{\left(\sum_{i=1}^{n} cos\ \theta_i\right)^2 + \left(\sum_{i=1}^{n} sin\ \theta_i\right)^2} \tag{4.2}$$

Where $\theta(f, i)$ represents the phase difference between two signals, in this case the selected signals would be the first and the second computed DSS component, this can be expressed as: $\phi_1(f, i) - \phi_2(f, i)$. For the final result, the difference will be averaged across n epochs.

Laterality Index

To estimate the lateralisation of the extracted sources, we computed the Laterality Index (LI). The neural origin for the DSS components was estimated by the dipole fitting procedure. This neural origin could be modelled by one or two symmetrical dipoles, as it was mentioned before while describing the dipole fitting procedure. For components whose origin was modelled by two symmetrical dipoles, we defined the LI based on the dipole magnitudes as it is shown in Equation 4.3. For components modelled by only one dipole, we calculated the LI based on the reconstructed responses and the noise level of the extracted component. If the dipole was in the right hemisphere ($x_{dip} > 0$) the noise floor was used to estimate the neural response of the left hemisphere, see Equation 4.4. If the dipole was in the left hemisphere ($x_{dip} < 0$) the noise floor was used to estimate the neural response of the right hemisphere, see Equation

4.5. Either with one or two dipoles an LI of +1 represents a response completely lateralised to the right hemisphere and an LI of -1 represents a response completely lateralised to the left hemisphere.

$$LI = \frac{mag_{right} - mag_{left}}{mag_{right} + mag_{left}} \tag{4.3}$$

$$if\ x_{dip} > 0\ then\ LI = \frac{\sqrt{P_{S+N}} - \sqrt{P_N}}{\sqrt{P_{S+N}} + \sqrt{P_N}} \tag{4.4}$$

$$if\ x_{dip} < 0\ then\ LI = \frac{\sqrt{P_N} - \sqrt{P_{S+N}}}{\sqrt{P_N} + \sqrt{P_{S+N}}} \tag{4.5}$$

4.2.5 Statistical Analyses

Detecting significant ASSR

To determine whether the ICA or the DSS components were carrying ASSR or not, the one-sample Hotelling t-squared test was performed in the frequency spectrum of the components (Hotelling 1931). These spectra were obtained by means of a Discrete Fourier Transformation. The statistical test compared the complex responses at the modulation frequency bin across n different epochs.

Obtained components were considered to have ASSR activity when the Hotelling t-squared test showed a significant difference ($\alpha \geq 0.05$) between the squared mean of the response, numerator of Equation 4.1, and the squared Standard Error of the R_{mf} distribution, denominator of Equation 4.1 (Hofmann & Wouters, 2012).

Error estimation for group analysis

The Quenouille and Tukey jackknife approach was utilised to estimate bias and variance (σ_{JK}) for the group analysis (Miller, 1974). The standard deviation of the mean value μ, which is the value including all M subjects, was estimated from the jackknife estimate of variance, see Equation 4.6. This jackknife statistic estimation is assumed to have a normal distribution (Efron & Stein, 1981).

$$\sigma_{JK} = \sqrt{\frac{M-1}{M} \sum_{m=1}^{M} [\zeta_m - \zeta_{all}]^2} \tag{4.6}$$

Where ζ_{all} represents the data of all subjects, ζ_m represents the data for one subject and M is the total number of subjects.

Two tailed t-test

Based on the mean and standard deviations obtained using the Jackknife method for the outcome measures, we calculated how significant the differences were between the control group (TR) and the group with dyslexia (DR) for the three age points using a paired t-test. We used the Bonferroni-Holm correction (Holm, 1979) every time a multiple comparison was performed.

4.3 Results

4.3.1 Source Localisation

The dipole locations for the first DSS component are shown in Figure 4.2 for the typical reader group and in Figure 4.3 for the readers with dyslexia. All the responses were processed in both hemispheres for all conditions, both groups and all ages. The averaged location for all the conditions was in the temporal gyrus. Although the error bars showed the subject dispersion around the mean, the low spatial resolution of EEG in addition with the lack of individual head models produced a decrease of the source localisation accuracy that was not reflected in the length of these error bars. Thus, we cannot assess whether there are differences in the source localisation for the two groups under study due to their proximity and the spatial resolution issues.

4.3.2 Response SNR

The SNR comparison between the two groups as a function of age is represented for 4 Hz, in Figure 4.4 and for 20 Hz, in Figure 4.5. It can be seen how at the age of 7 we could not find differences between the two groups for both modulation frequencies. While for 4 Hz the SNR was lower for the group with dyslexia at the age of 5 ($p < 0.01$) and 9 ($p < 0.1$); and for 20 Hz the SNR fluctuated from a higher value for the group with dyslexia at the age of 5 ($p < 0.1$) to a lower SNR for the group with dyslexia at the age of 9 years old ($p < 0.01$).

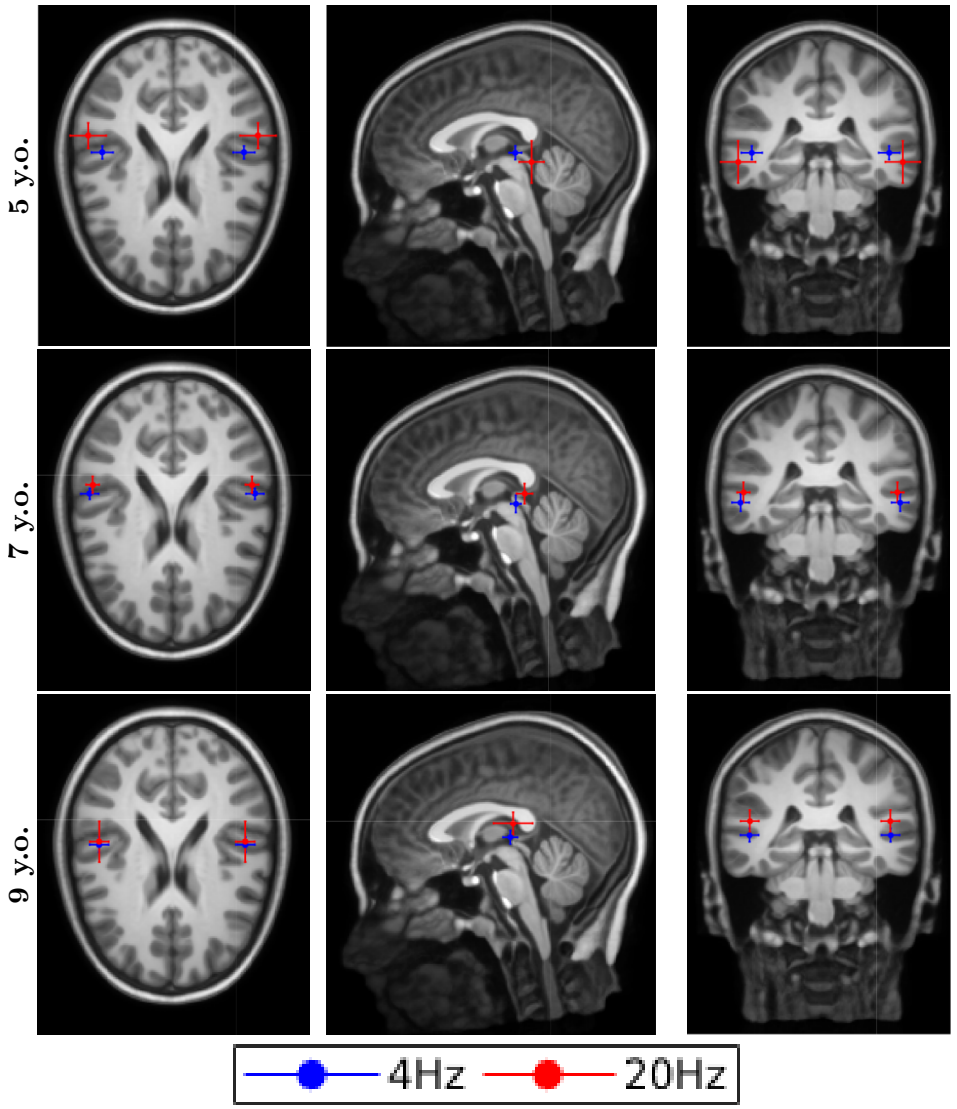


Figure 4.2: Dipole locations of the first DSS component for the typical readers along different ages.

4.3.3 Phase Coherence

Phase Coherence values can be found in Figure 4.6 for 4 Hz and in Figure 4.7 for 20 Hz. In both figures, it is represented how the differences in phase synchrony evolved with age between the typically developing group and the group with dyslexia. For 4 Hz, the typical readers presented a higher connectivity at the age of 5 and 9, while at 7 the group with dyslexia showed a higher Phase Coherence. For 20 Hz, there were no difference at the age of 5, at the age of 7 the typical readers presented higher connectivity values, while at the age of 9 the group with dyslexia presented higher Phase Coherence values.

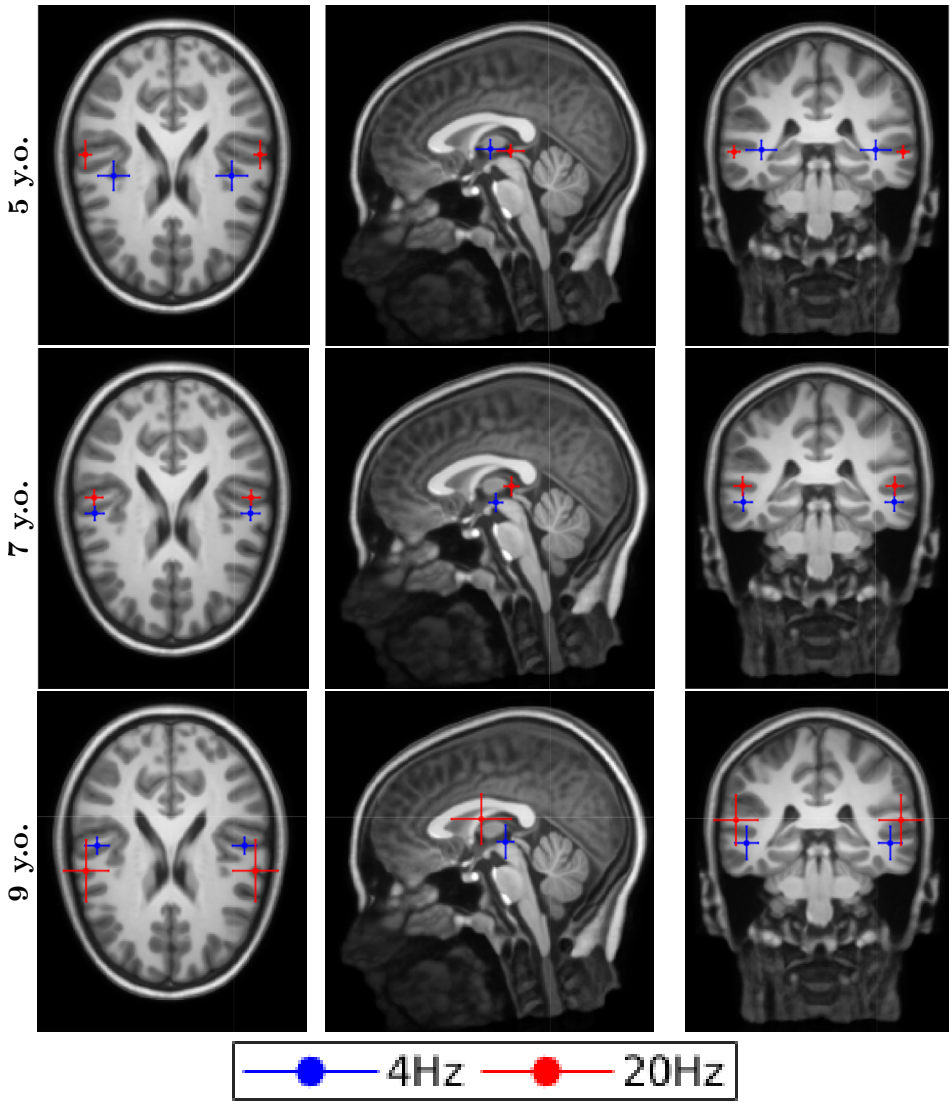


Figure 4.3: Dipole locations of the first DSS component for the readers with dyslexia along different ages.

4.3.4 Laterality Index

Hemispherical preference was calculated through the laterality index for 4 Hz, Figure 4.8, and for 20 Hz, Figure 4.9. During 4 Hz stimulation both groups presented right hemispherical preference across age. However, right lateralisation was stronger for the typically developing group at the age of 5 ($p < 0.1$) and 7 ($p < 0.01$) . At the age of 9, both groups presented similar lateralisation values towards the right hemisphere. For 20 Hz, stimulation the preference for a right lateralisation was also present. The group with dyslexia had a stronger right

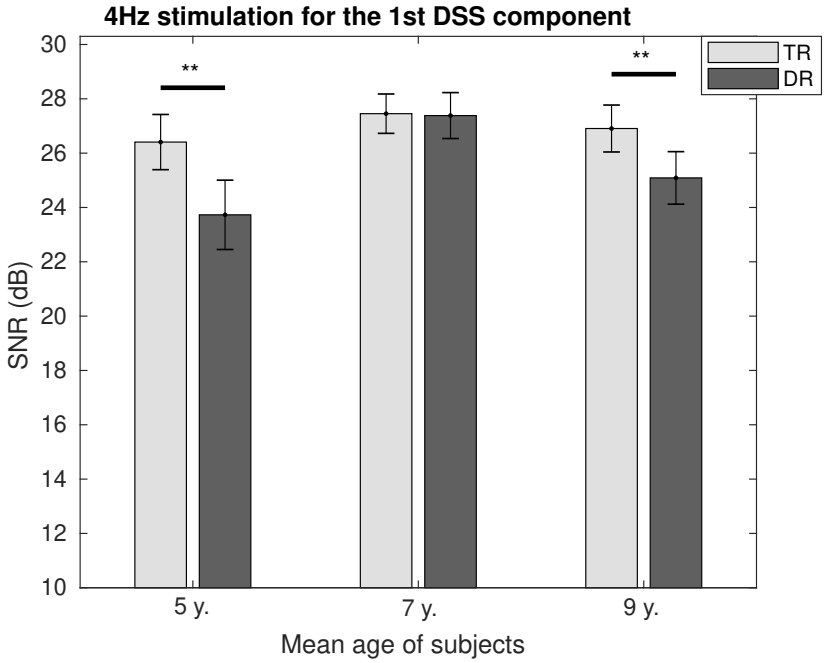


Figure 4.4: Group comparison of the SNR for the first DSS component at 4 Hz. Significant differences below a 0.05 threshold are marked with an $\star$ and thresholds below 0.01 are marked with $\star\star$ for all figures. All the p-values were corrected using the Bonferroni-Holm approach.

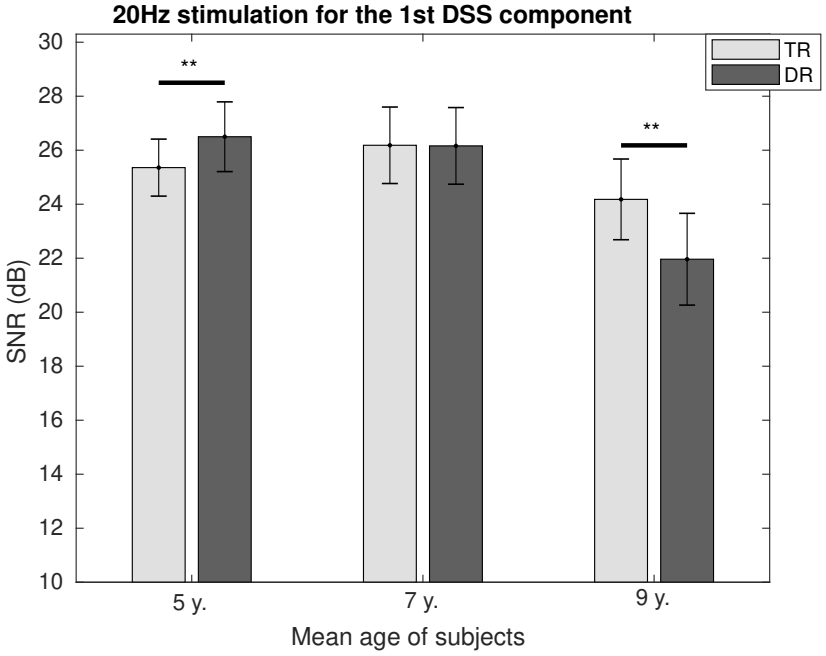


Figure 4.5: Group comparison of the SNR for the first DSS component at 20 Hz. Significant differences below a 0.05 threshold are marked with an $\star$ and thresholds below 0.01 are marked with $\star\star$ for all figures. All the p-values were corrected using the Bonferroni-Holm approach.

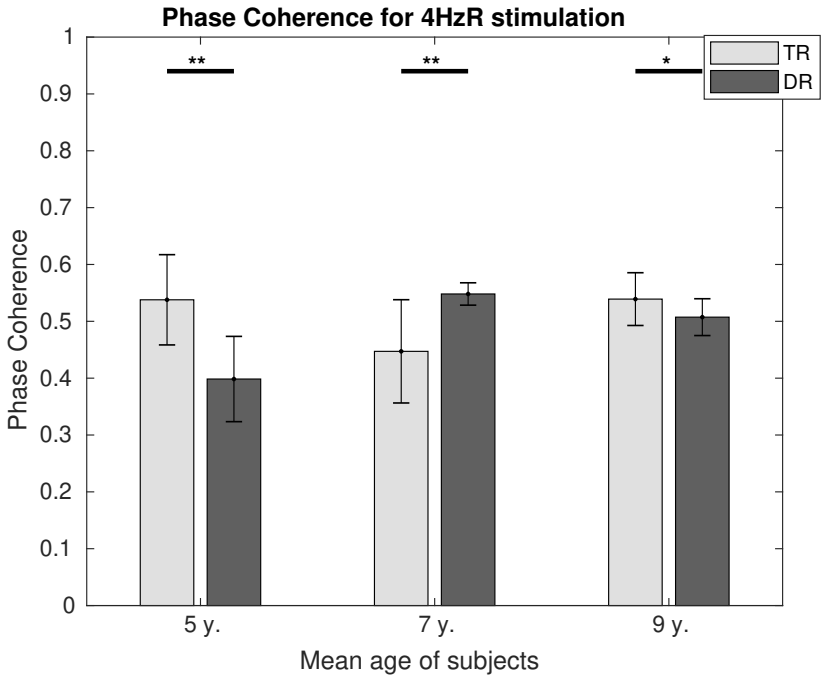


Figure 4.6: Comparison of the phase coherence for the two first DSS components at 4 Hz for both groups. Significant differences below a 0.05 threshold are marked with an $\star$ and thresholds below 0.01 are marked with $\star\star$ for all figures. All the p-values were corrected using the Bonferroni-Holm approach.

lateralisation when compared to the weaker right hemispherical preference typical readers showed at the age of 5 ($p < 0.1$) and at the age of 7 ($p < 0.01$). However, at the age of 9, we could not find differences between the two groups, despite both presented responses lateralised to the right.

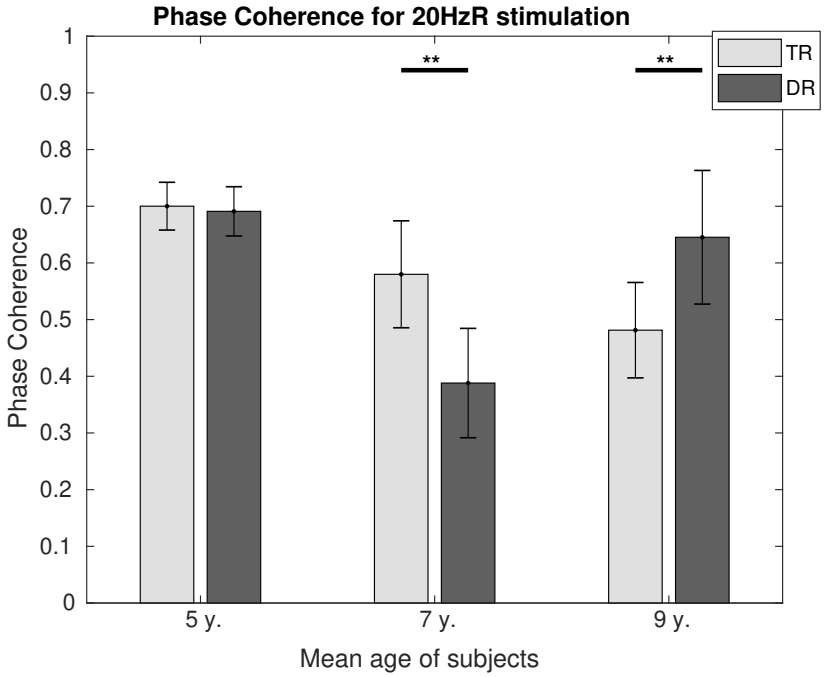


Figure 4.7: Comparison of the phase coherence for the two first DSS components at 20 Hz. Significant differences below a 0.05 threshold are marked with an $\star$ and thresholds below 0.01 are marked with $\star\star$ for all figures. All the p-values were corrected using the Bonferroni-Holm approach.

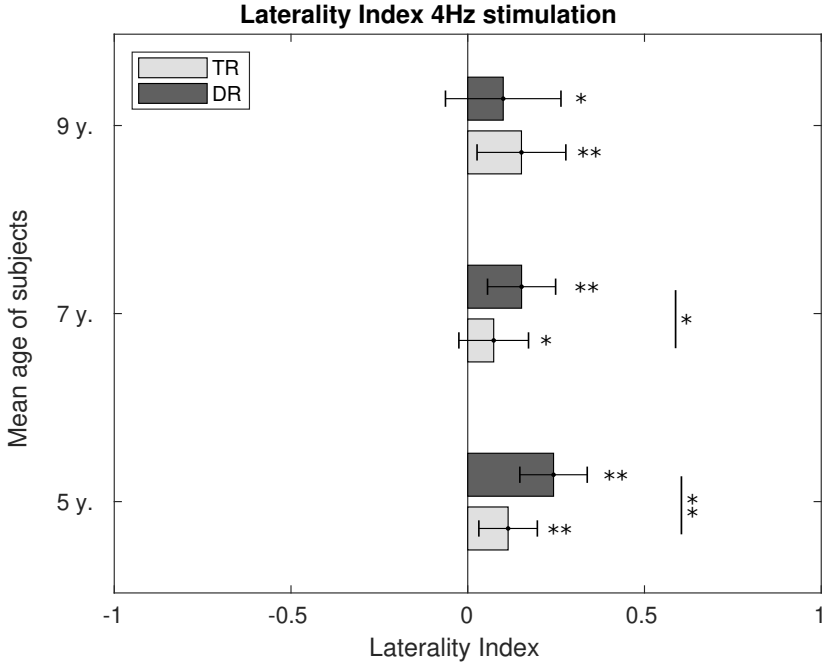


Figure 4.8: Comparison of the laterality index of the first DSS component at 4 Hz. LI values significantly different from zero were calculated and are marked in the Figure as well as the differences between the two groups. P-values below 0.05 are marked with an $\star$ and p-values below 0.01 are marked with $\star\star$ for all figures. All the p-values were corrected using the Bonferroni-Holm approach.

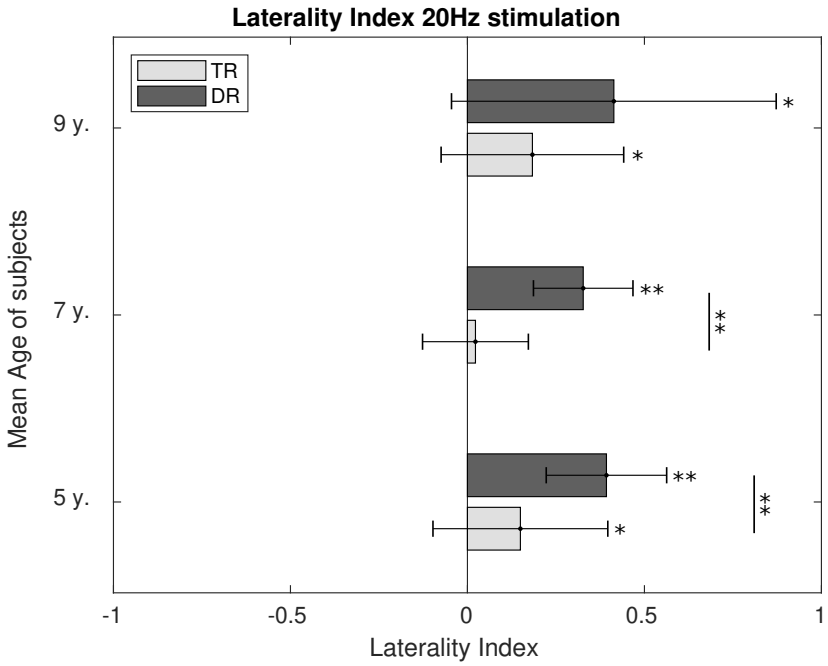


Figure 4.9: Comparison of the laterality index of the first DSS component at 20 Hz. LI values significantly different from zero were calculated and are marked in the Figure as well as the differences between the two groups. P-values below 0.05 are marked with an $\star$ and p-values below 0.01 are marked with $\star\star$ for all figures. All the p-values were corrected using the Bonferroni-Holm approach.

4.4 Discussion

4.4.1 Source Localisation

As it was stated in the results section our figures for the source localisation showed the averages (centre) and the jackknife estimates (error bars) for the dispersion around the mean. These error bars represent the distribution of the participants source location for each spatial direction. Apart from the inherent limitation of the EEG regarding the spatial resolution, which is low compared to other techniques such as MRI, we have to remark upon the use of general MRI templates for all the ages. Due to the problems we found creating the BEM templates for our young participants we decided to use an older functional BEM template based on 14-year-old MRI. Since we used an older template there are aspects that increase our limitations about spatial resolution: First, the size of the head and the distances between tissues are higher in adolescents than in children; another aspect is the geometrical distribution of these tissues, which differs from adolescents to children. In addition, by using a general template for all the subjects we are denying the presence of individual differences caused by a specific geometry of the head. The presented limitations cannot be quantified easily and be represented by an error bar. In summary, we showed these results as a qualitative measure of the nature of the responses. Based solely on the figures we could not observe differences between the processing of syllable-rate stimulation and phoneme-rate stimulation. The lack of difference was present along all ages for both groups. From these results we can conclude that with our methodology and our spatial resolution the primary regions for speech processing in the brain are the same for syllabic-rate stimulation (4 Hz) as for phonemic-rate stimulation (20 Hz) in typically developing children as well as in children with dyslexia.

4.4.2 Signal-to-noise ratio

Activity at 4 Hz (theta rhythm)

For accurate speech processing, the most important modulation frequencies are the ones below 16 Hz (Drullman et al., 1994a,b; Shannon et al., 1995). Moreover, modulation rates below 10 Hz have been associated in speech with the temporal rates of syllables (Edwards & Chang, 2013; Greenberg et al., 2003).

As it was shown in the Figure 4.4: at the age of five the children with dyslexia presented lower entrainment than the typically developing children; the same could be observed at the age of nine. This agrees with the hypotheses presented by Goswami (2011) where a lower entrainment was suggested in the theta (syllable) rate processing for the group with dyslexia. The age of seven is an age when intensive reading training has already started. At this age children with difficulties usually receive extra teaching support. The similarities in the level of neural entrainment found at this age might suggest that all the extra support received had its impact at a neurological level. In fact, this level of support intensifies in the later stages of reading development. Some intervention techniques for readers with dyslexia provide them with efficient tools to enhance their perception that might have an impact in syllable perception. Sometimes that comes at the cost of great mental effort that can be observed in a higher level of neural entrainment in adolescents and adults during stimulation with frequencies at syllable rates (Arns et al., 2007; De Vos et al., 2017a; Lizarazu et al., 2015; Marosi et al., 1995), see also chapter 3. This extra effort is not always reflected at the neural amplitude level. However, we hypothesise that it has its impact by enhancing the SNR observed in children with dyslexia making it comparable to the typical readers (Hämäläinen et al., 2012; Poelmans et al., 2012b).

Activity at 20 Hz (beta rhythm)

Modulation frequencies above 12 Hz are associated with the phoneme rate processing in speech.

As we showed in the results: before formal reading training (at 5 years of age) the group with dyslexia presented a higher level of entrainment. However, at the age of nine, the level of neural entrainment for this group is lower. We hypothesise that typically developing children will perform better after having received formal reading instruction for a long period of time and having trained their phonological representations, reflected in the levels of neural entrainment. This may be increased by an atypical maturation of beta oscillations in dyslectic brains (De Vos et al., 2017a). This atypical maturation may explain the lack of differences in the levels of neural entrainment for both groups (Hämäläinen et al., 2012; Lehongre et al., 2011). Furthermore, it has been suggested that strong compensatory mechanisms would try to enhance the phoneme rate processing in people with dyslexia. These mechanisms might

explain the higher levels of neural entrainment in adolescents with dyslexia, see chapter 3, or adults with dyslexia (Helenius et al., 2002) in comparison with typical readers.

4.4.3 Connectivity

Activity at 4 Hz (theta rhythm)

At the age of five the level of connectivity is higher for the typical readers. This level of synchrony between the two main generators has its reflection as well in the level of neural entrainment represented by the SNR. During intensive reading training (7 years of age) the SNRs show no differences between the two groups. However, we can see that this might be a result of a higher neural effort represented in the higher levels of connectivity for the group with dyslexia. At the age of nine, both the SNR and the Connectivity levels are higher for the typically developing children, suggesting a better neural processing of syllable-rate stimulation. The lower levels of neural entrainment and connectivity may reflect the effects of a disrupted neural network structure and mixed patterns of connectivity abnormalities in children with dyslexia(Frye et al., 2012; Koyama et al., 2013). Similar effects were found in resting-state experiments, where typically developing children presented higher levels of connectivity than the children with dyslexia in the theta frequency band (Fraga González et al., 2016; Xue et al., 2020). Strong compensatory mechanisms seem to appear in later stages of development. These mechanisms would cause the group with dyslexia to have higher levels of connectivity in adolescence (chapter 3) and in adulthood (Thiede et al., 2020).

Activity at 20 Hz (beta rhythm)

The suggestion of an atypical maturation of beta oscillations in dyslexia (De Vos et al., 2017a) may explain the different levels of connectivity that can be found at the ages of seven and nine. Typical readers show a higher phase coherence at 7 while children with dyslexia have a higher phase coherence at the age of nine. Higher levels of connectivity in beta oscillations for children older than 8 y.o. with dyslexia have also been reported in resting state studies (Xue et al., 2020) and are present in adolescence (chapter 3) and in adulthood (Thiede et al., 2020). This later maturation of beta oscillations found with connectivity may trigger the compensatory mechanisms in the neural entrainment levels (SNR) that appear in adolescents

(chapter 3) and adults (Helenius et al., 2002).

4.4.4 Laterality

It has been suggested that the right hemisphere is important for syllabic rate modulations (Boemio et al., 2005; Poeppel, 2003). We could indeed find during stimulation at 4 Hz a strong preference for right lateralisation even at the youngest age. The difference between groups that exists at 5 and 7 might reflect a late maturation process for the children with dyslexia. Both groups would find a similar level of maturation at the age of nine, since both groups show a similar lateralisation level towards the right hemisphere. Different studies also found a right hemisphere lateralisation in theta rhythms in children (Abrams et al., 2008; Vanvooren et al., 2015) and in adults (Bidelman & Howell, 2016; Boemio et al., 2005).

For phonemic rate stimulation (20 Hz), the preference for an ipsilateral lateralisation was clearly shown by the results, except at the age of 7 for the typically developing children. Both groups present similar levels of right hemispherical lateralisation at the age of nine. Before this age the group with dyslexia shows a consistent preference for right lateralisation that is matched by the typically developing group at the age of nine. The preference for a right hemispherical lateralisation in both groups reached at the age of nine would carry on towards adolescence as well (chapter 3). This ipsilateral preference in phonemic-rate stimulation has been shown previously in adolescents and adults in chapter 3 as well as in Jamison et al. (2006); Obleser et al. (2008).

4.5 Conclusion

Despite the well-known heterogeneity during developmental stages, especially in children and in dyslexia, we could extract meaningful common oscillatory patterns using our methodology. In this longitudinal study, we confirmed that the existence of atypical levels of neural entrainment and connectivity already exists in pre-reading stages. Overall, these measures reflected a lower capability of the dyslectic brain to synchronise with syllabic-rate stimulation, in the form of neural entrainment (SNR) and connectivity (Phase Coherence). In addition, our findings reinforced the hypothesis of a later maturation of the processing of beta rhythms in dyslexia. This study shows the importance of longitudinal studies in dyslexia, especially

in children, where differences between the two groups can change in the span of a year. To conclude, we hope we have provided important insights in syllabic and phonemic processing in order to understand the underlying differences of speech processing in developing children with dyslexia.

CHAPTER 5

General discussion and future prospects

5.1 Global Findings of this project

In this PhD project, we aimed to study how neural speech processing between readers with and without dyslexia evolved with age from a source analysis perspective. We used the synchronisation of the phase-locked signals evoked as a response to the temporal envelope modulations of ASSRs. To develop a source analysis perspective, we relied on the reconstruction of the brain activation patterns and their waveforms associated through the methodology developed in chapter 2. Together with the model of how electrical potentials traverse from their origin towards the scalp, i.e., the forward model; we needed a mathematical methodology capable of using this forward model to reconstruct the electrophysiological activity. The major challenges we faced during this stage were: (1) the lack of individual data for the creation of the forward model (i.e., head and brain scan and individual electrode locations); (2) the high oscillatory and correlation features of ASSRs and (3) the high inter-subject variability in developing children. In chapter 2, we specified how our approach used an age-related MRI template and their BEM head model calculated in order to develop our functional forward model. We aimed to extract the most prominent brain activity evoked by our auditory stimulation. This allowed to reconstruct and measure the most representative pattern of electrophysiological activity

during auditory stimulation for a group of subjects. This approach provided us with a set of outcome measures where we could find common trends in the data that were representative of the whole group.

In chapter 3, we evaluated how brain dynamics differed in adolescents with and without dyslexia during auditory stimulation capable of triggering phase-locked responses.

We showed that the major differences were not found in the brain activation pattern, or in other words, the location of the activity sources, but rather in the reconstructed brain activity, i.e., in the oscillatory waveforms. In chapter 4, we measured the brain response pattern through ASSRs in children with and without risk of dyslexia at three different age points. We wanted to evaluate how brain differences reported in literature could evolve with age in three important stages of reading: before formal reading instruction, during formal reading instruction and after one year of formal reading instruction. On the following pages we will review the major findings of each study carried out in the framework of this PhD thesis.

5.1.1 Development of the methodology

We focused our efforts on finding a brain source methodology that was independent of the head model and that had a low number of prior assumptions. This methodology was tested in order to extract group pattern activity with physiological plausibility. Overall we obtained higher SNRs for the group concatenation than the superposition or average of individual results. Furthermore, the group level offered a lower number of dispersion due to two effects: the first one is related to an enhanced detection caused by the use of a higher number of epochs, and the second one associated with the reduction of inter-subject variability produced by data concatenation. It is true that there might be relevant information in subject-dependent data, however, our aim was focused on the extraction of the most prominent ASSR activity across the whole group.

The goal of this project was to apply this methodology in further studies about speech processing in dyslexia. For that reason, we used different modulation frequencies for the ASSRs: low modulation rates ($4\ Hz, 10\ Hz$ and $20\ Hz$) and high modulation rates ($40\ Hz$ and $80\ Hz$). For low modulation frequencies, we could reconstruct the brain activation pattern

and their brain waves associated to the sources with relatively low dispersion and high SNRs. The location of the brain sources presented a symmetry consistent with the symmetrical activation of both auditory cortices and their locations were obtained in the vicinities of the auditory cortices. For high modulation frequencies, the brain activation pattern was not as clear. It is known that during auditory stimulation at 40 Hz a high number of sources are firing simultaneously from the brain cortex as well as from deeper regions (Farahani et al., 2017; Reyes et al., 2005). This caused our methodology to detect different sources of brain activity that were active during a significant number of epochs. Different sources of activity with different properties such as location and waveforms contributed to the high dispersion observed during the study. The multiple activation pattern together with what is known as the depth bias that appears in low-SNR scenarios (Fuchs et al., 1999; Lucka et al., 2012; De Peralta et al., 2009) could explain the high dispersion found at individual and group level for high modulation frequencies: 40 Hz and 80 Hz.

The reconstructed signals at the group level presented a behaviour that was already observed in scalp EEG recordings, for example the highest relative response amplitudes at 4 Hz (Vanvooren et al., 2015) or highest SNR at the modulation frequency of 40 Hz (Rance, 2008). The same could not be observed at the individual level, proving that a high number of epochs improves performance in ASSR analyses. We could conclude that our methodology could obtain the brain activation pattern and the waveform associated of the most prominent activity of a group. Especially in low modulation frequencies, where the most important physiological features are present (Picton et al., 2003). We developed our methodology towards studying differences in speech processing in dyslexia, and it is known that the most of the energy of the envelope modulation spectrum of speech is constrained in the range of 4 Hz to 16 Hz (Drullman et al., 1994a,b; Shannon et al., 1995).

5.1.2 Syllable rates processing in dyslexia

The stimulation frequency of 4 Hz evokes ASSR contained in the theta range, which lies in the range of temporal rates of syllables in speech. It was proposed in Goswami (2011) that major differences between readers with and without dyslexia should occur in frequencies related to the theta rhythm. This means a less efficient phase-locking of the main brain auditory

generators to stimulations happening in this frequency range.

In chapter 4, we could observe lower neural entrainment in theta for readers with dyslexia in our longitudinal dataset from children. Specifically at the ages of 5 and 9 years old. The markers for a lower neural entrainment were the SNR levels at the frequency of 4 Hz as well as the Phase Coherence levels, which in our experience they are intrinsically related to each other. However, lower entrainment in the theta frequency range for the group with dyslexia was not observed in chapter 3, where data were obtained from adolescents instead of children. The lack of differences between readers with and without dyslexia in the theta frequency range was also observed in other EEG studies (Arns et al., 2007; Marosi et al., 1995) as well as MEG (Lizarazu et al., 2015). In addition, other studies have never been able to show a theta rate synchronisation difference in adults with dyslexia (Hämäläinen et al., 2012; Poelmans et al., 2012b). This might indicate that the encoding of frequency ranges other than theta could become more important with age. We observed in adolescents a lower neural entrainment for the group with dyslexia during the stimulation at 10 Hz (alpha band). Alpha band has been associated with the upper limit of temporal rates at which syllables occur in speech (Edwards & Chang, 2013; Greenberg et al., 2003). Thus, we believe oscillations occurring in the alpha band become more important with age when it comes to syllable encoding. Overall, lower neural entrainment levels in readers with dyslexia during stimulation in this frequency band could be related to the speech-in-noise perception differences that have been shown in other studies in dyslexia (Boets et al., 2007; Dole et al., 2012; Poelmans et al., 2011; Ziegler et al., 2009; Van Hirtum et al., 2019b, 2021).

5.1.3 Phoneme rates processing in dyslexia

In this project, we studied phoneme rate processing through the auditory stimulation at the modulation frequency of 20 Hz, which belongs to the beta range. In chapter 4, we observed that typically developing children presented higher levels of neural entrainment after receiving formal reading instruction (9 y.o.). However, in chapter 3 adolescents with dyslexia showed an atypical higher neural entrainment at this modulation frequency. It has been hypothesised that there could be an atypical maturation process associated with auditory processing frequencies in the beta range for readers with dyslexia (De Vos et al., 2017a). This

suggestion was accompanied by the development of strong overcompensatory mechanisms, that may emerge in later stages of development. A brain with dyslexia would try to enhance phonemic rate processing, in line with a series of studies that showed improved responses to phonemic rate alterations in school-aged children as well as in adults with dyslexia (Helenius et al., 2002; Lohvansuu et al., 2014). These two effects together could explain why typically developing children after formal reading instruction present higher levels of neural entrainment in this frequency range, and why in adolescence and adulthood readers with dyslexia might present atypically higher levels of neural entrainment.

5.2 Future prospects

The main investigation line of this doctoral research focused on auditory processing differences between readers with and without dyslexia during speech-related stimulation and how these may arise with age.

However, all the findings presented in the chapters 3 and 4 are based on the methodology developed in chapter 2. This project has presented the limitations any source analysis study with EEG data would face. All the choices made were carefully evaluated over other options. However, they were not exempt of downsides and sometimes we were limited by the computational load when making our choices over other potential benefits. Thus, in order to improve the methodology and the derived studies, these limitations should be taken into account, together with the considerations and implications every choice had.

We selected the C_z electrode as a reference. The selection of C_z as reference has proven more reliable than the average based reference in EEG experiments with an array of 64 EEG electrodes or less (Fein et al., 1988; Srinivasan et al., 1998). This selection provided us with a reference that was stable across subjects; relatively far away from the generators; in the sagittal plane, to reduce the effect over spatially symmetrical responses; and with relatively low muscular artefacts. In return, the detection of deep sources, especially for high modulation frequencies, was significantly altered. Because the contribution of these deep sources is only detected by the parietal and occipital electrodes after referencing to C_z; coronal electrodes are highly sensitive to these brain sources. Thus, only very strong deep sources could be detected. This had an impact on the performance of the methodology presented in chapter 2 for high

frequencies.

ASSRs have proven very useful in different fields to study the neural processing of the temporal aspects of speech. However, using a electrophysiological phase-locked response will raise a number of considerations for any source analysis study that want to use them as the main stimulation paradigm. All ASSR generators carry their information in the same frequency, independently of their location. Most of the source analysis methods use separation criteria defined in at the time-series level. In our case, these criteria were two: First, the Shannon mutual information, for ICA, which uses the joint and marginal distributions of discrete signals. The second one, the reproducibility across epochs for DSS, which uses the proportion of epoch-averaged (evoked) activity. It is true that some separation methods can be adapted or have been defined to be applicable in the frequency domain. However, they perform much better with electrophysiological signals with a rich frequency spectrum where evoked activity is not only present at the modulation frequency.

Furthermore, most of the methods assume that the brain activity is produced by stationary sources. Although their changes in location are slow compared to the electrical propagation effects (Hallez et al., 2007), brain sources are not fully static. Distributed Source Models can work around this issue by providing brain activity information through a mesh of a high number of distributed dipoles. Despite being static, this mesh of dipoles can cover wide areas of the brain with high resolution offering an overview about how the activity pattern changes throughout the recording. Nevertheless, these methods require of a very detailed head model to yield reliable results. Very detailed head models, often FEM, need of subject specific high-quality MRIs or manual supervision.

Generally, in most studies, the individual information is useful from a clinical point of view. However, to either evaluate or classify a single individual, previous group studies are required in order to provide with evaluation or classification patterns. To achieve that, it is necessary to understand the underlying features that are common to a group of individuals. This can be done by analysing all the individual data in a group of subjects with a high level of detail and extracting the common patterns afterwards. This way of proceeding would be able to answer research questions using the common information of the group while retaining and considering the individual variability that has an important clinical value. However, as we have explained before, to achieve the best result often entails the use of significant amount

of resources, being these time or computing power. Furthermore, even the best choices have downsides that need to be considered as well.

In summary, for this project about temporal processing in subjects with and without dyslexia, we thought the development of a group analysis had more scientific motivations. Since the underlying mechanisms that produce differences in the neural entrainment levels during auditory processing in dyslexia remain unknown.

That was the main reason that steered us towards data-driven methods used to estimate spatial filters and why we chose to work with head models derived from BEM constructed from MRI averaged templates. For this research project, we did not have the resources to carry out a full group analysis taking into consideration individual differences in morphology and in electrode locations. We focused on extracting the most representative electrophysiological activity during auditory stimulation using the high temporal resolution that EEG offers.

As we have mentioned, we were aware of the limitations of our methodology, especially regarding source localisation at high modulation rates, and the rejection of inter-subject variability. However, we believe that despite the existence of higher heterogeneity in developing stages, we have shown that there are still common patterns of oscillatory activity that could be found across the whole group with a careful choice of the methodology. Some of these patterns pointed out differences between the two groups. Differences that can be already observed in pre-reading stages and are still during further developmental stages. To have such indicators at this early stage may prove useful for future clinical applications. Since dyslexia can only be formally diagnosed once children are able to read and write, before this reading stage, a risk for dyslexia can only be evaluated based on a family risk for dyslexia indicator. Thus, an in-depth analysis that could extract information that could differentiate a dyslectic brain from a typically developing one will have an important impact in the field of clinical applications. Because intervention has proven more effective when applied in these early stages.

Furthermore, we would like to remark the scientific information a longitudinal study may provide. It may compensate for the known high heterogeneity that exists in developing children, especially in the field of dyslexia. Its importance has also been suggested in the validation of existing theories or for the development of new ones (Goswami, 2015).

We can conclude that we have provided with an interesting starting point in the devel-

opment of methodologies whose main aim is to analyse the most representative electrophysiological activity present in a group. The studies derived from this methodology presented interesting insights about how different neural entrainment levels evolved with age and with the different stages of formal reading instruction. Overall, this project presents with some evidence that may be used in future studies aiming to find patterns between a dyslectic brain and a typically developing one even in very early stages. A study that could find differentiating patterns in dyslexia in pre-reading stages will have a significant clinical impact. Because it will allow the application of intervention plans when they are most effective.

References

Abdi, H., & Williams, L. J. (2010). Principal component analysis. *Wiley Interdisciplinary Reviews: Computational Statistics*, *2*, 433–459. doi:10.1002/wics.101.

Abrams, D. A., Nicol, T., Zecker, S., & Kraus, N. (2008). Right-Hemisphere Auditory Cortex Is Dominant for Coding Syllable Patterns in Speech. *Journal of Neuroscience*, *28*, 3958–3965. doi:10.1523/JNEUROSCI.0187-08.2008.

Adrián-Ventura, J., Soriano-Ferrer, M., Fuentes-Claramonte, P., Morte-Soriano, M., Parcet, M. A., & Ávila, C. (2020). Grey matter reduction in the occipitotemporal cortex in spanish children with dyslexia: A voxel-based morphometry study. *Journal of Neurolinguistics*, *53*, 100873. doi:https://doi.org/10.1016/j.jneuroling.2019.100873.

Akalin Acar, Z., & Makeig, S. (2013). Effects of Forward Model Errors on EEG Source Localization. *Brain Topography*, *26*, 378–396. doi:10.1007/s10548-012-0274-6.

Alaerts, J., Luts, H., Hofmann, M., & Wouters, J. (2009). Cortical auditory steady-state responses to low modulation rates. *International Journal of Audiology*, *48*, 582–593. doi:10.1080/14992020902894558.

Arns, M., Peters, S., Breteler, R., & Verhoeven, L. (2007). Different brain activation patterns in dyslexic children: Evidence from EEG power and coherence patterns for the double-deficit theory of dyslexia. *Journal of Integrative Neuroscience*, *06*, 175–190. doi:10.1142/S0219635207001404.

Artoni, F., Delorme, A., & Makeig, S. (2018). Applying dimension reduction to EEG data by Principal Component Analysis reduces the quality of its subsequent Independent Component decomposition. *NeuroImage*, *175*, 176–187. doi:10.1016/j.neuroimage.2018.03.016.

Bell, A. J., & Sejnowski, T. J. (1995). An Information-Maximization Approach to Blind Separation and Blind Deconvolution. *Neural Computation*, *7*, 1129–1159. doi:10.1162/neco.1995.7.6.1129. arXiv:arXiv:1511.06440v1.

Berlingeri, M., Danelli, L., Bottini, G., Sberna, M., & Paulesu, E. (2013). Reassessing the HAROLD model: Is the hemispheric asymmetry reduction in older adults a special case of compensatory-related utilisation of neural circuits? *Experimental Brain Research*, *224*, 393–410. doi:10.1007/s00221-012-3319-x.

Bidelman, G. M., & Howell, M. (2016). Functional changes in inter- and intra-hemispheric cortical processing underlying degraded speech perception. *NeuroImage*, *124*, 581–590. doi:10.1016/j.neuroimage.2015.09.020.

Biesmans, W., Bertrand, A., Wouters, J., & Moonen, M. (2015). Optimal spatial filtering for auditory steady-state response detection using high-density EEG. In *2015 IEEE International Conference on Acoustics, Speech and Signal Processing (ICASSP)* (pp. 857–861). IEEE. doi:10.1109/ICASSP.2015.7178091.

Boemio, A., Fromm, S., Braun, A., & Poeppel, D. (2005). Hierarchical and asymmetric temporal sensitivity in human auditory cortices. *Nature Neuroscience*, *8*, 389–395. doi:10.1038/nn1409.

Boets, B., Ghesquière, P., Van Wieringen, A., & Wouters, J. (2007). Speech perception in preschoolers at family risk for dyslexia: Relations with low-level auditory processing and phonological ability. *Brain and language*, *101*, 19–30.

Bohórquez, J., & Özdamar, Ö. (2008). Generation of the 40-Hz auditory steady-state response (ASSR) explained using convolution. *Clinical Neurophysiology*, *119*, 2598–2607. doi:10.1016/j.clinph.2008.08.002.

Van den Bos, K., Spelberg, H., Scheepsma, A., & De Vries, J. (1994). De klepel. vorm a en b. een test voor de leesvaardigheid van pseudowoorden. verantwoording, handleiding, diagnostiek en behandeling. *Nijmegen, the Netherlands: Berkhout*, .

Bouveyron, C., & Brunet-Saumard, C. (2014). Model-based clustering of high-dimensional data: A review. *Computational Statistics & Data Analysis*, *71*, 52 – 78. doi:https://doi.org/10.1016/j.csda.2012.12.008.

Brus, B. T., & Voeten, M. J. M. (1973). *Een-minuut-test: vorm A en B; schoolvorderingentest voor de technische leesvaardigheid, bestemd voor het tweede tot en met het zesde leerjaar van het basisonderwijs; verantwoording en handleiding*. Berkhout.

Buzsaki, G. (2006). *Rhythms of the Brain*. Oxford University Press.

Centanni, T., Pantazis, D., Truong, D., Gruen, J., Gabrieli, J., & Hogan, T. (2018). Increased variability of stimulus-driven cortical responses is associated with genetic variability in children with and without dyslexia. *Developmental Cognitive Neuroscience*, *34*, 7–17. doi:10.1016/j.dcn.2018.05.008.

Chait, M., Greenberg, S., Arai, T., Simon, J. Z., & Poeppel, D. (2015). Multi-time resolution analysis of speech: evidence from psychophysics. *Frontiers in Neuroscience*, *9*, 1–10. doi:10.3389/fnins.2015.00214.

de Cheveigné, A., & Arzounian, D. (2015). Scanning for oscillations. *Journal of Neural Engineering*, *12*, 066020. doi:10.1088/1741-2560/12/6/066020.

de Cheveigne, A., & Simon, J. Z. (2008). Denoising based on spatial filtering. *Journal of Neuroscience Methods*, *171*, 331–339. doi:10.1016/j.jneumeth.2008.03.015.

Coffey, E. B. J., Herholz, S. C., Chepesiuk, A. M. P., Baillet, S., & Zatorre, R. J. (2016). Cortical contributions to the auditory frequency-following response revealed by MEG. *Nature Communications*, *7*, 11070. doi:10.1038/ncomms11070.

Cong, F., He, Z., Hämäläinen, J., Leppänen, P. H., Lyytinen, H., Cichocki, A., & Ristaniemi, T. (2013). Validating rationale of group-level component analysis based on estimating number of sources in EEG through model order selection. *Journal of Neuroscience Methods*, *212*, 165–172. doi:10.1016/j.jneumeth.2012.09.029.

Cummins, F. (2009). Rhythm as entrainment: The case of synchronous speech. *Journal of Phonetics*, *37*, 16–28. doi:10.1016/j.wocn.2008.08.003.

Dalal, S., Sekihara, K., & Nagarajan, S. (2006). Modified Beamformers for Coherent Source Region Suppression. *IEEE Transactions on Biomedical Engineering*, *53*, 1357–1363. doi:10.1109/TBME.2006.873752. arXiv:NIHMS150003.

D'Croz-Baron, D. F., Bréchet, L., Baker, M., & Karp, T. (2021). Auditory and Visual Tasks Influence the Temporal Dynamics of EEG Microstates During Post-encoding Rest. *Brain Topography*, *34*, 19–28. doi:10.1007/s10548-020-00802-4.

De Cheveigné, A., & Parra, L. C. (2014). Joint decorrelation, a versatile tool for multichannel data analysis. *NeuroImage*, *98*, 487–505. doi:10.1016/j.neuroimage.2014.05.068.

De Peralta, R. G., Hauk, O., & Gonzalez, S. L. (2009). The neuroelectromagnetic inverse problem and the zero dipole localization error. *Computational Intelligence and Neuroscience*, *2009*. doi:10.1155/2009/659247.

De Vos, A., Vanvooren, S., Ghesquière, P., & Wouters, J. (2020). Subcortical auditory neural synchronization is deficient in pre-reading children who develop dyslexia. *Developmental Science*, *23*, 1–16. doi:10.1111/desc.12945.

De Vos, A., Vanvooren, S., Vanderauwera, J., Ghesquière, P., & Wouters, J. (2017a). A longitudinal study investigating neural processing of speech envelope modulation rates in children with (a family risk for) dyslexia. *Cortex*, *93*, 206–219. doi:10.1016/j.cortex.2017.05.007.

De Vos, A., Vanvooren, S., Vanderauwera, J., Ghesquière, P., & Wouters, J. (2017b). Atypical neural synchronization to speech envelope modulations in dyslexia. *Brain and Language*, *164*, 106–117. doi:10.1016/j.bandl.2016.10.002.

Delorme, A., & Makeig, S. (2004). EEGLAB: an open source toolbox for analysis of single-trial EEG dynamics including independent component analysis. *Journal of Neuroscience Methods*, *134*, 9–21. doi:10.1016/j.jneumeth.2003.10.009. arXiv:j.jneumeth.2003.10.009.

van Deursen, J., Vuurman, E., van Kranen-Mastenbroek, V., Verhey, F., & Riedel, W. (2011). 40-hz steady state response in alzheimer's disease and mild cognitive impairment. *Neurobiology of Aging*, *32*, 24 – 30. doi:https://doi.org/10.1016/j.neurobiolaging.2009.01.002.

Di Liberto, G. M., Peter, V., Kalashnikova, M., Goswami, U., Burnham, D., & Lalor, E. C. (2018). Atypical cortical entrainment to speech in the right hemisphere underpins phonemic deficits in dyslexia. *NeuroImage*, *175*, 70–79. doi:10.1016/j.neuroimage.2018.03.072.

Dimitrijevic, A., John, M. S., & Picton, T. W. (2004). Auditory Steady-State Responses and Word Recognition Scores in Normal-Hearing and Hearing-Impaired Adults. *Ear and Hearing*, *25*, 68–84. doi:10.1097/01.AUD.0000111545.71693.48.

Dimitrijevic, A., Smith, M. L., Kadis, D. S., & Moore, D. R. (2017). Cortical alpha oscillations predict speech intelligibility. *Frontiers in Human Neuroscience*, *11*, 1–10. doi:10.3389/fnhum.2017.00088.

Dole, M., Hoen, M., & Meunier, F. (2012). Speech-in-noise perception deficit in adults with dyslexia: Effects of background type and listening configuration. *Neuropsychologia*, *50*, 1543–1552.

Drullman, R., Festen, J. M., & Plomp, R. (1994a). Effect of reducing slow temporal modulations on speech reception. *The Journal of the Acoustical Society of America*, *95*, 2670–2680. doi:10.1121/1.409836.

Drullman, R., Festen, J. M., & Plomp, R. (1994b). Effect of temporal envelope smearing on speech reception. *The Journal of the Acoustical Society of America*, *95*, 1053–1064. doi:10.1121/1.408467.

Eden, G. F., Olulade, O. A., Evans, T. M., Krafnick, A. J., & Alkire, D. R. (2016). Chapter 65 - developmental dyslexia. In G. Hickok, & S. L. Small (Eds.), *Neurobiology of Language* (pp. 815 – 826). San Diego: Academic Press. doi:https://doi.org/10.1016/B978-0-12-407794-2.00065-1.

Edwards, E., & Chang, E. F. (2013). Syllabic ($\sim$ 2–5 Hz) and fluctuation ($\sim$ 1–10 Hz) ranges in speech and auditory processing. *Hearing Research*, *305*, 113–134. doi:10.1016/j.heares.2013.08.017.

Efron, B., & Stein, C. (1981). The Jackknife Estimate of Variance. *The Annals of Statistics*, *9*, 586–596. doi:10.1214/aos/1176345462.

Eichele, T., Rachakonda, S., Brakedal, B., Eikeland, R., & Calhoun, V. D. (2011). EEGIFT: Group Independent Component Analysis for Event-Related EEG Data. *Computational Intelligence and Neuroscience*, *2011*, 1–9. doi:10.1155/2011/129365.

Fant, G. (1970). *Acoustic Theory of Speech Production*. D A C S R Series. De Gruyter.

Farahani, E., Goossens, T., Wouters, J., & van Wieringen, A. (2017). Spatiotemporal reconstruction of auditory steady-state responses to acoustic amplitude modulations: potential sources beyond the auditory pathway. *NeuroImage*, *148*, 1–35. doi:10.1016/j.neuroimage.2017.01.032.

Farahani, E. D., Wouters, J., & van Wieringen, A. (2019). Contributions of non-primary cortical sources to auditory temporal processing. *NeuroImage*, *191*, 303–314. doi:10.1016/j.neuroimage.2019.02.037.

Farahani, E. D., Wouters, J., & Wieringen, A. (2021). Brain mapping of auditory steady-state responses: A broad view of cortical and subcortical sources. *Human Brain Mapping*, *42*, 780–796. doi:10.1002/hbm.25262.

Fedorov, A., Beichel, R., Kalpathy-Cramer, J., Finet, J., Fillion-Robin, J.-C., Pujol, S., Bauer, C., Jennings, D., Fennessy, F., Sonka, M., Buatti, J., Aylward, S., Miller, J., Pieper, S., & Kikinis, R. (2012). 3d slicer as an image computing platform for the quantitative imaging network. *Magnetic Resonance Imaging*, *30*, 1323–41.

Fein, G., Raz, J., Brown, F. F., & Merrin, E. L. (1988). Common reference coherence data are confounded by power and phase effects. *Electroencephalography and Clinical Neurophysiology*, *69*, 581–584. doi:10.1016/0013-4694(88)90171-X.

Fell, J., & Axmacher, N. (2011). The role of phase synchronization in memory processes. *Nature reviews. Neuroscience*, *12*, 105–118. doi:10.1038/nrn2979.

Fonov, V., Evans, A. C., Botteron, K., Almli, C. R., McKinstry, R. C., & Collins, D. L. (2011). Unbiased average age-appropriate atlases for pediatric studies. *NeuroImage*, *54*, 313–327. doi:10.1016/j.neuroimage.2010.07.033.

Fowler, R. (1986). *Linguistic Criticism*. An OPUS book. Oxford University Press.

Fraga González, G., Van der Molen, M., Žarić, G., Bonte, M., Tijms, J., Blomert, L., Stam, C., & Van der Molen, M. (2016). Graph analysis of EEG resting state functional networks in dyslexic readers. *Clinical Neurophysiology*, *127*, 3165–3175. doi:10.1016/j.clinph.2016.06.023.

Frye, R. E., Liederman, J., McGraw Fisher, J., & Wu, M.-H. (2012). Laterality of Temporoparietal Causal Connectivity during the Prestimulus Period Correlates with Phonological Decoding Task Performance in Dyslexic and Typical Readers. *Cerebral Cortex*, *22*, 1923–1934. doi:10.1093/cercor/bhr265.

Fuchs, M., Wagner, M., Köhler, T., & Wischmann, H.-A. (1999). Linear and Nonlinear Current Density Reconstructions. *Journal of Clinical Neurophysiology*, *16*, 267–295. doi:10.1097/00004691-199905000-00006.

Füllgrabe, C., Stone, M. A., & Moore, B. C. J. (2009). Contribution of very low amplitude-modulation rates to intelligibility in a competing-speech task. *The Journal of the Acoustical Society of America*, *125*, 1277–1280. doi:10.1121/1.3075591.

Gabriel, S., Lau, R. W., & Gabriel, C. (1996). The dielectric properties of biological tissues: II. Measurements in the frequency range 10 Hz to 20 GHz. *Physics in Medicine and Biology*, *41*, 2251–2269. doi:10.1088/0031-9155/41/11/002.

Gelfand, S. (2018). *Hearing: An Introduction to Psychological and Physiological Acoustics, Sixth Edition*. Taylor & Francis Group.

Ghitza, O. (2011). Linking Speech Perception and Neurophysiology: Speech Decoding Guided by Cascaded Oscillators Locked to the Input Rhythm. *Frontiers in Psychology*, *2*, 1–13. doi:10.3389/fpsyg.2011.00130.

Giraud, A.-L., Lorenzi, C., Ashburner, J., Wable, J., Johnsrude, I., Frackowiak, R., & Kleinschmidt, A. (2000). Representation of the temporal envelope of sounds in the human brain. *Journal of Neurophysiology*, *84*, 1588–1598. doi:10.1152/jn.2000.84.3.1588. arXiv:https://doi.org/10.1152/jn.2000.84.3.1588. PMID: 10980029.

Giraud, A.-L., & Poeppel, D. (2012). Cortical oscillations and speech processing: emerging computational principles and operations. *Nature Neuroscience*, *15*, 511–517. doi:10.1038/nn.3063. arXiv:15334406.

Goossens, T., Vercammen, C., Wouters, J., & van Wieringen, A. (2016). Aging Affects Neural Synchronization to Speech-Related Acoustic Modulations. *Frontiers in Aging Neuroscience*, *8*, 1–16. doi:10.3389/fnagi.2016.00133.

Goossens, T., Vercammen, C., Wouters, J., & van Wieringen, A. (2017). Masked speech perception across the adult lifespan: Impact of age and hearing impairment. *Hearing Research*, *344*, 109–124. doi:10.1016/j.heares.2016.11.004.

Goossens, T., Vercammen, C., Wouters, J., & van Wieringen, A. (2018). Neural envelope encoding predicts speech perception performance for normal-hearing and hearing-impaired adults. *Hearing Research*, *370*, 189–200. doi:10.1016/j.heares.2018.07.012.

Goossens, T., Vercammen, C., Wouters, J., & van Wieringen, A. (2019). The association between hearing impairment and neural envelope encoding at different ages. *Neurobiology of Aging*, *74*, 202–212. doi:10.1016/j.neurobiolaging.2018.10.008.

Goswami, U. (2011). A temporal sampling framework for developmental dyslexia. *Trends in Cognitive Sciences*, *15*, 3–10. doi:10.1016/j.tics.2010.10.001.

Goswami, U. (2012). Phonological representation. In N. M. Seel (Ed.), *Encyclopedia of the Sciences of Learning* (pp. 2625–2627). Boston, MA: Springer US. URL: https://doi.org/10.1007/978-1-4419-1428-6_148. doi:10.1007/978-1-4419-1428-6_148.

Goswami, U. (2015). Sensory theories of developmental dyslexia: three challenges for research. *Nature Reviews Neuroscience*, *16*, 43–54. doi:10.1038/nrn3836.

Granados Barbero, R., Vos, A., Ghesquière, P., & Wouters, J. (2021). Atypical processing in neural source analysis of speech envelope modulations in adolescents with dyslexia. *European Journal of Neuroscience*, (pp. 1–21). doi:10.1111/ejn.15515.

Grech, R., Cassar, T., Muscat, J., Camilleri, K. P., Fabri, S. G., Zervakis, M., Xanthopoulos, P., Sakkalis, V., & Vanrumste, B. (2008). Review on solving the inverse problem in EEG source analysis. *Journal of NeuroEngineering and Rehabilitation*, *5*, 1–33. doi:10.1186/1743-0003-5-25.

Greenberg, S., Carvey, H., Hitchcock, L., & Chang, S. (2003). Temporal properties of spontaneous speech—a syllable-centric perspective. *Journal of Phonetics*, *31*, 465–485. doi:10.1016/j.wocn.2003.09.005.

Guttorm, T. K., Leppänen, P. H., Poikkeus, A.-M., Eklund, K. M., Lyytinen, P., & Lyytinen, H. (2005). Brain Event-Related Potentials (ERPs) Measured at Birth Predict Later Language Development in Children with and Without Familial Risk for Dyslexia. *Cortex*, *41*, 291–303. doi:10.1016/S0010-9452(08)70267-3.

Hallez, H., Vanrumste, B., Grech, R., Muscat, J., De Clercq, W., Vergult, A., D'Asseler, Y., Camilleri, K. P., Fabri, S. G., Van Huffel, S., & Lemahieu, I. (2007). Review on solving the forward problem in EEG source analysis. *Journal of NeuroEngineering and Rehabilitation*, *4*, 46. doi:10.1186/1743-0003-4-46.

Halliday, D., Resnick, R., & Walker, J. (2013). *Fundamental of Physics Extended*. Wiley. doi:10.1017/CBO9781107415324.004. arXiv:arXiv:1011.1669v3.

Hämäläinen, J. A., Rupp, A., Soltész, F., Szücs, D., & Goswami, U. (2012). Reduced phase locking to slow amplitude modulation in adults with dyslexia: An MEG study. *NeuroImage*, *59*, 2952–2961. doi:10.1016/j.neuroimage.2011.09.075.

Hamm, J. P., Gilmore, C. S., & Clementz, B. A. (2012). Augmented gamma band auditory steady-state responses: Support for NMDA hypofunction in schizophrenia. *Schizophrenia Research*, *138*, 1–7. doi:10.1016/j.schres.2012.04.003. arXiv:NIHMS150003.

Hari, R., Hämäläinen, M., & Joutsiniemi, S.-L. (1989). Neuromagnetic steady-state responses to auditory stimuli. *The Journal of the Acoustical Society of America*, *86*, 1033–1039. doi:10.1121/1.398093.

Harms, M., & Melcher, J. (2002). Sound repetition rate in the human auditory pathway: Representations in the waveshape and amplitude of fmri activation. *Journal of neurophysiology*, *88*, 1433–50.

Haufe, S., Meinecke, F., Görgen, K., Dähne, S., Haynes, J.-D., Blankertz, B., & Bießmann, F. (2014). On the interpretation of weight vectors of linear models in multivariate neuroimaging. *NeuroImage*, *87*, 96–110. doi:10.1016/j.neuroimage.2013.10.067.

He, B., Sohrabpour, A., Brown, E., & Liu, Z. (2018). Electrophysiological Source Imaging: A Noninvasive Window to Brain Dynamics. *Annual Review of Biomedical Engineering*, *20*, 171–196. doi:10.1146/annurev-bioeng-062117-120853.

Hebart, M. N., & Baker, C. I. (2018). Deconstructing multivariate decoding for the study of brain function. *NeuroImage*, *180*, 4–18. doi:10.1016/j.neuroimage.2017.08.005.

Helenius, P., Salmelin, R., Richardson, U., Leinonen, S., & Lyytinen, H. (2002). Abnormal Auditory Cortical Activation in Dyslexia 100 msec after Speech Onset. *Journal of Cognitive Neuroscience*, *14*, 603–617. doi:10.1162/08989290260045846.

Herdman, A. T., Lins, O., Van Roon, P., Stapells, D. R., Scherg, M., & Picton, T. W. (2002). Intracerebral sources of human auditory steady-state responses. *Brain topography*, *15*, 69–86. doi:10.1023/A:1021470822922.

Hofmann, M., & Wouters, J. (2012). Improved electrically evoked auditory steady-state response thresholds in humans. *Journal of the Association for Research in Otolaryngology : JARO*, *13*, 573–589. doi:10.1007/s10162-012-0321-8.

Holm, S. (1979). Board of the Foundation of the Scandinavian Journal of Statistics A Simple Sequentially Rejective Multiple Test Procedure A Simple Sequentially Rejective Multiple Test Procedure. *Source: Scandinavian Journal of Statistics Scand J Statist*, *6*, 65–70. doi:10.2307/4615733. arXiv:arXiv:1011.1669v3.

Holmes, C. J., Hoge, R., Collins, L., Woods, R., Toga, A. W., & Evans, A. C. (1998). Enhancement of MR Images Using Registration for Signal Averaging. *Journal of Computer Assisted Tomography*, *22*, 324–333. doi:10.1097/00004728-199803000-00032.

Hotelling, H. (1931). The Generalization of Student's Ratio. *The Annals of Mathematical Statistics*, *2*, 360–378. doi:10.1214/aoms/1177732979.

Huang, G., Hu, Z., Zhang, L., Li, L., Liang, Z., & Zhang, Z. (2020). Removal of eye-blinking artifacts by ICA in cross-modal long-term EEG recording. In *2020 42nd Annual International Conference of the IEEE Engineering in Medicine & Biology Society (EMBC)* (pp. 217–220). IEEE. doi:10.1109/EMBC44109.2020.9176711.

Huster, R. J., Plis, S. M., & Calhoun, V. D. (2015). Group-level component analyses of EEG: validation and evaluation. *Frontiers in Neuroscience*, *9*, 1–14. doi:10.3389/fnins.2015.00254.

Hyvärinen, A., Karhunen, J., & Oja, E. (2001). Independent Component Analysis. *Analysis*, *26*, 481. doi:10.1016/j.acha.2006.03.003.

Hyvärinen, A., Särelä, J., & Vigário, R. (1999). Spikes and bumps: Artefacts generated by independent component analysis with insufficient sample size. *International Workshop on Independent Component Analysis and Blind Signal Separation (ICA'99), Aussois, France*, (pp. 425–429).

Hämäläinen, M. S., & Sarvas, J. (1989). Realistic conductivity geometry model of the human head for interpretation of neuromagnetic data. *IEEE Transactions on Biomedical Engineering*, *36*, 165–171. doi:10.1109/10.16463.

Im, K., Raschle, N. M., Smith, S. A., Ellen Grant, P., & Gaab, N. (2015). Atypical Sulcal Pattern in Children with Developmental Dyslexia and At-Risk Kindergarteners. *Cerebral Cortex*, *26*, 1138–1148. doi:10.1093/cercor/bhu305. arXiv:https://academic.oup.com/cercor/article-pdf/26/3/1138/17309443/bhu305.pdf.

Jamison, H. L., Watkins, K. E., Bishop, D. V., & Matthews, P. M. (2006). Hemispheric specialization for processing auditory nonspeech stimuli. *Cerebral Cortex*, *16*, 1266–1275. doi:10.1093/cercor/bhj068.

Javitt, D. C., & Sweet, R. A. (2015). Auditory dysfunction in schizophrenia: integrating clinical and basic features. *Nature Reviews Neuroscience*, *16*, 535–550. doi:10.1038/nrn4002.

Joris, P. X., Schreiner, C. E., & Rees, A. (2004). Neural Processing of Amplitude-Modulated Sounds. *Physiological Reviews*, *84*, 541–577. doi:10.1152/physrev.00029.2003.

Kayser, J., & Tenke, C. E. (2003). Optimizing PCA methodology for ERP component identification and measurement: Theoretical rationale and empirical evaluation. *Clinical Neurophysiology*, *114*, 2307–2325. doi:10.1016/S1388-2457(03)00241-4.

Koerner, T. K., & Zhang, Y. (2015). Effects of background noise on inter-trial phase coherence and auditory N1–P2 responses to speech stimuli. *Hearing Research*, *328*, 113–119. doi:10.1016/j.heares.2015.08.002.

Koyama, M. S., Di Martino, A., Kelly, C., Jutagir, D. R., Sunshine, J., Schwartz, S. J., Castellanos, F. X., & Milham, M. P. (2013). Cortical Signatures of Dyslexia and Remediation: An Intrinsic Functional Connectivity Approach. *PLoS ONE*, *8*, e55454. doi:10.1371/journal.pone.0055454.

Lehongre, K., Morillon, B., Giraud, A.-L., & Ramus, F. (2013). Impaired auditory sampling in dyslexia: further evidence from combined fMRI and EEG. *Frontiers in Human Neuroscience*, *7*, 1–8. doi:10.3389/fnhum.2013.00454.

Lehongre, K., Ramus, F., Villiermet, N., Schwartz, D., & Giraud, A.-L. (2011). Altered low-gamma sampling in auditory cortex accounts for the three main facets of dyslexia. *Neuron*, *72*, 1080–1090.

Liberman, A. M., Cooper, F. S., Shankweiler, D. P., & Studdert-Kennedy, M. (1967). Perception of the speech code. *Psychological Review*, *74*, 431–461. doi:10.1037/h0020279.

Lins, O. G., & Picton, T. W. (1995). Auditory steady-state responses to multiple simultaneous stimuli. *Electroencephalography and Clinical Neurophysiology/Evoked Potentials Section*, *96*, 420 – 432. doi:https://doi.org/10.1016/0168-5597(95)00048-W.

Lizarazu, M., Lallier, M., Molinaro, N., Bourguignon, M., Paz-Alonso, P. M., Lerma-Usabiaga, G., & Carreiras, M. (2015). Developmental evaluation of atypical auditory sampling in dyslexia: Functional and structural evidence. *Human Brain Mapping*, *36*, 4986–5002. doi:10.1002/hbm.22986.

Lohvansuu, K., Hämäläinen, J. A., Tanskanen, A., Ervast, L., Heikkinen, E., Lyytinen, H., & Leppänen, P. H. (2014). Enhancement of brain event-related potentials to speech sounds is associated with compensated reading skills in dyslexic children with familial risk for dyslexia. *International journal of psychophysiology*, *94*, 298–310.

Luce, R., & Luce, V. (1986). *Response Times: Their Role in Inferring Elementary Mental Organization*. Oxford Psychology Series. OUP USA.

Lucka, F., Pursiainen, S., Burger, M., & Wolters, C. H. (2012). Hierarchical Bayesian inference for the EEG inverse problem using realistic FE head models: Depth localization and source separation for focal primary currents. *NeuroImage*, *61*, 1364–1382. doi:10.1016/j.neuroimage.2012.04.017.

Luke, R., De Vos, A., & Wouters, J. (2017). Source analysis of auditory steady-state responses in acoustic and electric hearing. *NeuroImage*, *147*, 568–576. doi:10.1016/j.neuroimage.2016.11.023.

Luo, H., & Poeppel, D. (2007). Phase Patterns of Neuronal Responses Reliably Discriminate Speech in Human Auditory Cortex. *Neuron*, *54*, 1001–1010. doi:10.1016/j.neuron.2007.06.004.

Luts, H., & Wouters, J. (2004). Hearing assessment by recording multiple auditory steady-state responses: The influence of test duration. *International journal of audiology*, *43*, 471–8. doi:10.1080/14992020400050060.

Manju, V., Gopika, K. K., & Arivudai Nambi, P. M. (2014). Association of Auditory Steady State Responses with Perception of Temporal Modulations and Speech in Noise. *ISRN Otolaryngology*, *2014*, 1–8. doi:10.1155/2014/374035.

Marosi, E., Harmony, T., Becker, J., Reyes, A., Bernal, J., Fernández, T., Rodríguez, M., Silva, J., & Guerrero, V. (1995). Electroencephalographic coherences discriminate between children with different pedagogical evaluation. *International Journal of Psychophysiology*, *19*, 23–32. doi:10.1016/0167-8760(94)00059-N.

Marslen-Wilson, W., & Tyler, L. K. (1980). The temporal structure of spoken language understanding. *Cognition*, *8*, 1–71. doi:10.1016/0010-0277(80)90015-3.

McAnally, K. I., & Stein, J. F. (1997). Scalp potentials evoked by amplitude-modulated tones in dyslexia. *Journal of Speech, Language, and Hearing Research*, *40*, 939–945.

McClelland, J. L., & Elman, J. L. (1986). The TRACE model of speech perception. *Cognitive Psychology*, *18*, 1–86. doi:10.1016/0010-0285(86)90015-0.

McGrath, L. M., Peterson, R. L., & Pennington, B. F. (2020). The Multiple Deficit Model: Progress, Problems, and Prospects. *Scientific Studies of Reading*, *24*, 7–13. doi:10.1080/10888438.2019.1706180.

Meijs, J. W. H., Weier, O. W., Peters, M. J., & Oosterom, A. V. (1989). On the numerical accuracy of the boundary element method (eeg application). *IEEE Transactions on Biomedical Engineering*, *36*, 1038–1049. doi:10.1109/10.40805.

Menell, P., McAnally, K. I., & Stein, J. F. (1999). Psychophysical Sensitivity and Physiological Response to Amplitude Modulation in Adult Dyslexic Listeners. *Journal of Speech, Language, and Hearing Research*, *42*, 797–803. doi:10.1044/jslhr.4204.797.

Miller, R. G. (1974). The jackknife-a review. *Biometrika*, *61*, 1–15. doi:10.1093/biomet/61.1.1.

Miyazaki, T., Thompson, J., Fujioka, T., & Ross, B. (2013). Sound envelope encoding in the auditory cortex revealed by neuromagnetic responses in the theta to gamma frequency bands. *Brain Research*, *1506*, 64–75. doi:10.1016/j.brainres.2013.01.047.

Møller, A. R., Kern, J. K., & Grannemann, B. (2005). Are the non-classical auditory pathways involved in autism and PDD? *Neurological Research*, *27*, 625–629. doi:10.1179/016164105X25117.

Moore, B. C. (2012). *An introduction to the psychology of hearing*. Brill.

de Munck, J., van Dijk, B., & Spekreijse, H. (1988). Mathematical dipoles are adequate to describe realistic generators of human brain activity. *IEEE Transactions on Biomedical Engineering*, *35*, 960–966. doi:10.1109/10.8677.

Muñoz-Gutiérrez, P. A., Giraldo, E., Bueno-López, M., & Molinas, M. (2018). Localization of Active Brain Sources From EEG Signals Using Empirical Mode Decomposition: A Comparative Study. *Frontiers in Integrative Neuroscience*, *12*. doi:10.3389/fnint.2018.00055.

Obleser, J., Eisner, F., & Kotz, S. A. (2008). Bilateral Speech Comprehension Reflects Differential Sensitivity to Spectral and Temporal Features. *Journal of Neuroscience*, *28*, 8116–8123. doi:10.1523/JNEUROSCI.1290-08.2008.

Obleser, J., & Kayser, C. (2019). Neural Entrainment and Attentional Selection in the Listening Brain. *Trends in Cognitive Sciences*, *23*, 913–926. doi:10.1016/j.tics.2019.08.004.

O'Donnell, B. F., Vohs, J. L., Krishnan, G. P., Rass, O., Hetrick, W. P., & Morzorati, S. L. (2013). Chapter 6 - the auditory steady-state response (assr): a translational biomarker for schizophrenia. In E. Başar, C. Başar-Eroğlu, A. Özerdem, P. Rossini, & G. Yener (Eds.), *Application of Brain Oscillations in Neuropsychiatric Diseases* (pp. 101 – 112). Elsevier volume 62 of *Supplements to Clinical Neurophysiology*. doi:https://doi.org/10.1016/B978-0-7020-5307-8.00006-5.

Onton, J. (2009). High-frequency broadband modulation of electroencephalographic spectra. *Frontiers in Human Neuroscience*, *3*, 1–18. doi:10.3389/neuro.09.061.2009.

Onton, J., Westerfield, M., Townsend, J., & Makeig, S. (2006). Imaging human EEG dynamics using independent component analysis. *Neuroscience and Biobehavioral Reviews*, *30*, 808–822. doi:10.1016/j.neubiorev.2006.06.007.

Oostenveld, R., Fries, P., Maris, E., & Schoffelen, J. M. (2011). FieldTrip: Open source software for advanced analysis of MEG, EEG, and invasive electrophysiological data. *Computational Intelligence and Neuroscience*, *2011*. doi:10.1155/2011/156869. arXiv:156869.

Pastor, M., Artieda, J., Arbizu, J., Marti-Climent, J., Pañuelas, I., & Masdeu, J. (2002). Activation of human cerebral and cerebellar cortex by auditory stimulation at 40 hz. *Journal of Neuroscience*, *22*, 10501–10506. Cited By 101.

Pastor, M. A., Vidaurre, C., Fernández-Seara, M. A., Villanueva, A., & Friston, K. J. (2008). Frequency-specific coupling in the cortico-cerebellar auditory system. *Journal of Neurophysiology*, *100*, 1699–1705. doi:10.1152/jn.01156.2007. arXiv:https://doi.org/10.1152/jn.01156.2007. PMID: 18684912.

Pennington, B. (2006). From single to multiple deficit models of developmental disorders. *Cognition*, *101*, 385–413. doi:10.1016/j.cognition.2006.04.008.

Pennington, B. F., Santerre-Lemmon, L., Rosenberg, J., MacDonald, B., Boada, R., Friend, A., Leopold, D. R., Samuelsson, S., Byrne, B., Willcutt, E. G., & Olson, R. K. (2012). Individual prediction of dyslexia by single versus multiple deficit models. *Journal of Abnormal Psychology*, *121*, 212–224. doi:10.1037/a0025823.

Picton, T. (2011). *Human Auditory Evoked Potentials*. Plural Pub.

Picton, T. W., Dimitrijevic, A., Sasha John, M., & Van Roon, P. (2001). The use of phase in the detection of auditory steady-state responses. *Clinical Neurophysiology*, *112*, 1698–1711. doi:10.1016/S1388-2457(01)00608-3.

Picton, T. W., John, M. S., Dimitrijevic, A., & Purcell, D. (2003). Human auditory steady-state responses: Respuestas auditivas de estado estable en humanos. *International Journal of Audiology*, *42*, 177–219. doi:10.3109/14992020309101316. arXiv:https://doi.org/10.3109/14992020309101316.

Poelmans, H., Luts, H., Vandermosten, M., Boets, B., Ghesquière, P., & Wouters, J. (2011). Reduced sensitivity to slow-rate dynamic auditory information in children with dyslexia. *Research in Developmental Disabilities*, *32*, 2810–2819. doi:10.1016/j.ridd.2011.05.025.

Poelmans, H., Luts, H., Vandermosten, M., Boets, B., Ghesquière, P., & Wouters, J. (2012a). Auditory Steady State Cortical Responses Indicate Deviant Phonemic-Rate Processing in Adults With Dyslexia. *Ear and Hearing*, *33*, 134–143. doi:10.1097/AUD.0b013e31822c26b9.

Poelmans, H., Luts, H., Vandermosten, M., Ghesquière, P., & Wouters, J. (2012b). Hemispheric Asymmetry of Auditory Steady-State Responses to Monaural and Diotic Stimulation. *Journal of the Association for Research in Otolaryngology*, *13*, 867–876. doi:10.1007/s10162-012-0348-x.

Poeppel, D. (2003). The analysis of speech in different temporal integration windows: cerebral lateralization as 'asymmetric sampling in time'. *Speech Communication*, *41*, 245–255. doi:10.1016/S0167-6393(02)00107-3.

Popov, T., Oostenveld, R., & Schoffelen, J. M. (2018). FieldTrip Made Easy: An Analysis Protocol for Group Analysis of the Auditory Steady State Brain Response in Time, Frequency, and Space. *Frontiers in Neuroscience*, *12*, 026014. doi:10.3389/fnins.2018.00711. arXiv:1612.06880.

Poulsen, C., Picton, T. W., & Paus, T. (2007). Age-Related Changes in Transient and Oscillatory Brain Responses to Auditory Stimulation in Healthy Adults 19-45 Years Old. *Cerebral Cortex*, *17*, 1454–1467. doi:10.1093/cercor/bhl056.

Purcell, D. W., John, S. M., Schneider, B. A., & Picton, T. W. (2004). Human temporal auditory acuity as assessed by envelope following responses. *The Journal of the Acoustical Society of America*, *116*, 3581–3593. doi:10.1121/1.1798354.

Putilov, A., Münch, M., & Cajochen, C. (2013). Principal Component Structuring of the Non-REM Sleep EEG Spectrum in Older Adults Yields Age-Related Changes in the Sleep and Wake Drives. *Current Aging Science*, *6*, 280–293. doi:10.2174/18746098060314010120341 2.

Ramus, F. (2001). Talk of two theories. *Nature*, *412*, 393–394. doi:10.1038/35086683.

Rance, G. (2008). *The Auditory Steady-state Response: Generation, Recording, and Clinical Application*. Plural Publishing.

Raschle, N. M., Chang, M., & Gaab, N. (2011). Structural brain alterations associated with dyslexia predate reading onset. *NeuroImage*, *57*, 742 – 749. doi:https://doi.org/10.1016/j.neuroimage.2010.09.055. Special Issue: Educational Neuroscience.

Raven, J., & Court, J. (1996). *Manual for Raven's Progressive Matrices and Vocabulary Scales: Standard progressive matrices*. Manual for Raven's Progressive Matrices and Vocabulary Scales. Oxford Psychologists Press.

Reyes, S. A., Lockwood, A. H., Salvi, R. J., Coad, M. L., Wack, D. S., & Burkard, R. F. (2005). Mapping the 40-Hz auditory steady-state response using current density reconstructions. *Hearing Research*, *204*, 1–15. doi:10.1016/j.heares.2004.11.016.

Reyes, S. A., Salvi, R. J., Burkard, R. F., Coad, M. L., Wack, D. S., Galantowicz, P. J., & Lockwood, A. H. (2004). Pet imaging of the 40 hz auditory steady state response. *Hearing Research*, *194*, 73 – 80. doi:https://doi.org/10.1016/j.heares.2004.04.001.

Richards, J. E., Sanchez, C., Phillips-Meek, M., & Xie, W. (2016). A database of age-appropriate average MRI templates. *NeuroImage*, *124*, 1254–1259. doi:10.1016/j.neuroimage.2015.04.055.

Rosen, S. (1992). Temporal information in speech: acoustic, auditory and linguistic aspects. *Philosophical transactions of the Royal Society of London. Series B, Biological sciences*, *336*, 367–73. doi:10.1098/rstb.1992.0070.

Sanchez, C. E., Richards, J. E., & Almli, C. R. (2012). Age-Specific MRI Templates for Pediatric Neuroimaging. *Developmental Neuropsychology*, *37*, 379–399. doi:10.1080/87565641.2012.688900. arXiv:NIHMS150003.

Särelä, J., & Valpola, H. (2005). Denoising source separation. *Journal of Machine Learning Research*, *6*, 233–272.

Schoonhoven, R., Boden, C., Verbunt, J., & de Munck, J. (2003). A whole head MEG study of the amplitude-modulation-following response: phase coherence, group delay and dipole source analysis. *Clinical Neurophysiology*, *114*, 2096–2106. doi:10.1016/S1388-2457(03)00200-1.

Schorer, E. (1986). Critical modulation frequency based on detection of AM versus FM tones. *The Journal of the Acoustical Society of America*, *79*, 1054–1057. doi:10.1121/1.393377.

Schwarz, G. (1978). Estimating the dimension of a model. *Ann. Statist.*, *6*, 461–464. doi:10.1214/aos/1176344136.

Sek, A., & Moore, B. C. J. (1994). The critical modulation frequency and its relationship to auditory filtering at low frequencies. *The Journal of the Acoustical Society of America*, *95*, 2606–2615. doi:10.1121/1.409831.

Shahin, A. J., & Pitt, M. A. (2012). Alpha activity marking word boundaries mediates speech segmentation. *European Journal of Neuroscience*, *36*, 3740–3748. doi:10.1111/ejn.12008.

Shannon, R. V., Zeng, F.-G., Kamath, V., Wygonski, J., & Ekelid, M. (1995). Speech Recognition with Primarily Temporal Cues. *Science*, *270*, 303–304. doi:10.1126/science.270.5234.303.

Share, D. L. (2021). Common Misconceptions about the Phonological Deficit Theory of Dyslexia. *Brain Sciences*, *11*, 1510. doi:10.3390/brainsci11111510.

Shattuck, D. W., Mirza, M., Adisetiyo, V., Hojatkashani, C., Salamon, G., Narr, K. L., Poldrack, R. A., Bilder, R. M., & Toga, A. W. (2008). Construction of a 3d probabilistic atlas of human cortical structures. *NeuroImage*, *39*, 1064 – 1080. doi:https://doi.org/10.1016/j.neuroimage.2007.09.031.

Spencer, K. M. (2012). Baseline gamma power during auditory steady-state stimulation in schizophrenia. *Frontiers in Human Neuroscience*, *5*, 1–7. doi:10.3389/fnhum.2011.00190.

Srinivasan, R., Nunez, P., & Silberstein, R. (1998). Spatial filtering and neocortical dynamics: estimates of EEG coherence. *IEEE Transactions on Biomedical Engineering*, *45*, 814–826. doi:10.1109/10.686789.

Steinmann, I., & Gutschalk, A. (2011). Potential fmri correlates of 40-hz phase locking in primary auditory cortex, thalamus and midbrain. *NeuroImage*, *54*, 495 – 504. doi:https://doi.org/10.1016/j.neuroimage.2010.07.064.

Stevens, K. N. (1960). Toward a Model for Speech Recognition. *The Journal of the Acoustical Society of America*, *32*, 47–55. doi:10.1121/1.1907874.

Stoodley, C. J. (2016). Chapter 9 - the role of the cerebellum in developmental dyslexia. In P. Mariën, & M. Manto (Eds.), *The Linguistic Cerebellum* (pp. 199–221). San Diego: Academic Press. doi:https://doi.org/10.1016/B978-0-12-801608-4.00009-8.

Tang, H., Brock, J., & Johnson, B. W. (2016a). Sound envelope processing in the developing human brain: A MEG study. *Clinical Neurophysiology*, *127*, 1206–1215. doi:10.1016/j.clinph.2015.07.038.

Tang, H., Crain, S., & Johnson, B. W. (2016b). Dual temporal encoding mechanisms in human auditory cortex: Evidence from MEG and EEG. *NeuroImage*, *128*, 32–43. doi:10.1016/j.neuroimage.2015.12.053.

Teale, P., Collins, D., Maharajh, K., Rojas, D. C., Kronberg, E., & Reite, M. (2008). Cortical source estimates of gamma band amplitude and phase are different in schizophrenia. *NeuroImage*, *42*, 1481 – 1489. doi:https://doi.org/10.1016/j.neuroimage.2008.06.020.

Telkemeyer, S., Rossi, S., Koch, S. P., Nierhaus, T., Steinbrink, J., Poeppel, D., Obrig, H., & Wartenburger, I. (2009). Sensitivity of Newborn Auditory Cortex to the Temporal Structure of Sounds. *Journal of Neuroscience*, *29*, 14726–14733. doi:10.1523/JNEUROSCI.1246-09.2009.

Telkemeyer, S., Rossi, S., Nierhaus, T., Steinbrink, J., Obrig, H., & Wartenburger, I. (2011). Acoustic Processing of Temporally Modulated Sounds in Infants: Evidence from a Combined Near-Infrared Spectroscopy and EEG Study. *Frontiers in Psychology*, *1*. doi:10.3389/fpsyg.2011.00062.

Thiede, A., Glerean, E., Kujala, T., & Parkkonen, L. (2020). Atypical MEG inter-subject correlation during listening to continuous natural speech in dyslexia. *NeuroImage*, *216*, 116799. doi:10.1016/j.neuroimage.2020.116799.

Vakorin, V. A., Kovacevic, N., & McIntosh, A. R. (2010). Exploring transient transfer entropy based on a group-wise ICA decomposition of EEG data. *NeuroImage*, *49*, 1593–1600. doi:10.1016/j.neuroimage.2009.08.027.

Van der Reijden, C. S., Mens, L. H. M., & Snik, A. F. M. (2005). EEG Derivations Providing Auditory Steady-State Responses With High Signal-to-Noise Ratios in Infants. *Ear and Hearing*, *26*, 299–309. doi:10.1097/00003446-200506000-00006.

Van Dun, B., Wouters, J., & Moonen, M. (2007). Improving auditory steady-state response detection using independent component analysis on multichannel EEG data. *IEEE Transactions on Biomedical Engineering*, *54*, 1220–1230. doi:10.1109/TBME.2007.897327.

Van Dun, B., Wouters, J., & Moonen, M. (2009). Optimal electrode selection for multi-channel electroencephalogram based detection of auditory steady-state responses. *The Journal of the Acoustical Society of America*, *126*, 254–268. doi:10.1121/1.3133872.

Van Hirtum, T., Ghesquière, P., & Wouters, J. (2019a). Atypical neural processing of rise time by adults with dyslexia. *Cortex*, *113*, 128–140. doi:10.1016/j.cortex.2018.12.006.

Van Hirtum, T., Ghesquière, P., & Wouters, J. (2021). A Bridge over Troubled Listening: Improving Speech-in-Noise Perception by Children with Dyslexia. *Journal of the Association for Research in Otolaryngology*, . doi:10.1007/s10162-021-00793-4.

Van Hirtum, T., Moncada-Torres, A., Ghesquière, P., & Wouters, J. (2019b). Speech Envelope Enhancement Instantaneously Effaces Atypical Speech Perception in Dyslexia. *Ear and Hearing*, *40*, 1242–1252. doi:10.1097/AUD.0000000000000706.

Van Wieringen, A., & Wouters, J. (2008). LIST and LINT: Sentences and numbers for quantifying speech understanding in severely impaired listeners for Flanders and the Netherlands. *International Journal of Audiology*, *47*, 348–355. doi:10.1080/14992020801895144.

Vandermosten, M., Correia, J., Vanderauwera, J., Wouters, J., Ghesquière, P., & Bonte, M. (2020). Brain activity patterns of phonemic representations are atypical in beginning readers with family risk for dyslexia. *Developmental Science*, *23*, 1–15. doi:10.1111/desc.12857.

Vanvooren, S., Hofmann, M., Poelmans, H., Ghesquière, P., & Wouters, J. (2015). Theta, beta and gamma rate modulations in the developing auditory system. *Hearing Research*, *327*, 153–162. doi:10.1016/j.heares.2015.06.011.

Vanvooren, S., Poelmans, H., Hofmann, M., Ghesquière, P., & Wouters, J. (2014). Hemispheric Asymmetry in Auditory Processing of Speech Envelope Modulations in Prereading Children. *Journal of Neuroscience*, *34*, 1523–1529. doi:10.1523/JNEUROSCI.3209-13.2014.

Vanvooren, S., Poelmans, H., Hofmann, M., Luts, H., Dandache, S., Ghesquière, P., & Wouters, J. (2012). Auditory temporal processing in dyslexia: An ASSR study in young children. *International Journal of Psychophysiology*, *85*, 358. doi:10.1016/j.ijpsycho.2012.06.181.

Vellutino, F. R., Fletcher, J. M., Snowling, M. J., & Scanlon, D. M. (2004). Specific reading disability (dyslexia): what have we learned in the past four decades? *Journal of Child Psychology and Psychiatry*, *45*, 2–40. doi:10.1046/j.0021-9630.2003.00305.x.

Von Helmholtz, H. (1863). *Die Lehre von den Tonempfindungen als physiologische Grundlage für die Theorie der Musik*. Vieweg.

Xue, H., Wang, Z., Tan, Y., Yang, H., Fu, W., Xue, L., & Zhao, J. (2020). Resting-state EEG reveals global network deficiency in dyslexic children. *Neuropsychologia*, *138*, 107343. doi:10.1016/j.neuropsychologia.2020.107343.

Ziegler, J. C., & Goswami, U. (2005). Reading Acquisition, Developmental Dyslexia, and Skilled Reading Across Languages: A Psycholinguistic Grain Size Theory. *Psychological Bulletin*, *131*, 3–29. doi:10.1037/0033-2909.131.1.3.

Ziegler, J. C., Pech-Georgel, C., George, F., & Lorenzi, C. (2009). Speech-perception-in-noise deficits in dyslexia. *Developmental science*, *12*, 732–745.

Zwicker, E. (1952). Die grenzen der hörbarkeit der amplitudenmodulation und der frequenz-modulation eines tones. *Acta Acustica United With Acustica*, *2*, 125–133.

Scientific acknowledgments

The authors would like to thank Prof. John E. Richards from the University of South Carolina for sharing part of their Neurodevelopmental MRI Database used to create the head model. We also would like to thank Dr. Robert Oostenveld from the Donders Institute in The Netherlands for his continuing interest and for sharing his critical insights with us in the analyses of these data.

This study was supported by the European Union H2020 Marie Skłodowska-Curie Actions (MSCA)- ITN-2014-ETN Programme. Under the project "Advancing brain research in children's developmental neurocognitive disorders" (ChildBrain, 641652). This work was partly supported by the Research Council of KU Leuven (C14/17/046) through a research grant to Prof. Jan Wouters. Some of the resources and services used in this work were provided by the VSC (Flemish Supercomputer Centre), funded by the Research Foundation - Flanders (FWO) and the Flemish Government.

Personal contribution and conflict of interest statement

Personal contribution

All the work presented in this Thesis has been developed by Raúl Granados Barbero. This author conceived the presented idea, performed the implementation and the analytical computations. Raúl Granados Barbero analysed the data, interpreted the global findings of this work and wrote the whole manuscript.

Conflict of interest

The authors declare no conflicts of interest.